

University of Louisville

## ThinkIR: The University of Louisville's Institutional Repository

---

Electronic Theses and Dissertations

---

8-2019

### All season heat pipe system.

Adrienne Marie Parsons  
*University of Louisville*

Follow this and additional works at: <https://ir.library.louisville.edu/etd>



Part of the [Mechanical Engineering Commons](#)

---

#### Recommended Citation

Parsons, Adrienne Marie, "All season heat pipe system." (2019). *Electronic Theses and Dissertations*. Paper 3274.

<https://doi.org/10.18297/etd/3274>

This Doctoral Dissertation is brought to you for free and open access by ThinkIR: The University of Louisville's Institutional Repository. It has been accepted for inclusion in Electronic Theses and Dissertations by an authorized administrator of ThinkIR: The University of Louisville's Institutional Repository. This title appears here courtesy of the author, who has retained all other copyrights. For more information, please contact [thinkir@louisville.edu](mailto:thinkir@louisville.edu).

ALL SEASON HEAT PIPE SYSTEM

By

Adrienne Marie Parsons  
B.S., University of Louisville, 2008  
M.Eng., University of Louisville, 2009

A Dissertation  
Submitted to the Faculty of the  
J.B. Speed School of Engineering at the University of Louisville  
in Partial Fulfillment of the Requirements  
for the Degree of

Doctor of Philosophy  
in Mechanical Engineering

Department of Mechanical Engineering  
University of Louisville  
Louisville, KY

August 2019



ALL SEASON HEAT PIPE SYSTEM

By

Adrienne Marie Parsons  
B.S., University of Louisville, 2008  
M.Eng., University of Louisville, 2009

A Dissertation Approved on

July 26, 2019

By the following Dissertation Committee:

---

Dr. M. Keith Sharp (Co-Chair)

---

Dr. Ellen Brehob (Co-Chair)

---

Dr. Geoffrey Cobourn

---

Dr. Brian Robinson

## DEDICATION

This dissertation is dedicated to my husband and daughter

Matthew K. Parsons

and

Madalyn A. Parsons

my family is what drives me.

## ACKNOWLEDGEMENTS

First, I would like to thank my husband, Matthew, for his patience and encouragement. This was only possible because of him. Thank you for believing in me. Next, my parents Scott and Connie, they gave me the drive, knowledge and confidence to become an engineer. Without my foundation in learning, I would not have been able to persist. Also, many thanks to those in the Engineering Fundamentals Department who continually endorsed me, helped me and mentored me throughout this process. Finally, I want to thank my daughter, Madalyn. I hope I make you proud.

## ABSTRACT

### ALL SEASON HEAT PIPE SYSTEM

Adrienne M. Parsons

July 26, 2019

Our energy choices impact the earth's natural systems and climate. As this becomes increasingly important, the need for decreasing our energy usage is essential.

Conventional passive solar systems can significantly reduce the heating load. Similarly, passive ambient energy systems, such as ventilation and sky radiation, can reduce cooling loads. However, the integration of passive heating and cooling systems in the same building and the benefits of actively controlling these otherwise passive systems to maximize annual energy savings has largely been unexplored.

This study first evaluates the building cooling capacity of sky radiation, which was previously identified to have the greatest cooling potential among common ambient sources for climates across the U.S., and the design parameters of the system. Next, the study develops and varies the control strategies of a passive heating and cooling system with the objective of maximizing annual energy and cost savings. The systems were simulated with thermal networks using Matrix Laboratory (MATLAB), a computer software package. Nodal temperatures were simultaneously solved as functions of time using Typical Meteorological Year (TMY3) weather data. Auxiliary heating and cooling were added as needed to limit room temperature to a maximum of 23.9 °C and minimum of 18.3 °C. Results were compared to a Louisville baseline with LRR = 10 W/m<sup>2</sup>K,

horizontal radiator and one cover, which provided an annual sky fraction (fraction of cooling load provided by sky radiation) of 0.855. A decrease to 0.852 was found for an increase in radiator slope to 20°, and a drop to 0.832 for 53° slope (latitude + 15°, a typical slope for solar heating). These drops were associated with increases in average radiator temperature by 0.73°C for 20° and 1.99°C for 53°. A 30% decrease in storage capacity caused a decrease in sky fraction to 0.843. LRR and thermal storage capacity had strong effects on performance. Radiator slope had a surprisingly small impact, considering that the view factor to the sky at 53° tilt is less than 0.5.

Chapter 3 expanded on and analyzed the design of the windscreen for the sky radiator used for cooling as well as the effects of implementing the heat pipe augmented sky radiator to varying climates. When applying a windscreen of polyethylene, which is mostly transparent to long-wave radiation, a drawback of polyethylene is its susceptibility to degradations of the optical properties. Sky fractions of 100% were possible in cities with small cooling loads (Rock Springs, Seattle, San Diego and Denver). Sky fractions of over 50% were achieved in New Orleans and Houston and over 40% in Miami. A second study examined the degradation of polyethylene cover material. Louisville and two challenging climates (Miami and New Orleans) were simulated. In the Louisville, Miami and New Orleans climate, performance was reduced by 2.7%, 14.1% and 9.0% respectively, due to degradation of the cover's material.

Chapter 4 explores the combination of a solar heating heat pipe system and sky radiation heat pipe cooling system. Two configurations were modeled in the Louisville, KY climate. The first system configuration, called a Separate System (SS), consists of a sky radiator and thermal mass that are separate from a solar heat pipe system and its

thermal mass. The second system configuration, called a Combined System (CS), utilizes a shared thermal mass between the solar absorber and sky radiator. The control strategies simulated included: Seasonal, Ambient, Room and Matrix. The highest fraction of energy supplied by ambient sources for the SS was 0.707 with Matrix control, while for the CS, the highest fraction (0.704) was with Matrix temperature control with switchable attributes for heating and cooling. In Chapter 5, the two configurations in Chapter 4 were simulated with additional active control approaches. The four control strategies in Chapter 5 included variables: ambient temperature (current and forecasted), indoor air temperature, calculated auxiliary load and heating/cooling (current and forecasted) load. The highest ambient energy fractions (fraction of the total annual load served by the system) of the configurations using a SS for Louisville were 0.710, 0.708, 0.715 and 0.712 respectively. With an estimated cost savings of \$49-\$54/m<sup>2</sup> USD for the Louisville baseline climate using a SS. The ambient energy fraction only decreased by 1% for the CS (AUX-24HR ambient energy fraction of 0.709).

## TABLE OF CONTENTS

ACKNOWLEDGEMENTS .....	iv
ABSTRACT.....	v
LIST OF TABLES .....	6
LIST OF FIGURES .....	7
CHAPTER I .....	1
INTRODUCTION .....	1
1.1. DISSERTATION ORGANIZATION .....	1
1.2. DISSERTATION OBJECTIVES .....	3
CHAPTER II.....	6
THE COOLING POTENTIAL OF SKY RADIATION WITH VARIATIONS IN SYSTEM PARAMETERS .....	6
2.1. INTRODUCTION.....	6
2.1.1. Sky Radiator System Review.....	6
2.1.2. Objective .....	8
2.2. METHODS.....	9
2.2.1. Sky Radiator System.....	9
2.2.2. Network Parameters .....	10
2.2.3. Parameters Evaluated .....	19
2.2.4. Sky Fraction and Radiator Efficiency.....	20
2.3. RESULTS AND DISCUSSION.....	21
2.3.1. Limitations .....	30
2.4. CONCLUSIONS .....	31
CHAPTER III .....	32
THE EFFECTS OF MULTIPLE COVERS WITH CONDENSATION AND OPTICAL DEGRADATION OF A POLYETHYLENE WINDSCREEN ON THE PERFORMANCE OF A SKY COOLING SYSTEM .....	32
3.1. INTRODUCTION .....	32
3.1.1. Polyethylene as Windscreen Material .....	33
3.1.2. Objective .....	35

3.2. METHODS .....	36
3.2.1. Sky Fraction and Radiator Efficiency.....	51
3.3. RESULTS AND DISCUSSION.....	53
3.3.1. Effects of Condensation on System Performance .....	53
3.3.2. Degradation of Polyethylene .....	57
3.4. CONCLUSIONS .....	58
CHAPTER IV .....	61
CONTROL STRATEGIES AND DESIGN PARAMETERS FOR A COMBINED PASSIVE HEATING AND COOLING SYSTEM IN LOUISVILLE, KY .....	61
4.1. INTRODUCTION .....	61
4.1.1. Review of Passive Heating Systems .....	61
4.1.2. Review of Passive Cooling Systems.....	62
4.1.3. Review of Combined Passive Heating and Cooling.....	63
4.1.4. Objective .....	65
4.2. METHODS .....	66
4.2.1. Passive System Configurations.....	76
4.2.2. System Control Strategies.....	79
4.2.3. Energy Fractions .....	82
4.3. RESULTS AND DISCUSSION.....	84
4.4. CONCLUSIONS .....	92
CHAPTER V .....	94
ACTIVE CONTROL OF PASSIVE SYSTEMS FOR HEATING AND COOLING OF BUILDINGS .....	94
5.1. INTRODUCTION .....	94
5.1.1. Passive Heating and Cooling .....	94
5.1.2. Building Controls.....	97
5.1.3. Objective .....	99
5.2. METHODS .....	99
5.2.1. MATLAB Computer Simulation.....	99
5.2.2. Ambient Energy Fraction .....	109
5.2.3. System Configurations.....	112
5.2.4. Control Strategies .....	113
5.3. RESULTS AND DISCUSSION.....	118
5.3.1. Annual performance of SS and CS .....	118

5.3.2. Hourly performance of CS.....	125
5.4. CONCLUSIONS .....	128
CHAPTER VI .....	130
CONCLUSIONS.....	130
6.1. SUMMARY OF RESULTS .....	130
6.2. ADDITIONAL RECOMMENDATIONS.....	131
REFERENCES .....	133
CURRICULUM VITA .....	146

## LIST OF TABLES

<i>Table 1. Description of baseline values for sky radiator system. ....</i>	11
<i>Table 2. Description and baseline values of nodal temperatures and conductances. ....</i>	13
<i>Table 3. Description of parameters used to calculate conductance in thermal network. ....</i>	13
<i>Table 4. Description and baseline values of nodal temperatures and conductance. ....</i>	39
<i>Table 5. Description of variables and parameters used to calculate conductance in thermal network (Equations 24-67). ....</i>	40
<i>Table 6. Program simulation description .....</i>	51
<i>Table 7. Description and baseline values of nodal temperatures and conductances. ....</i>	68
<i>Table 8. Separate System design parameters. ....</i>	77
<i>Table 9. Combined System design parameters for cooling versus heating schemes. ....</i>	78
<i>Table 10. Control strategies for varying system type and design parameters.....</i>	81
<i>Table 11. The average and maximum system power for CS-R-V-53. ....</i>	87
<i>Table 12. Description and baseline values of nodal temperatures and conductances. ..</i>	101
<i>Table 13. Louisville, KY Utility Electric Rate Structure.....</i>	112
<i>Table 14. Annual cost savings of SS-AUX-24HR passive system using Louisville, KY utility rate structures.....</i>	125
<i>Table 15. Variables used in equations in Section 4.2. ....</i>	141
<i>Table 16. Variables and parameters used in MATLAB simulation and design. ....</i>	143

## LIST OF FIGURES

*Figure 1. Illustration of the passive sky radiator system. Four heat pipes are shown that transfer heat from the thermal storage to the radiator on the outside of the building and one heat pipe that transfers heat directly from the room to the radiator. .... 10*

*Figure 2. Heat pipe graphic [Poteat, et al. 2015]. The evaporator end is immersed in the thermal storage tank or is surrounded by room air, and the condenser end is attached to the radiator. .... 10*

*Figure 3. Thermal network for passive sky radiator system with covers. .... 11*

*Figure 4. Annual sky fraction at varying tilt angles relative to horizontal. .... 22*

*Figure 5. Annual sky fraction at varying thermal storage capacity. .... 23*

*Figure 6. Annual sky fraction at varying load to radiator ratio LRR. .... 24*

*Figure 7. Hourly efficiency of baseline radiator (May-September only). .... 25*

*Figure 8. Nodal temperatures for the hottest week (June 23-29). .... 26*

*Figure 9. Nodal temperatures for the dates of June 5-7. Highlighted in grey is 5:00PM to 5:00AM representing nighttime. .... 27*

*Figure 10. Components of heat transfer to the windscreen: Radiation from sky ( $k_{81}$ ), radiation and convection from radiator ( $k_{12}$ ), radiation and convection from ambient (including condensation when it occurs) ( $k_{91}$ ) and solar flux ( $E_1$ ) for a typical summer day, June 2nd for the baseline attributes. Condensation is present at 5:00AM and 6:00AM. .... 29*

<i>Figure 11. Components of heat transfer to the radiator: Radiation from sky (k82), convection and radiation from cover (k12), radiation from ambient (including condensation when it occurs) (k92), fin conduction from the condenser end of the heat pipe (k23), conduction through wall insulation from tank (k25) and solar flux (E2) for a typical summer day, June 2nd for the baseline attributes. Condensation is present at 5:00AM and 6:00AM. ....</i>	<i>29</i>
<i>Figure 12. Depiction of one-windscreen sky radiator system with uniform condensation layer .....</i>	<i>37</i>
<i>Figure 13. Node diagram for system with no windscreen. ....</i>	<i>38</i>
<i>Figure 14. Node diagram for system with one windscreen. ....</i>	<i>38</i>
<i>Figure 15. Node diagram for system with two windscreens. ....</i>	<i>39</i>
<i>Figure 16. Annual sky fractions when condensation is included with zero, one and two cover(s).....</i>	<i>54</i>
<i>Figure 17. Calculated annual cooling loads for differing U.S. cities. ....</i>	<i>54</i>
<i>Figure 18. Time that condensation was found on the outer cover with one and two-cover systems. ....</i>	<i>55</i>
<i>Figure 19. Comparison of sky fractions in all locations with cooling load of one cover system.....</i>	<i>56</i>
<i>Figure 20. Comparison of room temperature, ambient temperature and radiator temperature during a week in June in Louisville, KY for the two cover system. ....</i>	<i>56</i>
<i>Figure 21. Annual sky fractions in Louisville, New Orleans and Miami, when the cover is replaced in the months shown. ....</i>	<i>58</i>

<i>Figure 22. Nodal diagram depicting the thermal conductances for cooling (top) and heating (bottom) for a one cover system.</i>	76
<i>Figure 23. Separate System configuration.</i>	77
<i>Figure 24. Combined System configuration with slope = latitude + 15°. (Slope = 0° was also simulated, but not depicted in this figure).</i>	78
<i>Figure 25. Combined System heat pipe configurations for cooling (left) and heating (right).</i>	79
<i>Figure 26. Process flowchart used to determine heating or cooling mode for the Matrix control strategy.</i>	81
<i>Figure 27. Heating and cooling mode hours for all control strategies (see Table 10).</i>	85
<i>Figure 28. Ambient energy fractions for varying control strategies and attributes (see Table 10).</i>	88
<i>Figure 29. Room temperature during a cooling period for Matrix control strategy (see Table 10).</i>	90
<i>Figure 30. Room temperature during a heating period for Matrix control strategy (see Table 10).</i>	91
<i>Figure 31. Nodal diagram depicting the calculations for thermal conductance for cooling (top) and heating (bottom) for a one cover system [Parsons &amp; Sharp, 2019].</i>	102
<i>Figure 32. [Left] The SS configuration. [Right] The CS configuration with slope at latitude.</i>	113
<i>Figure 33. Ambient temperature (AT) implementation diagram</i>	115
<i>Figure 34. Building load (BL) implementation diagram.</i>	116
<i>Figure 35. Room temperature (R/AT) implementation diagram.</i>	117

<i>Figure 36. Auxiliary load (AUX) implementation diagram.</i> .....	118
<i>Figure 37. Ambient energy fractions for the differing SS control strategies in Louisville, KY.</i> .....	121
<i>Figure 38. Heating and cooling hours for CS control strategies in Louisville, KY. ....</i>	121
<i>Figure 39. Average indoor temperatures and standard deviation (<math>\sigma=0.5</math>) of the control strategies in Louisville, KY for SS and CS. ....</i>	122
<i>Figure 40. Absorber heating efficiency versus loss potential to insolation ratio in January of the SS-AUX-24HR. ....</i>	123
<i>Figure 41. Radiator cooling efficiency in July of the SS-AUX-24HR at different sky-radiator temperature differences over black body radiation.</i> .....	123
<i>Figure 42. A 36 hour period in March (25-26th) of AT, R/AT, BL-24HR, and AUX-24HR room temperatures compared to ambient temperature of CS.</i> .....	127
<i>Figure 43. A 36 hour period in October (10-11<sup>th</sup>) of AT, R/AT, BL-24HR, and AUX-24HR room temperatures compared to ambient temperature of CS.</i> .....	128

## CHAPTER I INTRODUCTION

### 1.1. DISSERTATION ORGANIZATION

The impact of our energy choices on the earth's natural systems and climate are increasingly evident. The industrial activities of our modern civilization have continually raised atmospheric carbon dioxide levels in the last 150 years. The fifth assessment report by the Intergovernmental Panel on Climate Change [2014] concluded there is a better than 95 percent probability that human-produced greenhouse gases such as carbon dioxide, methane and nitrous oxide have caused much of the observed increase in Earth's temperatures over the past 50 years. Climate change continues to become an increasingly pertinent issue, and the need for decreasing our energy usage is essential in order to mitigate the effects of climate change. Air conditioning accounts for about 12% of United States (U.S.) home energy expenditures, and represents a lucrative opportunity where meaningful reductions can be realized. Conventional passive solar systems can significantly reduce a building's heating load. Similarly, passive ambient energy systems, such as ventilation and sky radiation, can reduce cooling loads. The integration of passive heating and cooling systems in the same building and maximizing annual energy savings by actively controlling these otherwise passive systems, has recently become popular and using a passive heat pipe system for both heating and cooling has been largely unexplored. MATLAB computer simulations were run for the theoretical models for each chapter's objective.

For this study, Chapter 2 examines a moderate climate (Louisville, KY) to evaluate the effects of radiator orientation, thermal storage capacity and cooling load to radiator area ratio (LRR) on a passive cooling sky radiator heat pipe system. Results were compared to a Louisville climate, with a baseline  $LRR = 10 \text{ W/m}^2\text{K}$ , horizontal radiator orientation and one cover. This chapter has been published by the *Journal of Solar Energy Engineering including Wind Energy and Building Energy Conservation*.

Next, Chapter 3 expanded on the design for the solar heat pipe sky radiator to analyze the windscreen for the sky radiator. This study also expanded the climates examined for the sky radiator in Chapter 2. Concerning the use of polyethylene windscreens, which are mostly transparent to long-wave radiation, multiple studies have discussed their susceptibility to optical property degradation. To account for this noted drawback, this chapter analyzes the performance degradation of a sky radiator equipped with a polyethylene windscreen. This chapter has been published by the *International Journal of Sustainable Energy*.

Due to the multitude of benefits a dual system would have on energy savings, Chapter 4 explores the combination of a solar heating heat pipe system and sky radiation heat pipe cooling system. In this chapter, two configurations were modeled in the Louisville, KY climate. The first system configuration, called Separate System (SS), consists of a sky radiator and thermal mass that are separate from a solar heat pipe system and its thermal mass. The second system configuration, called Combined System (CS), utilizes a shared thermal mass between the solar absorber and sky radiator. Four control strategies were

simulated for both systems. This chapter has been published by *International Journal of Sustainable Energy*.

In designing passive systems that will heat and cool, analyzing system's controls, in order to further reduce a building's heating and cooling load, would be significant in generating less energy. Chapter 5 considers the passive heating and cooling of a building, and the benefits of actively controlling the system through process controls to increase annual energy and cost savings. The two configurations in Chapter 4 were furthered by four newly examined control strategies that were simulated for both systems. All simulations utilized a differing control strategy to identify when to switch from cooling-only to heating-only. System parameters are compared each hour(s) to decide if the system should be in heating or cooling. Additionally, control strategies are simulated over multiple prediction horizons.

The final chapter, Chapter 6, includes a summary of the conclusions from the studies and recommendations for next steps in this research. The content within Chapters 2, 3, and 4 are identical to each respective publication with the following changes:

- To comply with university dissertation guidelines, this document is restricted to one official abstract summarizing the entire dissertation. Therefore, the abstracts were not included in the individual chapters.
- To comply with university dissertation guidelines, the references for each publication are compiled together and located after the body of this dissertation.
- To comply with university guidelines, and to ease confusion, the figures, tables and equations have been updated for uniformity within this document.

## **1.2. DISSERTATION OBJECTIVES**

As energy becomes more costly, both in terms of environmental and monetary costs, alternative applications for energy use become paramount. This study aims to further the

theoretical research on using a passive heat pipe system to heat and cool a space. The following aims of this study agreed upon in May of 2016 by this dissertation committee:

- 1. Evaluating the performance of a heat pipe system during the cooling season, as well as parameters that will affect the system's efficiency.**
- 2. Assessing the affect condensation and cover degradation have on the radiator efficiency.**
- 3. Simulating a heat pipe system that conditions a space for both the heating and cooling seasons.**

These research objectives are met through computer simulations imitating a theoretical prototype.

The initial research objective was to investigate a building's cooling capacity of sky radiation using a heat pipe system, while exploring different design parameters of the system. Different design parameters affect the radiative cooling system performance by increasing power density, by better matching of cooling availability to cooling demands, and by decreasing costs. For the initial investigation, the effects of radiator orientation, thermal storage capacity and cooling LRR are all assessed. Three climates were used to evaluate five cover configurations – zero, one and two covers with unconstrained temperature, and zero and one cover with temperature limited to the dew point of ambient air to simulate condensation on the cover.

Next, the sky radiator system's cooling performance is evaluated to include the effects of condensation and degradation of the radiator cover. The objective also established cooling capabilities across climates in the U.S.

The final objective is the theoretical development of a heat pipe system that includes space conditioning for the heating and cooling season. Computer simulations were used along with multiple control strategies and weather prediction methods to simulate two system types with a single passive heat pipe system that incorporates a heat pipe solar wall

in the winter and solar heat pipe sky radiator in the summer to condition a space. Multiple control strategies were studied and improved upon.

## CHAPTER II THE COOLING POTENTIAL OF SKY RADIATION WITH VARIATIONS IN SYSTEM PARAMETERS

### 2.1. INTRODUCTION

Radiative cooling is based on the principle of heat loss by long wave radiation from the building to the sky temperature. It is a particularly promising sustainable source for space cooling, having demonstrated the highest sensible cooling potential in most of the climates in the continental U.S. [Robinson, *et al.* 2013b]. A passive sky radiator provides an effective means of counterbalancing a large fraction of a building's cooling needs. Performance prediction algorithms are, therefore, useful to ensure effective design features and configurations for a particular application. When integrated with whole building simulations, such tools can provide valuable information for consideration during the design process. However, investigations of the benefits of particular features of sky radiation systems are limited. Therefore, this study evaluated three parameters expected to be important, namely, radiator orientation, thermal storage capacity and cooling load to radiator area ratio.

#### 2.1.1. Sky Radiator System Review

A number of radiative cooling systems designs have been investigated, such as movable insulation, air-based systems, open or closed water-based systems, photovoltaic/thermal systems, and heat pipe systems [Eicker, *et al.* 2011]. One of the first applications of

radiative cooling was tested about 50 years ago and used movable insulation. [Santamouris 2007]. Another early radiative cooling experimental design focused on radiative cooling by air flowing in a narrow channel [Brunold, *et al.* 1989]. In the system, a channel was created along a wall and roof with vents in the test room and to the environment, and a thin aluminum sheet used as the main radiator was located in the middle of the channel for air to circulate freely around. During the winter the vents were opened during the daytime when the sheet was heated by solar radiation, and in the summer the vents were only opened during the night.

Berdahl, *et al.* [1983] provided an empirical relationship for effective sky temperature as a function of ambient temperature and dew point temperature that is useful for modelling the radiant heat transfer between sky and radiator. Parameters that have been found to enhance the sky radiator system include the addition of a titanium dioxide painted surface that provides selective emittance of thermal radiation and low absorption of solar wavelengths [Kimball 1985], and the utilization of a polyethylene cover. The polyethylene cover allows long wave radiation to pass, while reducing convective losses and preventing passage of a portion of short wave radiation. [Catalanotti, *et al.* 1975, Andretta, *et al.* 1981, Das & Iqbal 1987].

Combining the efforts of these studies, it was found that sky radiation is a viable means for cooling a space, as well as for dehumidifying air. Such a system can be implemented to supply sensible and latent cooling to buildings at moisture levels that humans find comfortable in the different climate zones of the continental United States, with and without a means of energy storage [Robinson, *et al.* 2013b, Springer & Sharp 2015]. With sky radiation experiencing a recent increase in interest [Vall & Castell

2017], this study evaluates important preliminary design parameters for a heat pipe augmented sky radiator system to inform the development for a mass produced residential cooling system.

### **2.1.2. Objective**

With the widely recognized need to reduce carbon emissions and the large contribution that renewable space conditioning can have in reducing fossil fuel consumption, it is important to explore how different design parameters affect radiative cooling system performance by increasing power density, by better matching of cooling availability to cooling demands, and by decreasing costs. To the authors' knowledge, little research has been conducted on differing design parameters for a heat pipe augmented sky radiator system. The basic design evaluated in this study is shown in Figure 1. Heat pipes (Figure 2) provide two-phase heat transfer from storage and from the room to a covered plate that radiates heat to the sky. For this initial investigation, a moderate climate (Louisville, KY) was used to evaluate the effects of radiator orientation, thermal storage capacity and cooling load to radiator area ratio (LRR). Each of these parameters were varied to investigate the performance impact of various installation conditions. Differing radiator orientations were investigated to analyze system performance where a flat installation is not possible or practical. Analyzing this system over a range of LRR demonstrates system effectiveness in buildings with differing envelopes, for instance, new, small buildings with low loss coefficients and old, large construction with high loss coefficients. Finally, various cover and storage capacity characteristics were analyzed so that system performance versus cost can be balanced to satisfy market targets.

## 2.2. METHODS

Nodal temperatures were simultaneously solved as functions of time using Typical Meteorological Year (TMY3) weather data with MATLAB programming software. Auxiliary cooling was applied as needed to limit room temperature to a maximum of 23.9°C and no heat sources were assumed in the room. A thin layer of water was added to the polyethylene cover when it reached the dew point to simulate the effects of condensation.

### 2.2.1. Sky Radiator System

A nine-node network was used to simulate the system (Figure 3). Characteristics of the simulated system are given in Table 1. All simulations used a white (zinc oxide) painted radiator plate [Duffie & Beckman 2013]. Five heat pipes were simulated with four heat pipes immersed in a thermal storage tank containing water, and one transferring cooling directly into the space. Direct cooling of room air is designed to provide immediate cooling that is more in phase with the typical peak daily cooling load. The heat pipe used R-124 refrigerant as the two-phase heat transfer fluid. The algorithm was modeled after Robinson, *et al.* [2013a] to provide a similar design tool for this new system [Susheela & Sharp 2001, Albanese, *et al.* 2012 Robinson, *et al.* 2013a, Robinson & Sharp 2014].

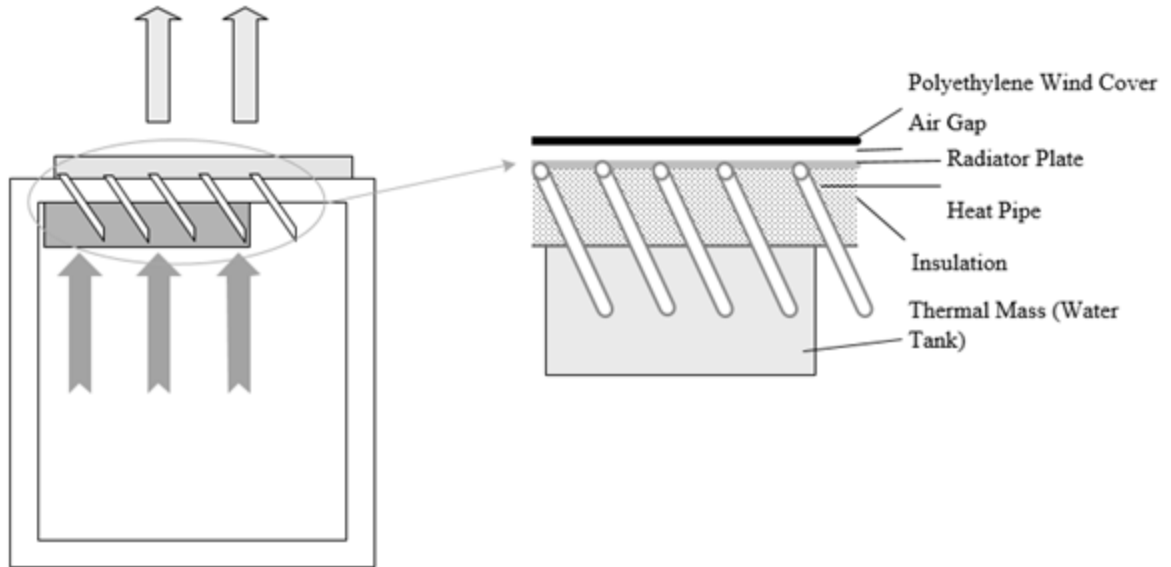


Figure 1. Illustration of the passive sky radiator system. Four heat pipes are shown that transfer heat from the thermal storage to the radiator on the outside of the building and one heat pipe that transfers heat directly from the room to the radiator.

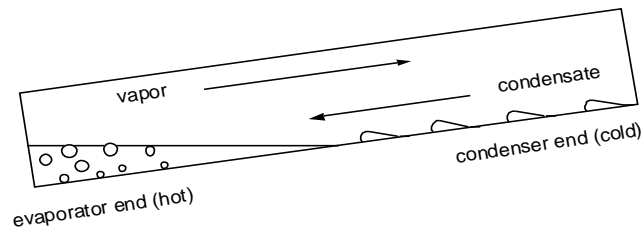


Figure 2. Heat pipe graphic [Poteat, et al. 2015]. The evaporator end is immersed in the thermal storage tank or is surrounded by room air, and the condenser end is attached to the radiator.

### 2.2.2. Network Parameters

Table 2 provides a description of the conductances and nodal temperatures shown in the thermal networks in Figure 3. The thermal network was constructed from previous work on a thermal heat pipe system for space heating [Susheela & Sharp 2001, Albanese,

*et al.* 2012 Robinson, *et al.* 2013a, Robinson & Sharp 2014] with additional features such as condensation and a windscreen node for the cooling system.

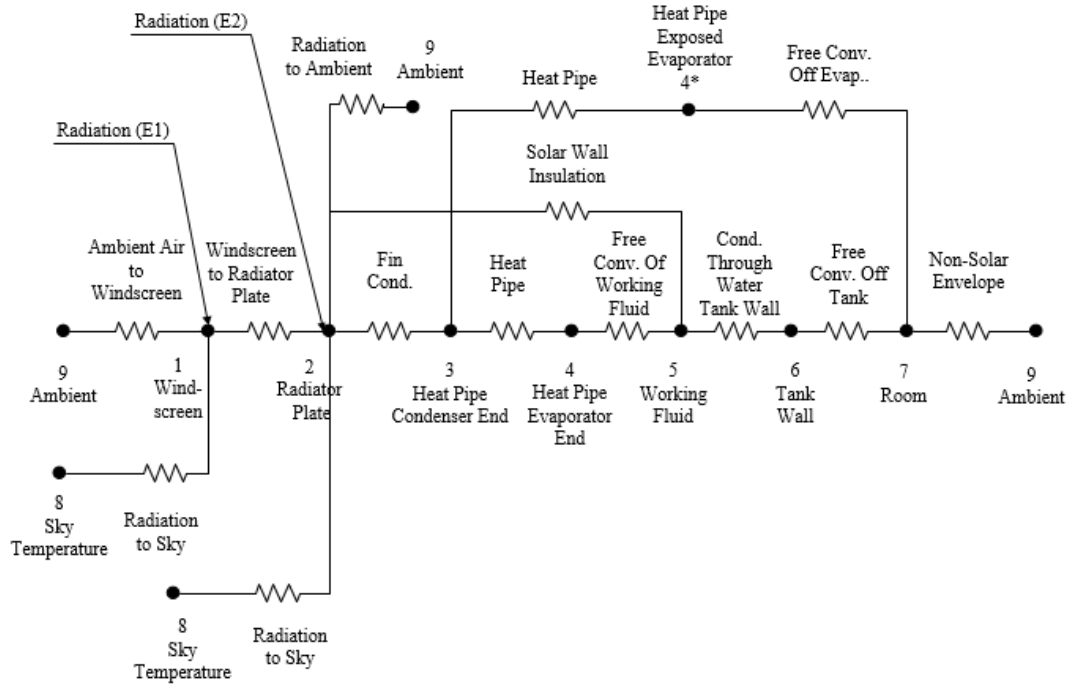


Figure 3. Thermal network for passive sky radiator system with covers.

Table 1. Description of baseline values for sky radiator system.

Sky radiator system parameters	Value
Cover thickness	50E-6 (m)
Cover long wavelength emittance	0.15
Cover long wavelength extinction coefficient	1.0E-5 (m <sup>-1</sup> )
Cover long wavelength transmittance	0.72
Radiator plate material	Copper
Radiator plate selective surface	White Zinc Oxide
Radiator plate long wavelength emittance	0.929
Radiator plate thickness	3.18E-3 (m)
Radiator plate insulation thickness	2.5E-2 (m)
Radiator insulation conductance	2.5E-2 (W/mK)
Radiator plate height	2.10 (m)
Radiator plate width	1.25 (m)
Heat pipe two phase heat transfer fluid	R-124

Heat pipe number	5 (4 to Tank and 1 to Room)
Heat pipe spacing	0.359 (m)
Heat pipe material	Copper
Water tank number	1
Water tank height	1.42 (m)
Water tank length	1.10 (m)
Water tank width	0.203 (m)
Water tank wall thickness	3.18E-3 (m)
Water tank wall conductivity	0.5 (W/mK)
Ground reflectance	0.3
Load to radiator area ratio	10 (W/m <sup>2</sup> K)

Sky temperature was modeled by [Berdahl, *et al.* 1984]

$$T_{sky} = T_o \left[ 0.711 + 0.005 \sigma_{dp,o} + 0.0003 T_{dp,o}^2 + 0.013 \cos(15t) \right]^{1/4} \quad (1)$$

where  $T_{sky}$  and  $T_o$  are the sky and outdoor dry-bulb temperature in degrees Kelvin,  $T_{dp,o}$  is the outdoor dew-point temperature in degrees Celsius, and  $t$  is the number of hours from midnight.

For the conductance values described in Table 2 that are functions of temperature, an iterative process was used to match the conductance values to the nodal temperatures solved by energy balance equations [Albanese, *et al.* 2012] given by

$$mc_p \frac{T_i(t + \Delta t) - T_i(t)}{\Delta t} = \sum_j k_{ij} (T_j - T_i) + E_i \quad (2)$$

where the heat transfer between the nodes is solved by using  $k_{ij}$ , the conductance between the two nodes, and multiplying by the temperature difference between the nodes. Solar fluxes  $E_i$  occur only to the cover and radiator plate, and thermal capacity  $mc_p$  was included only for the thermal storage tank. The network conductances were set or calculated as described in Table 2, with parameters as described in Table 3:

Table 2. Description and baseline values of nodal temperatures and conductances.

Parameter Description	Variable
Windscreen temperature <sup>T</sup>	$T_1$
Radiator plate temperature <sup>T</sup>	$T_2$
Heat pipe condenser end temperature <sup>T</sup>	$T_3$
Heat pipe evaporator end temperature <sup>T</sup>	$T_4$
Exposed heat pipe evaporator end temperature <sup>T</sup>	$T_{4*}$
Tank water temperature <sup>T</sup>	$T_5$
Tank wall temperature <sup>T</sup>	$T_6$
Room temperature <sup>T</sup>	$T_7$
Sky temperature <sup>T</sup>	$T_8$
Ambient temperature <sup>T</sup>	$T_9$
Solar flux to the windscreen <sup>E+</sup>	$E_1$
Solar flux to the radiator plate <sup>E+</sup>	$E_2$
Natural convection and radiation from plate to cover <sup>H</sup>	$k_{12}$
Conduction from plate to condenser <sup>H</sup>	$k_{23}$
Two phase heat transfer from immersed evaporator to condenser <sup>H</sup>	$k_{34}$
Two phase heat transfer from exposed evaporator to condenser <sup>H</sup>	$k_{34*}$
Natural convection from evaporator to water <sup>H</sup>	$k_{45}$
Natural convection from evaporator to room <sup>H</sup>	$k_{4*7}$
Conduction through tank wall <sup>H</sup>	$k_{56}$
Natural convection and radiation <sup>H</sup>	$k_{67}$
Overall heat loss from room to ambient (LRR) <sup>H</sup>	$k_{79}$
Wind convection and radiation from cover to ambient <sup>H+</sup>	$k_{91}$
Wind convection and radiation from radiator plate to ambient <sup>H+</sup>	$k_{92}$
Radiation from windscreen to sky <sup>H+</sup>	$k_{81}$
Radiation from radiator plate to sky <sup>H+</sup>	$k_{82}$

T- Indicates units of degrees Kelvin

E-Indicates units of W/m<sup>2</sup>

H- Indicates units of W/m<sup>2</sup>-K

+ - Indicates condensation is included

Table 3. Description of parameters used to calculate conductance in thermal network.

Variable	Description	Constant
$A_{WS}$	Surface area of windscreen	2.62 (m <sup>2</sup> )
$A_{Rad}$	Surface area of radiator	2.62 (m <sup>2</sup> )
$A_{HP}$	Surface area of heat pipe	5.18E-4 (m <sup>2</sup> )
$A_{Insul}$	Surface area of insulation	2.62 (m <sup>2</sup> )
$A_{Tank}$	Surface area of tank	4.17 (m <sup>2</sup> )
$A_{EVAP}$	Surface area of evaporator	1.04E-1 (m <sup>2</sup> )
$A_i$	Anisotropy index	--
$\alpha$	Thermal diffusivity	(m <sup>2</sup> /s)
$\alpha_{building}$	Terrain parameter (class III)	8.50 E-1

$\alpha_n$	Normal absorptivity (radiator)	1.80 E-1
$\alpha_b$	Beam absorptivity (radiator)	--
$\alpha_{b_{Cover}}$	Beam absorptivity (cover)	--
$\alpha_d$	Diffuse absorptivity (radiator)	--
$\alpha_{d_{Cover}}$	Diffuse absorptivity (cover)	--
$\alpha_g$	Ground absorptivity (radiator)	--
$\alpha_{g_{Cover}}$	Ground absorptivity (cover)	--
$\beta$	Radiator orientation	0°
$\beta'$	Volumetric coefficient of expansion	(1/K)
$e_{ws}$	Windscreen emissivity (long wave)	1.50 E-1
$e_{Rad}$	Radiator emissivity (long wave)	9.29 E-1
$e_{Tank}$	Tank emissivity	9.30 E-1
$f$	Correction factor	--
$\gamma_{building}$	Terrain parameter (class III)	2.00 E-1
$g$	Gravitational constant	9.81 (m/s <sup>2</sup> )
$H_{building}$	Modeled building height	3 (m)
$H_{tower}$	Weather tower height	10 (m)
$h_w$	Wind heat transfer coefficient [Sherman & Modera 1986]	--
$I$	Total radiation on horizontal surface (hourly)	TMY3 Data
$I_b$	Isotropic beam radiation (hourly)	--
$I_d$	Isotropic diffuse radiation (hourly)	TMY3 Data
$k_{air}$	Conductivity of air	--
$k_{HP}$	Conductivity of heat pipe material	401 (W/mK)
$k_{Insul}$	Conductivity of insulation material	2.5E-2 (W/mK)
$k_{Rad}$	Conductivity of radiator material	401 (W/mK)
$k_{Tank}$	Conductivity of tank	5E-1 (W/mK)
$k_{water}$	Conductivity of thermal fluid (water)	5.8 E-1
$K$	Extinction coefficient of polyethylene for solar wavelengths	1.0E-5 (m <sup>-1</sup> )
$L$	Thickness of windscreen	50 E-6(m)
$L_{HP}$	Length of adiabatic section	2.54E-2 (m)
$L_{Insul}$	Thickness of insulation	0.7 (m)
$L_{Rad}$	Thickness of radiator	3.18E-3 (m)
$L_{Tank}$	Thickness of tank	3.18E-3 (m)
$L_{cond}$	Thickness of condensation	1.2E-4 (m)
$n_1$	Refractive index (air)	1.0
$n_2$	Refractive index (polyethylene)	1.54
$n_3$	Refractive index (water)	1.33
$N_{fins}$	Number of fins	5
$N_{HP}$	Number of heat pipes	5

$N_{HPR}$	Number of heat pipes exposed to room	1
$N_{HPW}$	Number of heat pipes in thermal fluid	4
$N_{Tank}$	Number of tanks	1
$Nu_{air}$	Calculated Nusselt number of air	--
$Nu$	Calculated Nusselt number	--
$OD_{HP}$	Outside diameter of heat pipe	2.86E-2 (m)
$\rho_g$	Ground reflectance	0.3
$Ra_{air}$	Rayleigh number of air	--
$R_b$	Beam radiation Ratio	--
$R_{cond}$	Resistance of condenser end	8.58E-5 (K/W)
$R_{evap}$	Resistance of evaporator end	9.13E-5 (K/W)
$\sigma$	Stefan Boltzmann constant	5.67E-8 (W/m <sup>2</sup> K <sup>4</sup> )
$\tau_b$	Beam transmissivity	--
$\tau_d$	Diffuse transmissivity	--
$\tau_g$	Ground transmissivity	--
$\tau_{WS}$	Windscreen long wave transmissivity	0.72
$\tau_w$	Condensation long wave transmissivity	0.80
$\theta_1$	Angle of incidence in medium 1	--
$\theta_2$	Angle of refraction in medium 2	--
$\nu$	Kinematic viscosity	(m <sup>2</sup> /s)
$V_j$	Wind velocity (hourly)	--
$WSV$	Weather tower wind velocity	TMY3 Data
$W_{HP}$	Distance between heat pipe centers	3.59E-1 (m)

--Calculated parameter

Each conductance term was normalized by the radiator area. The conductance from ambient temperature to the outer windscreen including condensation is

$$k_{91} = \left( \left( \frac{1}{h_w} + \frac{L_{cond}}{k_{water}} \right)^{-1} + \tau_w e_{ws} \sigma (T_1^2 + T_9^2) (T_1 + T_9) \left( \frac{1 - \cos\beta}{2} \right) \right) \frac{A_{WS}}{A_{Rad}} \quad (3)$$

The thickness of the condensation,  $L_{cond}$ , was modeled after Pieters & Deltour [1997] as the maximum condensate film thickness on polyethylene. Without condensation, the  $k_{91}$  conductance term is calculated the same as Equation 1.3, without the water conductance

and the water transmissivity terms. The wind heat transfer coefficient [Burch & Luna, 1980] is calculated by first finding the wind speed velocity [Sherman & Modera, 1986].

The radiation from radiator to sky is

$$k_{92} = \left( \tau_w \tau_{ws} e_{Rad} \sigma (T_2^2 + T_9^2) (T_2 + T_9) \left( \frac{1 - \cos \beta}{2} \right) \right) \frac{A_{Rad}}{A_{Rad}}. \quad (4)$$

The far infrared radiation from the windscreen to the sky is calculated using,

$$k_{81} = \tau_w e_{ws} \sigma (T_1^2 + T_8^2) (T_1 + T_8) \left( \frac{1 + \cos \beta}{2} \right) \frac{A_{ws}}{A_{Rad}}. \quad (5)$$

Similarly, the far infrared radiation from sky to radiator is

$$k_{82} = \tau_w \tau_{ws} e_{Rad} \sigma (T_2^2 + T_8^2) (T_2 + T_8) \left( \frac{1 + \cos \beta}{2} \right) \frac{A_{Rad}}{A_{Rad}}. \quad (6)$$

Similar to  $k_{91}$ ,  $k_{92}$ ,  $k_{81}$  and  $k_{82}$  without condensation do not include the water terms shown.

The solar absorption of the windscreen was calculated from the model of Hay, Davies,

Klucher and Reindl, HDKR [Duffie & Beckman, 2013] where anisotropy index,

correction factor, and beam radiation ratio are calculated based on equations in Duffie &

Beckman [2013]. The solar absorption of the cover is

$$E_1 = (I_b + I_d A_i) R_b \alpha_{b_{Cover}} + (I_d (1 - A_i) \alpha_{d_{Cover}} \left( \frac{1 + \cos(\beta)}{2} \right) \left( 1 + f \sin^3 \left( \frac{\beta}{2} \right) \right) + I \rho_g \alpha_{g_{Cover}} \left( \frac{1 - \cos(\beta)}{2} \right). \quad (7)$$

To calculate the beam absorptivity and transmittance, the beam transmittance was calculated using derived expressions from Fresnel [Duffie & Beckman, 2013] for the reflection of un-polarized radiation passing from medium 1 with refractive index  $n_i$  to

medium 2 with refractive index  $n_2$ . When condensation is not present, medium 1 is air, and medium 2 is the cover. When condensation occurs, medium 1 is water.

Beam absorptivity for the cover and radiator was derived from Duffie & Beckman Equations 5.3.5 & 4.11.1 respectively [2013]. Diffuse and ground transmittance and absorption of diffuse and ground-reflected radiation were calculated using equations from Brandemuehl and Beckman [1980]. The angle of refraction is found using Snell's law. For the solar absorption by the radiator, a transmissivity term is added to represent the fraction of radiation passing through the cover

$$E_2 = (I_b + I_d A_i) R_b * 1.01 \tau_b \alpha_b + (I_d (1 - A_i) * 1.01 \tau_d \alpha_d \left( \frac{1 + \cos(\beta)}{2} \right) \left( 1 + f \sin^3 \left( \frac{\beta}{2} \right) \right) + I \rho_g * 1.01 \tau_g \alpha_g \left( \frac{1 - \cos(\beta)}{2} \right). \quad (8)$$

The conductance between the windscreen and the radiator includes both radiation and convection terms

$$k_{12} = \frac{k_{air} Nu_{air}}{L} \left( \frac{A_{WS}}{A_{Rad}} \right) + \left( \frac{1}{\frac{1}{e_{Rad}} + \frac{1}{e_{WS}} - 1} \right) \sigma (T_1^2 + T_2^2) (T_1 + T_2) \left( \frac{A_{WS}}{A_{Rad}} \right), \quad (9)$$

where the Nusselt number is a function of Rayleigh number for tilt angles found in experiments by Hollands et al. (1976) The Rayleigh number is calculated as

$$Ra = \frac{g \beta' \Delta T L^3}{\nu \alpha} \quad (10)$$

An equation developed by Susheela & Sharp [2001] is used for the conductance between the radiator plate and the condenser end of the heat pipe

$$k_{23} = \left( \frac{1}{\frac{1}{3k_{Rad}L_{Rad}} \left( \frac{W_{HP} - OD_{HP}}{2} \right)^2} \right) N_{fins} \left( \frac{A_{HP}}{A_{Rad}} \right). \quad (11)$$

The conductance of the heat pipe from condenser to evaporator end in the thermal storage fluid is [Susheela & Sharp 2001]

$$k_{34} = 0.04 \left( N_{HP,room} \left( \frac{k_{HP}}{L_{HP}} \right) \left( \frac{A_{HP}}{A_{Rad}} \right) + N_{HP,tank} \left( \frac{1}{R_{evap} + R_{cond}} \right) \frac{1}{A_{rad}} + \frac{k_{Insul}}{L_{Insul}} \left( \frac{A_{Insul}}{A_{Rad}} \right) \right). \quad (12)$$

The conductance of the heat pipe from condenser to evaporator end exposed to room air is [Susheela & Sharp 2001]

$$k_{34*} = 0.25 \left( N_{HP} \left( \frac{k_{HP}}{L_{HP}} \right) \left( \frac{A_{AHP}}{A_{Rad}} \right) + N_{HP} \left( \frac{1}{R_{evap} + R_{cond}} \right) \frac{1}{A_{rad}} + \frac{k_{Insul}}{L_{Insul}} \left( \frac{A_{Insul}}{A_{Rad}} \right) \right). \quad (13)$$

The convective conductance between the heat pipe evaporator end and thermal storage fluid is

$$k_{45} = \frac{N_{HP,W} k_{Water} Nu}{OD_{HP}} \left( \frac{A_{Evap}}{A_{Rad}} \right), \quad (14)$$

where the Nusselt number is calculated using equation from Churchill and Chu [1975] for the fluid in the tank and the Rayleigh number is calculated using Equation 14. For the heat pipes exposed to the room the convective conductance is

$$k_{47*} = \frac{N_{HP,R} k_{air} Nu}{OD_{HP}} \left( \frac{A_{Evap}}{A_{Rad}} \right), \quad (15)$$

where the Nusselt was calculated same as fluid in the tank and Rayleigh number was calculated using Equation 14. The conduction through the tank wall was accounted for using

$$k_{56} = \frac{k_{Tank}}{L_{Tank}} \left( \frac{A_{Tank}}{A_{Rad}} \right). \quad (16)$$

The conductance due to convection and radiation from the tank wall to the room is

$$k_{67} = \frac{N_{Tank} k_{air} Nu}{L_{Tank}^*} \left( \frac{A_{Tank}}{A_{Rad}} \right) + e_{Tank} \sigma (T_6 + T_7) (T_6^2 + T_7^2) \left( \frac{A_{Tank}}{A_{Rad}} \right), \quad (17)$$

where the Nusselt numbers for the top and bottom of the tank were calculated the same as Susheela & Sharp [2001] and for the vertical sides were calculated per Bergman et al. [2011], with Rayleigh numbers calculated using Equation 14. This study assumed film-wise condensation, and used a model with either a totally wet surface or a totally dry surface with the model neglecting the latent heat of condensation and evaporation (the cover temperature was also limited to the dew point temperature as a simplified approximation of the effect of latent heat). The simplified model neglected humidity and internal loads inside the room.

### 2.2.3. Parameters Evaluated

The effects on thermal performance of radiator orientation, thermal storage capacity and LRR were tested in the Louisville, KY climate.

*Orientation:* The tilts of the sky radiator evaluated were 0°, 20°, 23°(Latitude - 15°), 30°, 38°(Latitude), 40° and 53°(Latitude + 15°). The baseline orientation was 0°.

*Storage capacity:* Thermal capacity was decreased for multiple trials. The baseline capacity, 100%, was 0.32 m<sup>3</sup> of water per m<sup>2</sup> of radiator area. Capacity was decreased by 10%, 20%, 30%, 40%, 50%, 60% and 90%.

*LRR*: The cooling load to radiator area ratio was evaluated at 5, 10, 20, 25 and 50 W/m<sup>2</sup>K. The baseline LRR was 10 W/m<sup>2</sup>K. An LRR of 5 W/m<sup>2</sup>K represents a well-insulated envelope or large radiator, and a LRR of 50 W/m<sup>2</sup>K models a space with a poorly-insulated envelope or small radiator.

#### 2.2.4. Sky Fraction and Radiator Efficiency

The rate of heat gain from outdoors to the room is given by

$$\dot{q}_{CL,i} = (k_{79}(T_9 - T_7))^+ \quad (18)$$

where the superscript indicates only positive values, and the conductance and temperatures are indicated in Table 2. The index  $i$  signifies that this calculation is performed for each hour of the simulation.  $\dot{q}_{CL,i}$  represents the rate of cooling that must be supplied to maintain constant indoor temperature, thus the hourly cooling load is estimated as  $\dot{q}_{CL,i}$  times the hour time interval. Note that the cooling load includes loads when indoor temperature is below the indoor comfort temperature set point of 23.9°C. The portion of the load that was covered by the sky radiation system, from storage and from the exposed condenser, is

$$\dot{q}_{RAD,i} = (k_{67}(T_7 - T_6) + k_{4*7}(T_7 - T_{4*}))^+. \quad (19)$$

Auxiliary cooling is applied only when required to limit the indoor temperature  $T_7$  to no greater than 23.9°C, and is given by

$$\dot{q}_{AUX,i} = \dot{q}_{CL,i} - \dot{q}_{RAD,i} \quad (20)$$

with  $T_7 = 23.9^\circ\text{C}$ . The cooling load and auxiliary cooling were summed over the entire year. The fraction of the total annual load served by the sky radiator is defined as the sky fraction,

$$f_{sky} = 1 - \frac{\sum_{i=1}^{8760} q_{AUX,i}}{\sum_{i=1}^{8760} q_{CL,i}}, \quad (21)$$

where 8760 is the number of hours in the year. Hourly theoretical radiative heat transfer assuming the sky to be a perfect black body is

$$\dot{q}_{BB,i} = \sigma(T_2^4 - T_8^4), \quad (22)$$

where  $\sigma$  is the Stefan-Boltzman constant, and the temperatures are from Tables 4 and 5.

The radiator efficiency is then defined as

$$\eta = \frac{\sum_{i=1}^{8760} q_{RAD,i}}{\sum_{i=1}^{8760} q_{BB,i}} \quad (23)$$

### 2.3. RESULTS AND DISCUSSION

Annual sky fractions for the Louisville, KY climate with different radiator orientations are shown in Figure 4. As expected, larger sky fractions were associated with lower radiator tilt angles that provide a greater view factor to the sky. Tilting the surface toward the horizon causes the sky view factor to decrease. A one-cover horizontal radiator with condensation had an annual sky fraction of 0.855. A decrease to 0.852 was found for an increase in radiator slope to  $20^\circ$ , and a drop to 0.832 for  $53^\circ$  slope (latitude +

15°, a typical slope for solar heating). These drops were associated with increases in average radiator temperature by 0.73°C for 20° and 1.99°C for 53°.

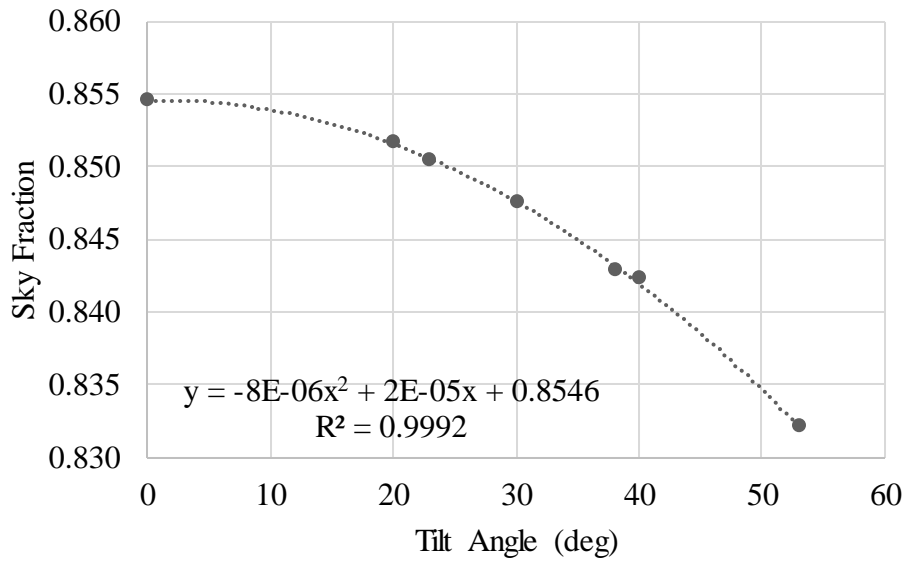
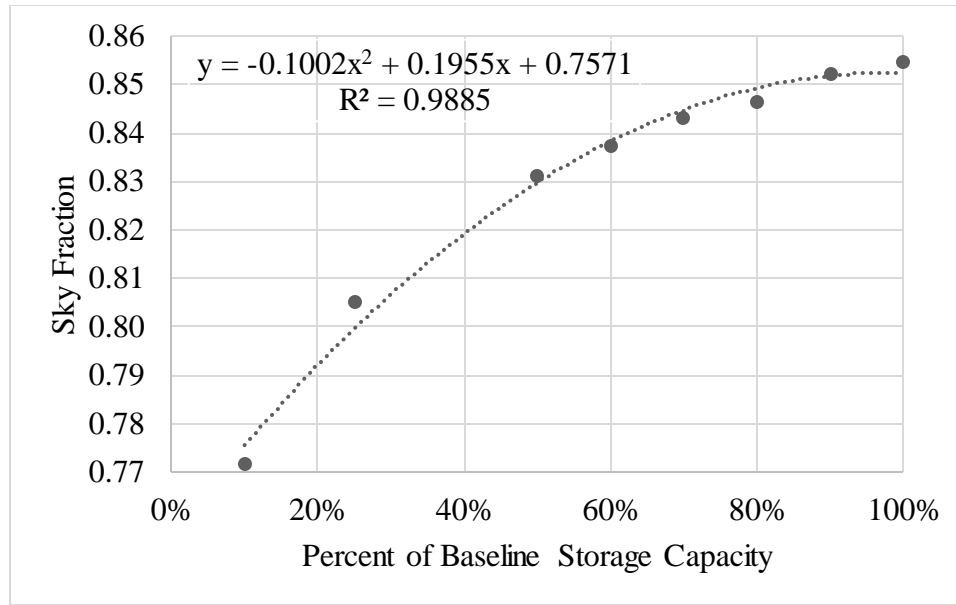


Figure 4. Annual sky fraction at varying tilt angles relative to horizontal.

The fraction of the load that can be served by the radiator for varying thermal storage capacity is shown in Figure 5. A 30% decrease in storage capacity caused a decrease in sky fraction to 0.843, while a 90% decrease in in storage capacity caused a decrease in sky fraction to 0.772, only a 10% decrease in sky fraction compared to the baseline.



*Figure 5. Annual sky fraction at varying thermal storage capacity.*

The load to radiator ratio LRR had a substantial impact on system performance. Sky fractions were 0.528 and 0.959 for LRR of 50 and 5, respectively (Figure 6). By decreasing the LRR to 5, almost the entire cooling load can be served by the sky radiator.

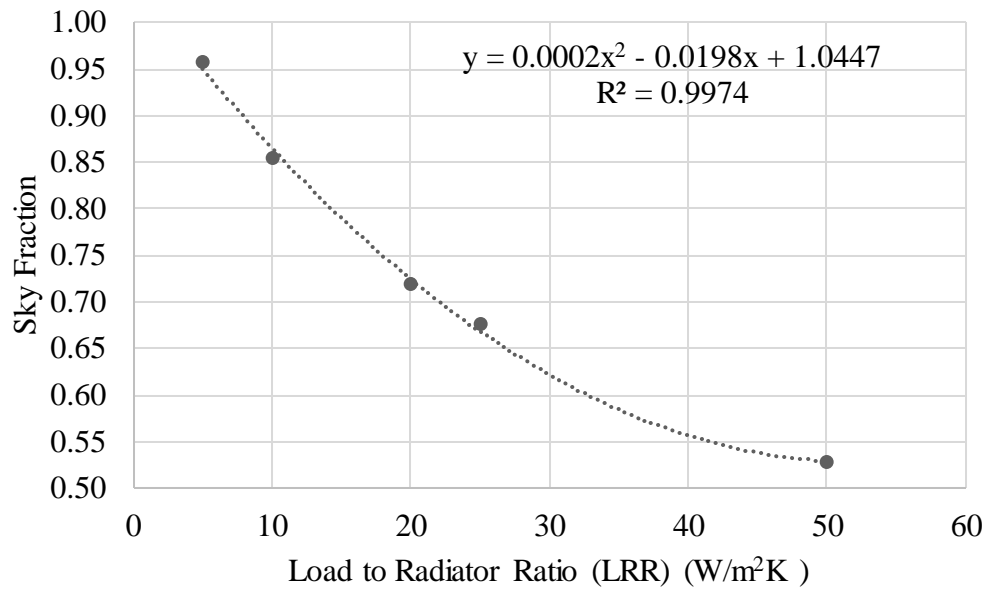
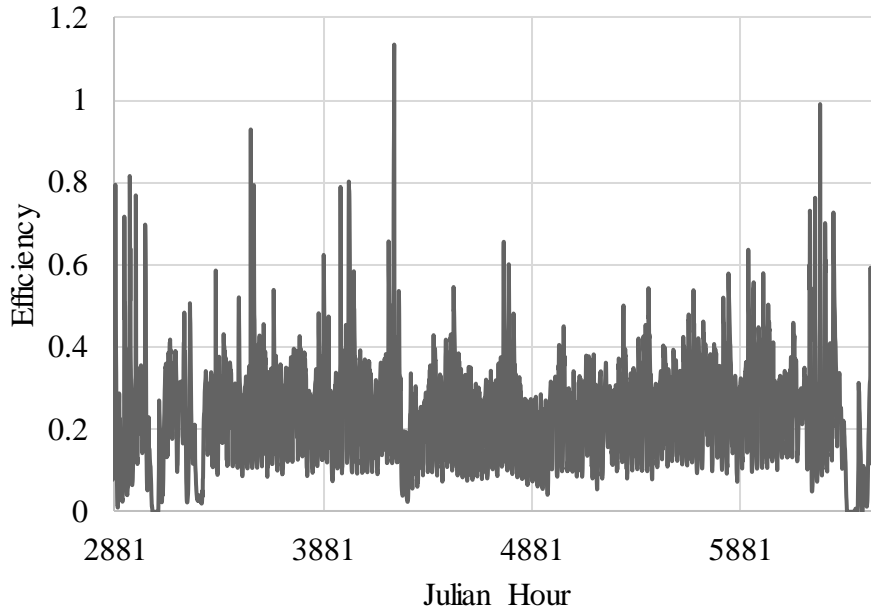


Figure 6. Annual sky fraction at varying load to radiator ratio LRR.

The hourly efficiency for the Louisville baseline configuration is shown in Figure 7. The average efficiency during the May through September cooling season was approximately 25%. Note that the efficiency can exceed 100% when ambient temperature is cool enough to augment radiation to the sky. The summer average (May-September) cooling power was 15.1 W/m<sup>2</sup>, while the maximum was 34 W/m<sup>2</sup>. These results are smaller than those of Joubert & Dobson [2017], who tested a small model of passive night-sky radiation cooling/heating system consisting of an unglazed radiator panel, a cold water storage tank, a hot water storage tank, a room and the interconnecting pipework. During the night, their system was able to reject energy at an average rate of 55 W/m<sup>2</sup>. Their larger losses may be attributed to their nighttime tank temperature being consistently greater than ambient temperature during the period of testing (8-13 April, autumn in Stellenbosch, South Africa), which would contribute to high radiator efficiency, as well as allowing losses from their uninsulated thermal storage tank and

pipng. In contrast, the current simulations in Louisville, KY, exhibited summer nighttime tank and radiator temperatures below ambient temperature (Figure 8).



*Figure 7. Hourly efficiency of baseline radiator (May-September only).*

Nodal temperatures for the hottest week of the TMY3 data are shown in Figure 8. The tank temperature tended to stay relatively constant while the windscreen and radiator most significantly tracked ambient temperature. When the sun was out, the radiator surpassed ambient temperature. In spite of the warm ambient temperature, the radiator was cooled to below storage temperature every night. Over this period, the average ambient and tank temperatures were 23 °C and 19°C, respectively. This decrease in tank temperature is similar to the lowest radiator outlet temperature that Goldstein et al. [2017] were able to achieve. Over three days of testing during October in Stanford, CA, their panels were able to cool water from 1 to 5 °C below the ambient air temperature, depending on flow rate, with water entering the radiator at near ambient temperature.

Again, this warmer radiator inlet temperature may have contributed to their larger cooling power, which was 20-40 W/m<sup>2</sup> at a low flow rate and 30-70 W/m<sup>2</sup> at a high flow rate. Neither short nor long-wave emittance of their radiator surface was reported, but short-wave emittance was small enough to allow cooling of up to nearly 40 W/m<sup>2</sup> at the higher flow rate during peak insolation.

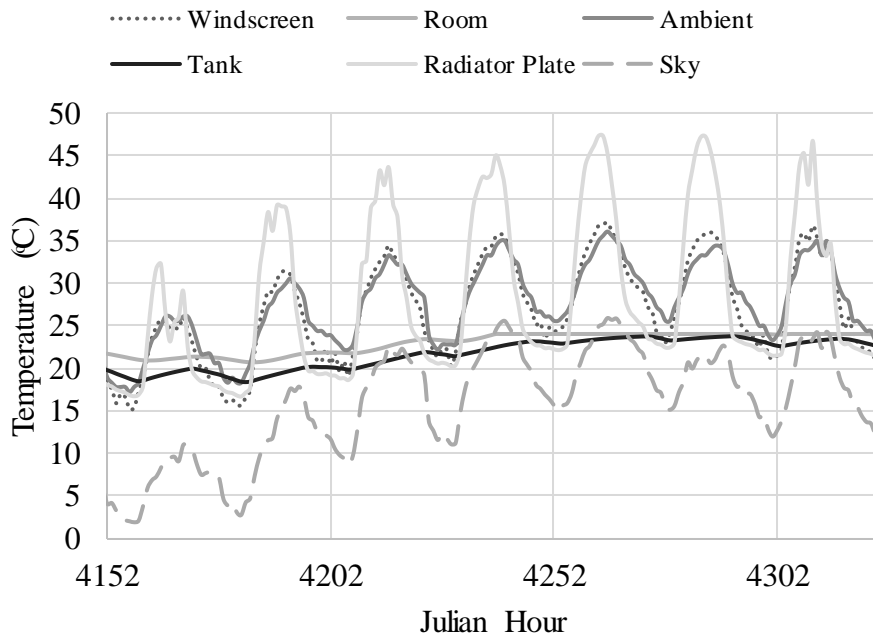


Figure 8. Nodal temperatures for the hottest week (June 23-29).

Nodal temperatures for a relatively clear day followed by a cloudy night, with nighttime highlighted in grey, are shown in Figure 9. Clouds tend to increase the sky temperature versus a clear sky, however ambient temperature has a stronger effect. The impact of humidity, which is the indicator of cloudiness in the Berdahl, *et al.* [1983] equation, can be seen in the lower sky temperature at the end of the first night relative to the end of the second night, when ambient temperature is similar, but humidity is greater. The efficiency of the sky radiator tends to follow the difference between windscreen and

ambient temperature, since this difference is a factor in unwanted heat gains to the radiator, which detract from its cooling capacity.

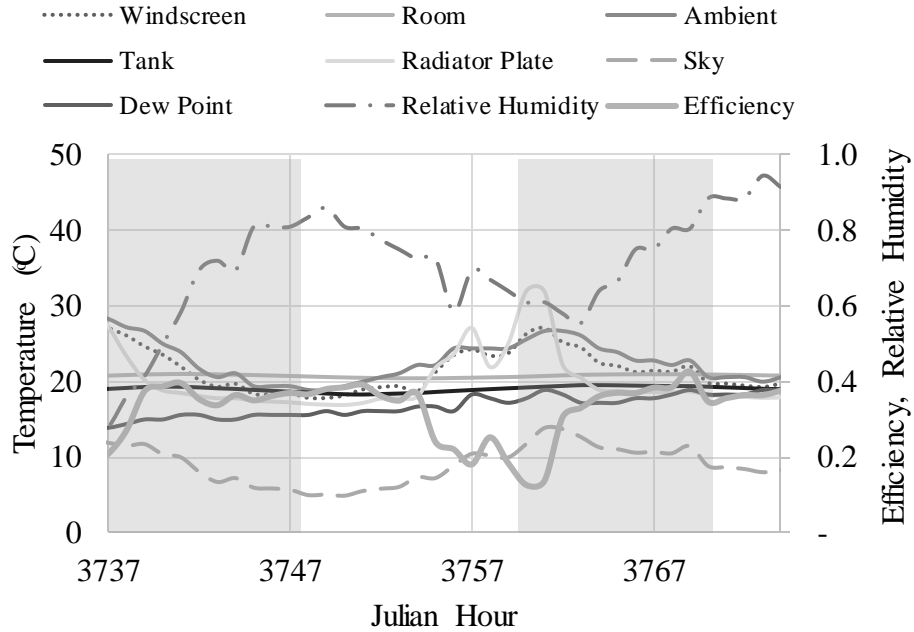


Figure 9. Nodal temperatures for the dates of June 5-7. Highlighted in grey is 5:00PM to 5:00AM representing nighttime.

Components of heat transfer to the cover and radiator plate are shown in Figures 10 and 11. In Figure 10, the solar flux absorbed by the cover is increased significantly due to the condensation, which occurs at 5:00AM and 6:00AM (Figure 10). Otherwise, the extinction coefficient of the cover for solar wavelengths is very low, thus the cover absorbs very little of the incident solar radiation. For most of the 24-hour period, the cover was cooler than ambient, thus it was heated by convection. However, from 9:00 am to 1:00 pm the ambient temperature was below the cover temperature and therefore cooling of the cover occurred during the daytime.

During the daytime, solar flux dominates the other components of heat transfer to the radiator (Figure 11), which is not as selective as that of Goldstein, et al. [2017]. Heat

transfer from the radiator to the sky and to the cover also increase during the day.

However, these increases do not represent capacity for useful cooling, but rather that the sun has elevated the radiator temperature. During nighttime, radiation to the sky dominates and allows for cooling. Heat transfer from the cover to the radiator (Figure 11) during nighttime is small and mostly positive compared to convection from ambient to the cover (Figure 10), suggesting that the cover is serving a useful purpose for these conditions. Conduction of heat through the wall to the radiator is small and is not visible on the graph. The model includes a small heat transfer in the reverse direction along the wall of the heat pipe when the condenser is hotter than the evaporator. These cooling losses provide a more realistic assessment of the performance of the system.  $k_{91}$  and  $k_{92}$  in Figures 10 and 11, respectively, represent radiative and convective heat transfer from ambient, but for the radiator slope of zero for this baseline case, no radiation occurs from ambient.

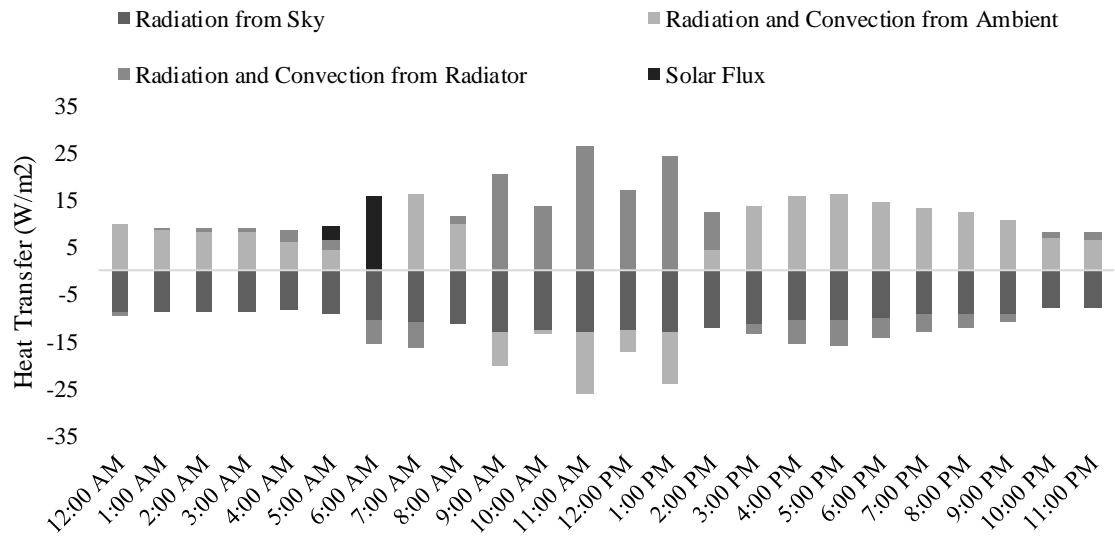


Figure 10. Components of heat transfer to the cover: Radiation from sky ( $k81$ ), radiation and convection from radiator ( $k12$ ), radiation and convection from ambient (including condensation when it occurs) ( $k91$ ) and solar flux ( $E1$ ) for a typical summer day, June 2nd for the baseline attributes. Condensation is present at 5:00AM and 6:00AM.

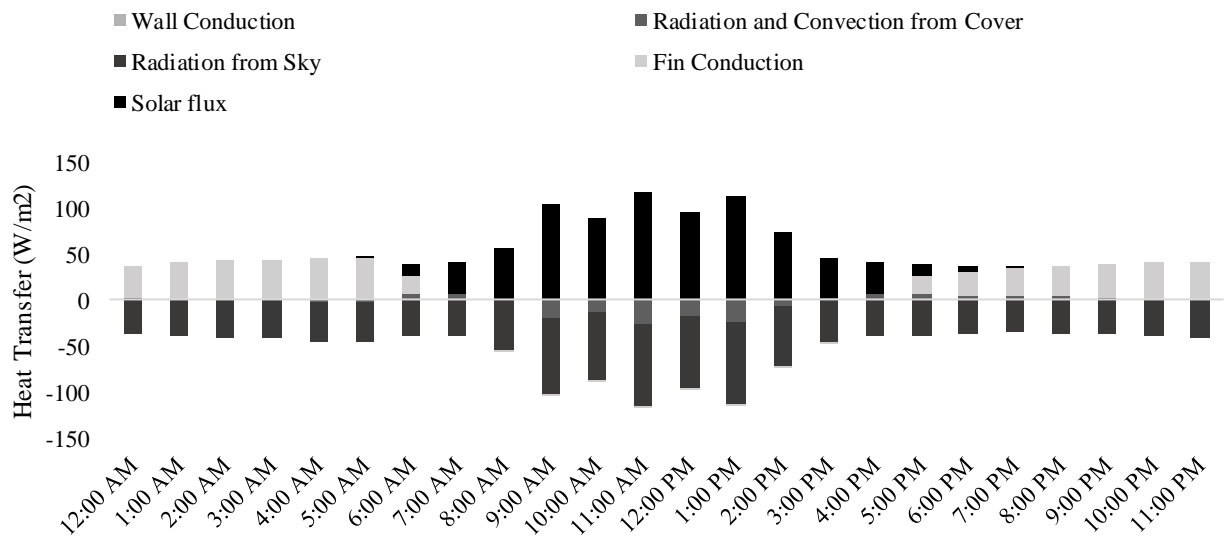


Figure 11. Components of heat transfer to the radiator: Radiation from sky ( $k82$ ), convection and radiation from cover ( $k12$ ), radiation from ambient (including condensation when it occurs) ( $k92$ ), fin conduction from the condenser end of the heat pipe ( $k23$ ), conduction through wall insulation from tank ( $k25$ ) and solar flux ( $E2$ ) for a

*typical summer day, June 2nd for the baseline attributes. Condensation is present at 5:00AM and 6:00AM.*

### **2.3.1. Limitations**

Limitations of this study include the narrow range of climate chosen. In particular, less humid climates and those with greater diurnal temperature swings may promote greater system performance. Additional results for more diverse climates will better exemplify all the zones in the United States. Also, an important limitation on the performance of a sky radiator system may be using a single cover system. Given the relatively low transmittance of thermal radiation for polyethylene (0.72 was used in this study) compared to low-wavelength transmittance for solar collector covers ( $> 0.90$ ), a system with no cover may provide greater cooling in climates with low nighttime temperatures. Additional covers should be modeled to verify if the addition of covers can decrease condensation and increase sky fraction. This will help to better understand the effects of condensation on system performance and how it varies with climate.

Simplifications of the model include lumping internal heat generation into the envelope loss coefficient. While this is a common technique for reducing computational effort and is appropriate where internal heat generation is small compared to the envelope loss, results may be influenced for buildings in which these terms are more similar in magnitude, such as in large commercial buildings. Thermal mass in the conditioned space was also not included and may be important in buildings with comparatively small envelope losses. Humidity control and associated latent cooling loads were not included and may be important particularly in humid climates.

Recently, radiators using innovative materials have achieved cooling during daytime (e.g., Goldstein, et al. [2017]). Because this capability may reduce the need for thermal storage, further modeling incorporating these radiator attributes with a complete building and sky radiator system should be considered.

## **2.4. CONCLUSIONS**

This study evaluated several design parameters in a passive sky radiator system, including orientation, thermal storage and LRR. In the Louisville climate, LRR and thermal storage capacity had strong effects on performance. These influences are as expected, in light of the well-documented importance of load to collector area ratio (LCR) and thermal storage capacity in passive and active solar heating systems. On the other hand, radiator slope had a surprisingly small impact in Louisville. This effect may be different in other climates. An efficiency of 25% for the sky radiator in the summer months for the Louisville climate gave promising performance results. This efficiency is less than that for typical solar collectors, which may be attributed to the greater potential for radiative exchange with the sun (temperature  $\sim 5800$  K) compared to the sky ( $\sim 0$  K for outer space, but  $\sim 280$  K for effective terrestrial sky temperature). Though relative humidity is modeled to increase sky temperature, ambient temperature and solar flux had stronger effects.

These results provide some initial insight into the significance of sky radiator design parameters and confirm the potential for a heat pipe augmented system used for passive cooling of buildings by radiation to the sky.

CHAPTER III  
THE EFFECTS OF MULTIPLE COVERS WITH CONDENSATION AND OPTICAL  
DEGRADATION OF A POLYETHYLENE WINDSCREEN ON THE  
PERFORMANCE OF A SKY COOLING SYSTEM

### 3.1. INTRODUCTION

Global climate change has already had measurable and observable effects on the environment. It is widely recognized that these changes will continue to rise in large part due to the greenhouse gases produced from fossil fuel consumption. Therefore, the need to reduce carbon emissions is imperative. With buildings accounting for a large fraction of energy use in the US and around the world, renewable space conditioning can have an impact in reducing fossil fuel consumption.

The potential use of sky temperature as a form of passive cooling has been recognized for decades [Yellot 1973, Robinson, *et al.* 2013]. Parsons & Sharp [2016] reviewed a number of such systems for space cooling, while Springer & Sharp [2015] showed that sky radiation can also be used for humidity control. A recent study found that a very selective radiator surface consisting of multiple layers of HfO<sub>2</sub> and SiO<sub>2</sub> was able to achieve a 4°C to 5°C drop from ambient temperature even when the sun was out [Raman, *et al.* 2014]. Goldstein *et al.* [2017] demonstrated a similar drop between 3°C to 5°C below dry bulb air temperature using fluid cooling panels to radiate to the sky. Simulations predicted 18 to 50% daily electricity savings by connecting the sky radiator to the condenser of a vapor-compression cooling system in Las Vegas, NV. Others have

demonstrated day and night cooling with material of randomized, glass polymer hybrid metamaterial [Zhai *et al.*, 2017]. Chotivisarut, *et al.* [2012], simulated and modeled an active system that uses a set of thermosiphon heat pipes to radiate heat to the night sky from a storage tank, cooling the water in the storage tank, then pumping the cooled water from the insulated tank to a set of cooling coils located in a small room, showing potential for cooling load reduction in certain climate zones. While an increase in sky radiation studies have shown the potential of sky radiation to achieve a temperature below ambient, few have been performed to quantify annual energy savings in space cooling applications. Still, fewer, have compared savings across climates, and none of which we are aware have studied the effect of condensation or cover aging on annual energy savings. This paper addresses these niches with simulations of a passive heat-pipe-based sky radiation system with conventional materials for a residential space cooling application with three different cover configurations across a range of climates

### **3.1.1. Polyethylene as Windscreen Material**

While a bare radiator surface can, in principle, work well in the absence of wind or where nighttime temperatures are low, such conditions are rare in many climates. Even a slight breeze causes forced convection on the surface, with a heat transfer coefficient much higher than for natural convection. Under these conditions, heat gain from outdoor air (in warm climates) offsets the heat radiated to the night sky [Johnson 1975]. Thus, cooling potential can be significantly increased with the presence of a windscreen. On the other hand, in climates with large diurnal temperature swings (for instance, the Rocky Mountain west), convection from cool nighttime air can augment cooling of the radiator

surface. Therefore, it is to be expected that the benefit of a windscreen may vary with climatic location. Two additional effects on the performance of a sky radiator this study will take into account are the presence of condensation on the cover and the decrease in the transmittance properties of polyethylene over time. Condensation represents another climatic factor, since it depends on outdoor temperature and humidity.

The windscreen can be any transparent material capable of withstanding environmental loads and exhibiting high transmissivity properties [Johnson 1975]. A windscreen of polyethylene, which is mostly transparent to long-wave radiation, has been widely used and can increase net cooling by reducing convective heat gain to the radiator plate. Polyethylene as a cover material is low cost, light weight and has desirable transmittance properties [Xing, *et al.* 2016] for the sky radiator. Plastics possess the advantage of being able to withstand hail and other impacts since they are flexible [Yellott 1973]. A drawback of polyethylene is its susceptibility to degradation and mechanical failure from harsh conditions caused by high temperature, solar radiation and wind [Bosi, *et al.* 2014, Xing, *et al.* 2016].

A polyethylene cover allows most long wave radiation to pass. Radiation transmission through the cover is affected by several factors, including the type of material, dirt and dust deposition, and discoloration caused by aging. The long wave transmissivity of a 50  $\mu\text{m}$  polyethylene cover for infrared radiation deteriorates from 0.8 for dry polyethylene to almost zero for polyethylene wetted by condensation [Pieters & Deltour 1997]. It was shown by Pieters & Deltour [1997] that in a temperate maritime climate, heating requirements were under-estimated by about 15% for glass greenhouses and over-estimated by about 20% for a polyethylene-covered greenhouse when

condensation was not modeled. Assuming uniformly diffuse radiation, condensate was found to lower the hemispherical transmittance by 8% for single and double glass, 5% for low-emissivity glass, 11% for low-density polyethylene and 13% for anti-dust polyethylene [Pollet & Pieters 2000]. There has been much research on transmittance of cladding materials covered with condensate, mainly focused on common non-treated plastic films or sheets. Using an outdoor test stand to measure the effect of condensate on the transmittance of low density polyethylene film for diffuse radiation, it was reported that transmittance was reduced by 8% [Geoola, *et al.* 1994]. Balemans [1990] found condensation reduced transmissivity through polyethylene at normal incidence by about 17%. Using an indoor test stand, transmittance was found to decrease between 9 and 19% on polyethylene due to condensation [Scultz & Bartnig 1996]. Although many studies describe the influence condensation has on transmissivity, few studies with sky radiation include this factor.

In addition to condensation, aging of the polyethylene also leads to substantial degradation in its transmissivity of long-wave radiation [Hamza, *et al.* 1998]. It was found that aging the polyethylene for 100 days caused a 33.3% decrease in performance through the decrease of heat dissipation and increase of radiation gain by a night sky radiator system. Based on these previous works, the effects of condensation and aging were included in the simulations of a heat pipe sky radiator system, due to their effect on the radiative properties of polyethylene and its prevalent use as a windscreen cover.

### **3.1.2. Objective**

In an initial study by Parsons & Sharp [2016], it was found that condensation had an effect on radiative properties of the sky radiator with one cover in the Louisville, KY climate. This study motivated the current one that includes transmittance of the condensate through zero, one and two cover(s). The objective of this new study was to evaluate the impacts of condensation on the overall performance of passive systems with different numbers of polyethylene covers in a range of climates. One city in each of the 11 ASHRAE climate zones across the United States was simulated. For this set of simulations, the cover was simulated using conventional 50  $\mu\text{m}$  polyethylene with long-wave transmittance of 0.72 to simulate a readily available cover design. Windscreen degradation was studied in Louisville, KY, Miami, FL and New Orleans, LA. To account for degradation of the polyethylene long-wavelength transmittance in the model, a linear decrease in transmittance over time was used [Hamza, *et al.* 1998]. Additionally, annual cover replacement was modeled. The replacement dates modeled were May 1<sup>st</sup>, June 1<sup>st</sup>, July 1<sup>st</sup> and Aug 1<sup>st</sup>. Condensation was included for each simulation.

### **3.2. METHODS**

A computer simulation program was created to simultaneously solve nodal temperatures as functions of time. The design of the system was modeled after a previous design of solar heat pipes used for heating only [Albenese *et al.* 2012, Robinson *et al.* 2015]. The computer model developed simulated the following nodes: thin polyethylene cover(s), radiator plate with a selective surface (white ZnO paint), heat pipe condenser end, heat pipe evaporator end, thermal storage fluid, fluid container wall, and room.

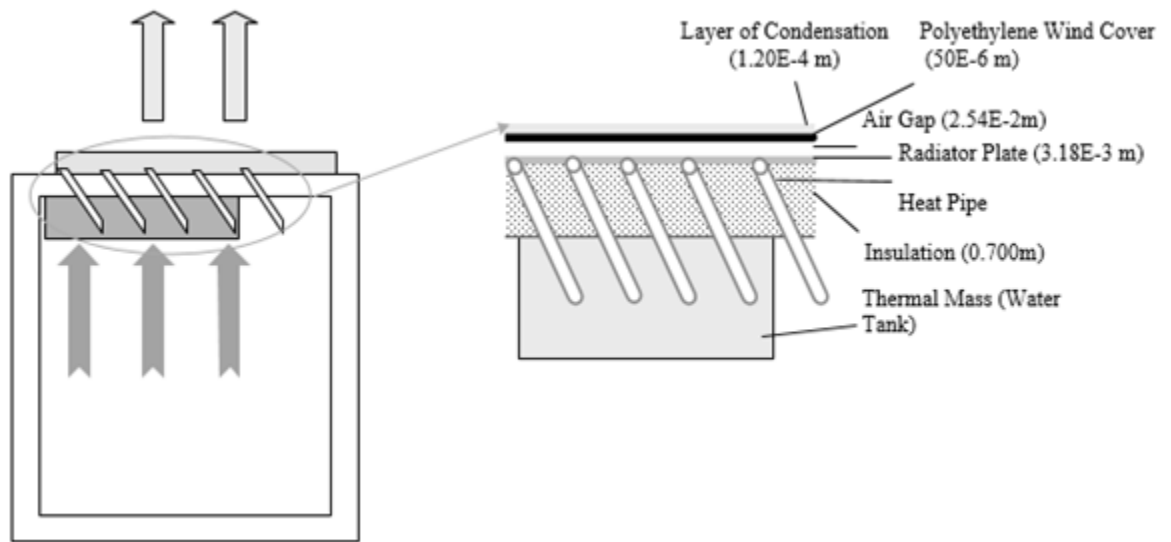


Figure 12. Depiction of one-windscreen sky radiator system with uniform condensation layer

The three node diagrams shown in Figures 13, 14 and 15 describe the thermal networks for a system with zero, one and two covers, respectively. Typical Meteorological Year (TMY3) weather data was used in the simulations, and auxiliary cooling was applied as needed to limit room temperature to a maximum of 24°C. The key heat transfer conductances among nodes were the load to radiator ratio (LRR), which characterized the ratio of building heat gain to radiator size, one way heat transfer through the heat pipe, polyethylene cover solar flux, sky radiation and wind convection, and radiator plate solar flux, sky radiation, and convective and radiative transfer. Conductances and nodal temperatures used in the thermal networks are listed in Table 4. Variables and parameter values used to solve for conductances are provided in Table 5.

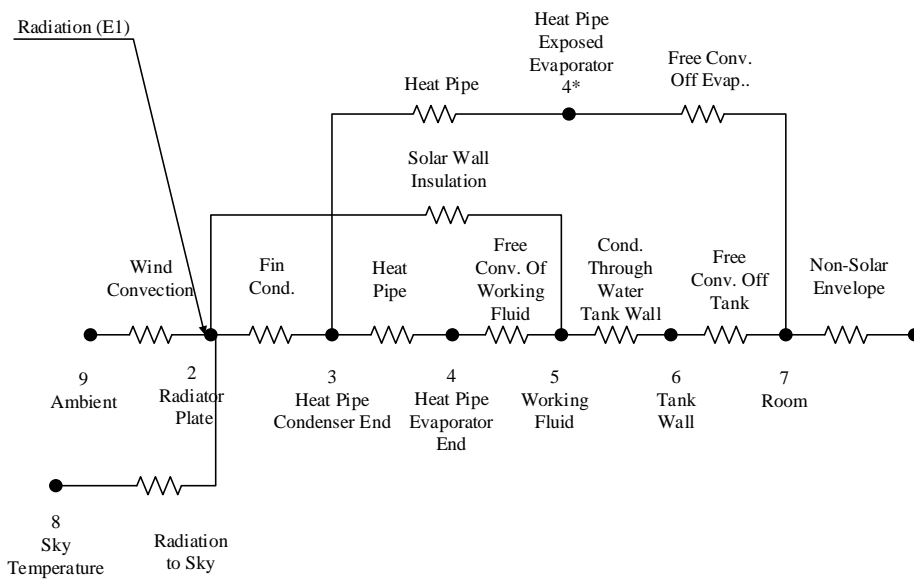


Figure 13. Node diagram for system with no windscreen.

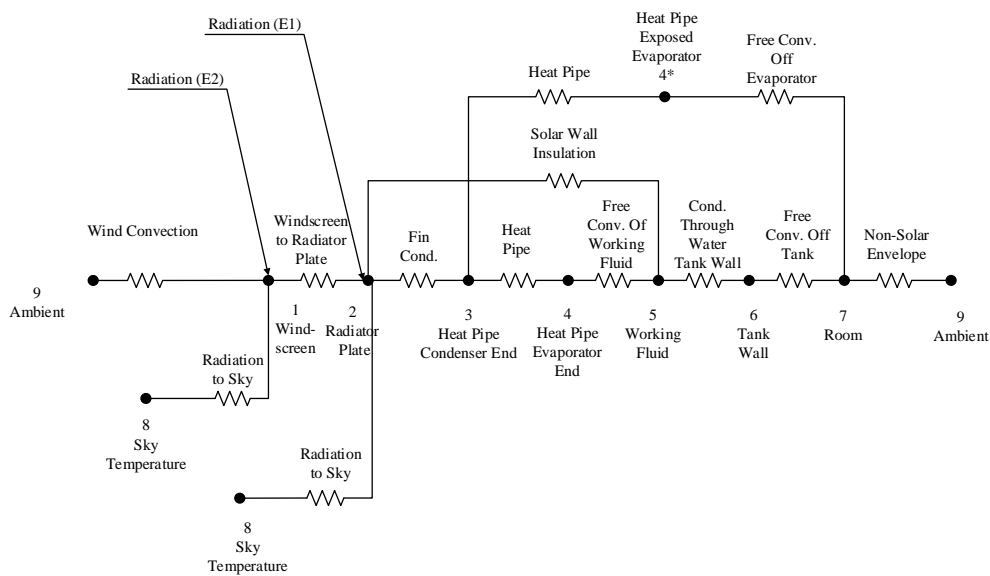


Figure 14. Node diagram for system with one windscreen.

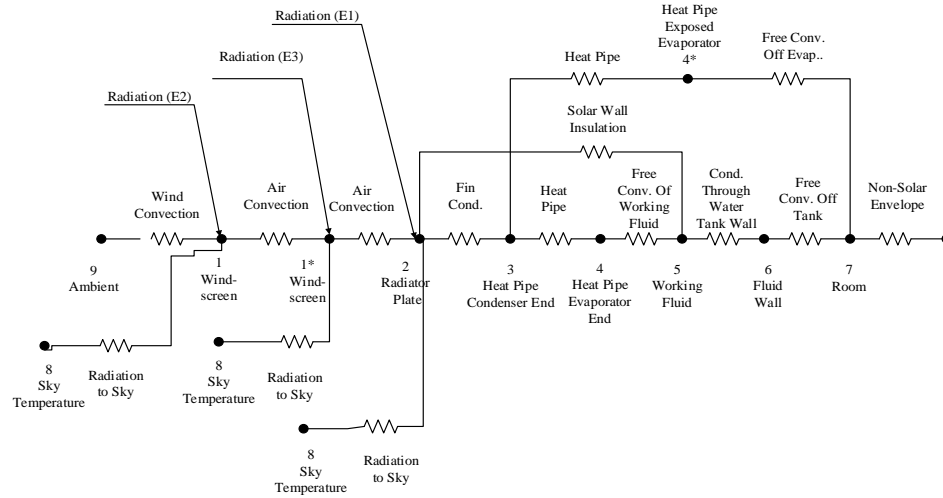


Figure 15. Node diagram for system with two windscreens.

Table 4. Description and baseline values of nodal temperatures and conductance.

Parameter Description	Variable
Windscreen temperature $T$	$T_1, T_{1^*}$
Radiator plate temperature $T$	$T_2$
Heat pipe condenser end temperature $T$	$T_3$
Heat pipe evaporator end temperature $T$	$T_4$
Exposed heat pipe evaporator end temperature $T$	$T_{4^*}$
Tank water temperature $T$	$T_5$
Tank wall temperature $T$	$T_6$
Room temperature $T$	$T_7$
Sky temperature $T$	$T_8$
Ambient temperature (TMY3 Data) $T$	$T_9$
Solar flux to the radiator plate $E$	$E_1$
Solar Flux to the windscreen $E$	$E_2$
Solar Flux to the second windscreen $E$	$E_3$
Natural convection and radiation from plate to windscreen $H$	$k_{12}$
Natural convection and radiation between two windscreens	$k_{11^*}$
Conduction from plate to condenser $H$	$k_{23}$
Two phase heat transfer from immersed evaporator to condenser $H$	$k_{34}$
Two phase heat transfer from exposed evaporator to condenser $H$	$k_{34^*}$
Natural convection from evaporator to water $H$	$k_{45}$
Natural convection from evaporator to room $H$	$k_{4^*7}$
Conduction through tank wall $H$	$k_{56}$
Natural convection and radiation $H$	$k_{67}$
Overall heat loss from room to ambient (LRR=10 W/m <sup>2</sup> -K) $H$	$k_{79}$
Wind convection and radiation from windscreen to ambient $H$	$k_{91}$
Wind convection and radiation from second windscreen to ambient $H^+$	$k_{91^*}$
Wind convection and radiation from radiator plate to ambient $H^+$	$k_{92}, k_{92^*}$

Radiation from windscreen to sky <sup>H+</sup>	$k_{81}$
Radiation from second windscreen to sky <sup>H+</sup>	$k_{81}^*$
Radiation from radiator plate to sky <sup>H+</sup>	$k_{82}$
Radiation from radiator plate to sky through two windscreens <sup>H+</sup>	$k_{82}^*$

T Indicates units of degrees Kelvin

E-Indicates units of W/m<sup>2</sup>

H- Indicates units of W/m<sup>2</sup>-K

+ - Indicates condensation term is included when needed

Table 5. Description of variables and parameters used to calculate conductance in thermal network (Equations 24-67).

Variable	Description	Constant
$A_{WS}$	Surface area of windscreen*	2.62 (m <sup>2</sup> )
$A_{Rad}$	Surface area of radiator*	2.62 (m <sup>2</sup> )
$A_{HP}$	Surface area of heat pipe*	5.18E-4 (m <sup>2</sup> )
$A_{Insul}$	Surface area of insulation*	2.62 (m <sup>2</sup> )
$A_{Tank}$	Surface area of tank*	4.17 (m <sup>2</sup> )
$A_{Evap}$	Surface area of evaporator*	0.104 (m <sup>2</sup> )
$A_i$	Anisotropy index	--
$\alpha$	Thermal diffusivity	--(m <sup>2</sup> /s)
$\alpha_{Building}$	Terrain parameter (class III)*	0.850
$\alpha_n$	Normal absorptivity (radiator)*	0.180
$\alpha_b$	Beam absorptivity (radiator)	--
$\alpha_{b_{WS}}$	Beam absorptivity (windscreen)	--
$\alpha_d$	Diffuse absorptivity (radiator)	--
$\alpha_{d_{WS}}$	Diffuse absorptivity (windscreen)	--
$\alpha_g$	Ground absorptivity (radiator)	--
$\alpha_{g_{WS}}$	Ground absorptivity (windscreen)	--
$\beta$	Radiator orientation*	0°
$\beta'$	Volumetric coefficient of expansion	(1/K)
$e_{WS}$	Windscreen emissivity (long wave)*	0.150
$e_{Rad}$	Radiator emissivity (long wave)*	0.929
$e_{Tank}$	Tank emissivity*	0.930
$f$	Correction factor	--
$\Gamma_{Building}$	Terrain parameter (class III)*	0.200
$g$	Gravitational constant	9.81 (m/s <sup>2</sup> )
$H_{Building}$	Modeled building height*	3.00 (m)
$H_{Tower}$	Weather tower height*	10.0 (m)
$hw$	Wind heat transfer coefficient [Sherman & Modera 1986]	--
$h$	Annual hour	--
$I$	Total radiation on horizontal surface (hourly)	TMY3 Data
$I_b$	Isotropic beam radiation (hourly)	--

$I_d$	Isotropic diffuse radiation (hourly)	TMY3 Data
$k_{Air}$	Conductivity of air	--
$k_{HP}$	Conductivity of heat pipe material*	401 (W/mK)
$k_{Insul}$	Conductivity of insulation material*	2.50E-2 (W/mK)
$k_{Rad}$	Conductivity of radiator material*	401 (W/mK)
$k_{Tank}$	Conductivity of tank*	0.500 (W/mK)
$k_{Water}$	Conductivity of thermal fluid (water)*	0.580
$K$	Extinction coefficient of polyethylene*	1.00E-5 (m <sup>-1</sup> )
$L$	Thickness of windscreen*	50E-6 (m)
$L_{HP}$	Length of adiabatic section*	2.54E-2 (m)
$L_{Insul}$	Thickness of insulation*	0.700 (m)
$L_{Rad}$	Thickness of radiator*	3.18E-3 (m)
$L_{Tank}$	Thickness of tank wall*	3.18E-3(m)
$L_{Cond}$	Thickness of condensation*	1.20E-4 (m)
$L_{W-W}$	Distance between windscreens	2.54E-2 (m)
$L_{W-R}$	Distance between windscreen and radiator	2.54E-2 (m)
$n_1$	Refractive index (air)*	1.00
$n_2$	Refractive index (polyethylene)*	1.54
$n_3$	Refractive index (water)*	1.33
$N$	Number of windscreens	0,1,2
$N_{Fins}$	Number of fins*	5
$N_{HP}$	Number of heat pipes*	5
$N_{HPR}$	Number of heat pipes exposed to room*	1
$N_{HPW}$	Number of heat pipes in thermal fluid*	4
$N_{Tank}$	Number of tanks*	1
$Nu_{Air}$	Calculated Nusselt number of air	--
$Nu$	Calculated Nusselt number	--
$OD_{HP}$	Outside diameter of heat pipe*	2.86E-2 (m)
$\rho_g$	Ground reflectance*	0.3
$P$	Prandtl number	--
$Ra_{Air}$	Rayleigh number of air	--
$R_b$	Beam radiation Ratio	--
$R_{Cond}$	Resistance of condenser end*	8.58E-5 (K/W)
$R_{Evap}$	Resistance of evaporator end*	9.13E-5 (K/W)
$\sigma$	Stefan Boltzmann constant*	5.67 E-8 (W/m <sup>2</sup> K <sup>4</sup> )
$t$	Number of hours from midnight	(hours)
$\tau_b$	Beam transmissivity	--
$\tau_d$	Diffuse transmissivity	--
$\tau_g$	Ground transmissivity	--
$\tau_{WS}$	Windscreen long wave transmissivity*	0.72
$\tau_{Cond}$	Condensation long wave transmissivity*	0.80
$T_{Sky}$	Sky temperature	--
$T_{dp,o}$	Outdoor dew-point temperature	TMY3 Data
$T_o$	Outdoor dry bulb (K)	TMY3 Data
$\theta_1$	Angle of incidence in medium 1	--

$\theta_2$	Angle of refraction in medium 2	--
$\nu$	Kinematic viscosity	(m <sup>2</sup> /s)
$V_j$	Wind velocity (hourly)	--
$WSV$	Weather tower wind velocity	TMY3 Data
$W_{HP}$	Distance between heat pipe centers*	0.359 (m)
$LRR$	Load to radiator ratio*	10 (W/mK)
	Radiator plate material*	Copper
	Radiator plate selective surface*	White Zinc Oxide
	Radiator plate height*	2.10 (m)
	Radiator plate width*	1.25 (m)
	Radiator plate height*	2.10 (m)
	Radiator plate width*	1.25 (m)
	Heat pipe two phase heat transfer fluid*	R-124
	Heat pipe material*	Copper
	Water tank height*	1.42 (m)
	Water tank length*	1.11 (m)
	Water tank width*	0.203 (m)

--Calculated Parameter

\*Baseline Parameter

Sky temperature was modeled by [Berdahl, *et al.* 1984]

$$T_8 = T_o \left[ 0.711 + 0.0056T_{dp,o} + 0.00037T_{dp,o}^2 + 0.013 \cos(15t) \right]^{\frac{1}{4}} \quad (24)$$

where  $T_8$  and  $T_o$  are the sky and outdoor dry-bulb temperatures in degrees Kelvin,  $T_{dp,o}$  is the outdoor dew-point temperature in degrees Celsius, and  $t$  is the number of hours from midnight. For the conductance values described in Table 4 that are functions of temperature, an iterative process was used to match the conductance values to the nodal temperatures solved by energy flux equations [Albanese, *et al.* 2012] given by

$$\dot{q}_{ij} = k_{ij}(T_j - T_i) \quad (15)$$

where heat transfer between the nodes is solved by using  $k_{ij}$ , the conductance between the two nodes, and multiplying by the temperature difference between nodes  $i$  and  $j$ . The network conductances were calculated with Eqns 3-37, with variables and constants described in Tables 4 and 5. Each conductance term was normalized by the radiator area and included view factors where needed.

The conductance from ambient temperature to the outer windscreen including condensation is

$$k_{91} = \left( \left( \frac{1}{h_w} + \frac{L_{cond}}{k_{water}} \right)^{-1} + \tau_{Cond} e_{ws} \sigma (T_1^2 + T_9^2) (T_1 + T_9) \left( \frac{1 - \cos\beta}{2} \right) \right) \frac{A_{WS}}{A_{Rad}}. \quad (26)$$

For radiation from ambient to the second (inner) windscreen,

$$k_{91*} = \left( \tau_{Cond} \tau_{WS} e_{ws} \sigma (T_{1*}^2 + T_9^2) (T_{1*} + T_9) \left( \frac{1 - \cos\beta}{2} \right) \right) \frac{A_{WS}}{A_{Rad}}. \quad (27)$$

The thickness of the condensation,  $L_{cond}$ , was modeled after Pieters & Deltour [1997] as the maximum condensate film thickness on polyethylene. Without condensation, the  $k_{91}$  and  $k_{91*}$  conductance terms are calculated the same as Equation 26 and 27, respectively, without the water conductance and the condensation transmissivity terms. The wind heat transfer coefficient [Burch & Luna 1980] is calculated by first finding the wind velocity [Sherman & Modera 1986]

$$V_j = WSV * \alpha_{building} \left( \frac{H_{building}}{H_{tower}} \right)^{y_{building}} \quad (28)$$

Then the convection coefficient is

$$h_w = 2.8 + (4.8V_j)$$

(29)

The radiation from radiator to ambient through one cover is

$$k_{92} = \tau_{Cond} \tau_{ws} e_{Rad} \sigma (T_2^2 + T_9^2) (T_2 + T_9) \left( \frac{1 - \cos \beta}{2} \right) \frac{A_{Rad}}{A_{Rad}}.$$

(30)

And for a two-cover system,

$$k_{92*} = \tau_{ws}^2 e_{Rad} \sigma (T_2^2 + T_9^2) (T_2 + T_9) \left( \frac{1 - \cos \beta}{2} \right) \frac{A_{Rad}}{A_{Rad}}.$$

(31)

The far infrared radiation from the outer windscreen to the sky is

$$k_{81} = \tau_{Cond} e_{ws} \sigma (T_1^2 + T_8^2) (T_1 + T_8) \left( \frac{1 + \cos \beta}{2} \right) \frac{A_{ws}}{A_{Rad}}.$$

(32)

and for the inner cover of a two-cover system,

$$k_{81*} = \tau_{ws} \tau_{Cond} e_{ws} \sigma (T_{1*}^2 + T_8^2) (T_{1*} + T_8) \left( \frac{1 + \cos \beta}{2} \right) \frac{A_{ws}}{A_{Rad}}.$$

(33)

Similarly, the far infrared radiation from radiator to sky through one cover is

$$k_{82} = \tau_{Cond} \tau_{ws} e_{Rad} \sigma (T_2^2 + T_8^2) (T_2 + T_8) \left( \frac{1 + \cos \beta}{2} \right) \frac{A_{Rad}}{A_{Rad}}.$$

(34)

And for the two-cover system,

$$k_{82*} = \tau_{Cond} \tau_{ws}^2 e_{Rad} \sigma (T_2^2 + T_8^2) (T_2 + T_8) \left( \frac{1 + \cos \beta}{2} \right) \frac{A_{Rad}}{A_{Rad}}.$$

(35)

Similar to  $k_{91}$ , the conductances  $k_{91*}$ ,  $k_{92}$ ,  $k_{92*}$ ,  $k_{81}$ ,  $k_{81*}$ ,  $k_{82}$  and  $k_{82*}$  without condensation do not include the condensation terms shown. The solar absorption of the outer

windscreen was calculated from the model of Hay, Davies, Klucher and Reindl, HDKR [Duffie & Beckman 2013]

$$E_2 = (I_b + I_d A_i) R_b \alpha_{b_{ws}} + (I_d (1 - A_i) \alpha_{d_{ws}} \left( \frac{1 + \cos(\beta)}{2} \right) \left( 1 + f \sin^3 \left( \frac{\beta}{2} \right) \right) + I \rho_g \alpha_{g_{ws}} \left( \frac{1 - \cos(\beta)}{2} \right). \quad (36)$$

where  $A_i$ ,  $f$  and  $R_b$  are calculated based on equations in Duffie & Beckman [2013]. The solar absorption of the inner windscreen was calculated as

$$E_3 = (I_b + I_d A_i) R_b * 1.01 \tau_b \alpha_{b_{ws}} + (I_d (1 - A_i) * 1.01 \tau_d \alpha_{d_{ws}} \left( \frac{1 + \cos \beta}{2} \right) \left( 1 + f \sin^3 \left( \frac{\beta}{2} \right) \right) + I \rho_g * 1.01 \tau_g \alpha_{g_{ws}} \left( \frac{1 - \cos \beta}{2} \right). \quad (37)$$

The factor 1.01 approximates the effect of multiple reflections. Isotropic beam radiation is calculated as

$$I_b = I - I_d . \quad (38)$$

The beam short-wave transmittance was calculated using derived expressions from Fresnel [Duffie & Beckman 2013] for the reflection of un-polarized radiation passing from medium 1 with refractive index  $n_1$  to medium 2 with refractive index  $n_2$ . When condensation is not present, medium 1 is air, and medium 2 is the windscreen. When condensation occurs, medium 1 is water.

$$\tau_b = \exp\left(-\frac{KL}{\cos\theta_2}\right) 0.5 \left( \frac{1 - \frac{\tan^2(\theta_2 - \theta_1)}{\tan^2(\theta_2 + \theta_1)}}{1 + (2N - 1) \frac{\tan^2(\theta_2 - \theta_1)}{\tan^2(\theta_2 + \theta_1)}} + \frac{1 - \frac{\sin^2(\theta_2 - \theta_1)}{\sin^2(\theta_2 + \theta_1)}}{1 + (2N - 1) \frac{\sin^2(\theta_2 - \theta_1)}{\sin^2(\theta_2 + \theta_1)}} \right). \quad (39)$$

Beam absorptivity for the windscreen was derived from Duffie & Beckman [2013] as,

$$\alpha_{b_{WS}} = 1 - \tau_b \quad (40)$$

Beam absorptivity for the radiator was then calculated with

$$\alpha_b = \alpha_n(1 - 1.5879x10^{-3}\theta_2 + 2.7314x10^{-4}\theta_2^2 - 2.3026x10^{-5}\theta_2^3 + 9.0244x10^{-7}\theta_2^4 - 1.8000x10^{-8}\theta_2^5 + 1.7734x10^{-10}\theta_2^6 - 6.9937x10^{-13}\theta_2^7). \quad (41)$$

Transmittance and absorption of diffuse and ground-reflected radiation were calculated using Equations 42 and 43, respectively, for angle of incidence  $\theta_1$

$$\theta_1 = 59.7 - 0.1388\beta + 0.001497\beta^2 \quad (42)$$

$$\theta_1 = 90 - 0.5788\beta + 0.002693\beta^2. \quad (43)$$

The angle of refraction for each is

$$\theta_2 = \sin^{-1} \left[ \frac{n_i}{n_2} \sin(\theta_1) \right]. \quad (44)$$

For the solar absorption by the radiator, short-wave transmissivity terms are added to represent the fractions of each type of radiation passing through the windscreen

$$E_1 = (I_b + I_d A_i) R_b * 1.01 \tau_b \alpha_b + (I_d (1 - A_i) * 1.01 \tau_d \alpha_d \left( \frac{1 + \cos(\beta)}{2} \right) \left( 1 + f \sin^3 \left( \frac{\beta}{2} \right) \right) + I \rho_g * 1.01 \tau_g \alpha_g \left( \frac{1 - \cos(\beta)}{2} \right). \quad (45)$$

When no windscreen is present,  $E_1$  is calculated the same as Equation 45, but without the factor 1.01 and with  $\tau_b = \tau_d = \tau_g = 1$ .

The conductance between the windscreens is

$$k_{11*} = \frac{k_{Air} Nu_{Air}}{L_{W-R}} \left( \frac{A_{WS}}{A_{Rad}} \right) + \left( \frac{1}{\frac{1}{e_{WS}} + \frac{1}{e_{WS}} - 1} \right) \sigma (T_1^2 + T_{1*}^2) (T_1 + T_{1*}) \left( \frac{A_{WS}}{A_{Rad}} \right). \quad (46)$$

The conductance between the windscreen and the radiator includes both radiation and convection

$$k_{12} = \frac{k_{Air} Nu_{Air}}{L_{W-R}} \left( \frac{A_{WS}}{A_{Rad}} \right) + \left( \frac{1}{\frac{1}{e_{Rad}} + \frac{1}{e_{WS}} - 1} \right) \sigma (T_1^2 + T_2^2) (T_1 + T_2) \left( \frac{A_{WS}}{A_{Rad}} \right), \quad (47)$$

where the Nusselt number is a function of Rayleigh number and tilt angle as found in experiments by Hollands, *et al.* [1976]

$$Nu_{Air} = 1 + 1.44 \left[ 1 - \frac{1708 (\sin 1.8\beta)^{1.6}}{Ra_{Air} \cos \beta} \right] \left[ 1 - \frac{1708}{Ra_{Air} \cos \beta} \right]^+ + \left[ \left( \frac{Ra_{Air} \cos \beta}{5830} \right)^{\frac{1}{3}} - 1 \right]^+, \quad (48)$$

where the meaning of the + exponent is that only positive values of the terms in the square brackets are used. Zero is used if the term is negative. The Rayleigh number is

$$Ra = \frac{g \beta' \Delta T L_X^3}{\nu \alpha} \quad (49)$$

where  $L_X$  is the distance between windscreen and radiator or between windscreens. An equation developed by Susheela & Sharp [2001] is used for the conductance between the radiator plate and the condenser end of the heat pipe

$$k_{23} = \left( \frac{1}{\frac{1}{3k_{Rad}L_{Rad}} \left( \frac{W_{HP} - OD_{HP}}{2} \right)^2} \right) N_{fins} \left( \frac{A_{HP}}{A_{Rad}} \right). \quad (50)$$

The conductance of the heat pipe from condenser to evaporator end in the thermal storage fluid is [Susheela & Sharp 2001]

$$k_{34} = 0.04(N_{HP,room} \left( \frac{k_{HP}}{L_{HP}} \right) \left( \frac{A_{HP}}{A_{Rad}} \right) + N_{HP,tank} \left( \frac{1}{R_{evap} + R_{cond}} \right) \frac{1}{A_{rad}} + \frac{k_{Insul}}{L_{Insul}} \left( \frac{A_{Insul}}{A_{Rad}} \right)). \quad (51)$$

The conductance of the heat pipe from condenser to evaporator end exposed to room air is [Susheela & Sharp 2001]

$$k_{34*} = 0.25(N_{HP} \left( \frac{k_{HP}}{L_{HP}} \right) \left( \frac{A_{AHP}}{A_{Rad}} \right) + N_{HP} \left( \frac{1}{R_{evap} + R_{cond}} \right) \frac{1}{A_{rad}} + \frac{k_{Insul}}{L_{Insul}} \left( \frac{A_{Insul}}{A_{Rad}} \right)). \quad (52)$$

The convective conductance between the heat pipe evaporator end and thermal storage fluid is

$$k_{45} = \frac{N_{HP,W} k_{Water} Nu}{OD_{HP}} \left( \frac{A_{Evap}}{A_{Rad}} \right), \quad (53)$$

where the Nusselt number for the fluid in the tank is

$$Nu = \left( 0.60 + \frac{0.387R a^{\frac{1}{6}}}{\left( 1 + \left( \frac{0.559\nu}{a} \right)^{\frac{9}{16}} \right)^{\frac{8}{27}}} \right)^2, \quad (54)$$

where the Rayleigh number is calculated using Equation 54. For the heat pipes exposed to the room, the convective conductance is

$$k_{47*} = \frac{N_{HP,R} k_{air} Nu}{OD_{HP}} \left( \frac{A_{Evap}}{A_{Rad}} \right), \quad (55)$$

where the Nusselt and Rayleigh numbers are calculated using Equations 48 and 49, respectively. The conduction through the tank wall is

$$k_{56} = \frac{k_{Tank}}{L_{Tank}} \left( \frac{A_{Tank}}{A_{Rad}} \right). \quad (56)$$

The conductance due to convection and radiation from the tank wall to the room is

$$k_{67} = \frac{N_{Tank} k_{air} Nu}{L_{Tank*}} \left( \frac{A_{Tank}}{A_{Rad}} \right) + e_{Tank} \sigma (T_6 + T_7) (T_6^2 + T_7^2) \left( \frac{A_{Tank}}{A_{Rad}} \right), \quad (57)$$

where the Nusselt number for the top and bottom of the tank [Susheela & Sharp 2001] and vertical sides [Bergman et al. 2011] are

$$Nu_{Sides} = 0.68 + \frac{0.670 Ra^{\frac{1}{4}}}{\left( 1 + \frac{0.492}{P^{\frac{9}{16}}} \right)^{\frac{4}{9}}}, \quad Ra < 10^9$$

$$Nu_{Sides} = \left( 0.825 + \frac{0.387 Ra^{\frac{1}{6}}}{\left( 1 + \frac{0.492}{P^{\frac{9}{16}}} \right)^{\frac{8}{27}}} \right)^2, \quad Ra > 10^9$$
(58)

$$Nu_{Top} = 0.54 Ra^{0.25}, \quad 10^4 < Ra < 10^7,$$

$$Nu_{Top} = 0.15 Ra^{0.333}, \quad 10^7 < Ra < 10^{11}, \quad (59)$$

$$Nu_{Bottom} = 0.27Ra^{0.25}, \quad (60)$$

The Rayleigh number is calculated using equation 49 for each surface of the tank. Two types of condensation have been distinguished:

*Film-wise Condensation* - When water spreads out as a continuous film over the surface.

*Drop-wise Condensation* – When separate drops are formed on the surface.

[Jakob 1936]

To explore its greatest effect, film-wise condensation was assumed for this study. The model represents either a totally wet surface or a totally dry surface and neglects the latent heat of condensation and evaporation (the cover temperature was also limited to the dew point temperature as a simplified approximation of the effect of latent heat). The totally wet surface along with the other nodal layers is shown in Figure 12.

For this study, the design chosen uses 50  $\mu\text{m}$  polyethylene cover that would be stiff enough to withstand environmental issues with a long-wave transmissivity of 0.72 [Hamza, *et al.* 1998] consistent with 0.73 long wave transmissivity, used in recent studies of a polyethylene with thickness 100  $\mu\text{m}$  [Xing, *et al.* 2016]. The degradation of the typical polyethylene cover's long-wave transmittance was modeled by a linear relationship with time. Results from Hamza *et al* [1998] were linearly fit, and the long-wave transmittance was modeled to decrease as

$$\tau_{WS} = 0.72 - 1.207 \times 10^{-4} h, \quad (61)$$

where  $\tau_{WS}$  is the transmittance of the cover and  $h$  is the age of the cover in hours. A transmittance of 0.42 was used as a lower limit. Simulations were run with four different dates on which the cover is replaced annually, May 1<sup>st</sup>, June 1<sup>st</sup>, July 1<sup>st</sup> and Aug 1<sup>st</sup>. Cities modeled were Louisville, Miami and New Orleans. Condensation on one cover was included for each run. For this study, the cases simulated are listed in Table 6.

*Table 6. Program simulation description*

City	Simulation Description
Louisville New Orleans Miami	No cover with baseline attributes
	One cover with baseline attributes
	Two covers with baseline attributes
	Polyethylene degradation with May cover replacement and baseline attributes
	Polyethylene degradation with June cover replacement and baseline attributes
	Polyethylene degradation with July cover replacement and baseline attributes
	Polyethylene degradation with August cover replacement and baseline attributes
Albuquerque, NM Madison, WI Rock Springs, WY Denver, CO Seattle, WA Denver, CO San Diego, CA Washington, D.C Houston, TX	No cover with baseline attributes
	One cover with baseline attributes
	Two covers with baseline attributes

\*Baseline attributes include parameters listed in Table 5 with no cover degradation.

### 3.2.1. Sky Fraction and Radiator Efficiency

The rate of heat gain from outdoors to the room is given by

$$\dot{q}_{CL,i} = (k_{79}(T_9 - T_7))^+ \quad (62)$$

where the superscript indicates only positive values, and the conductance and temperatures are given in Table 4. The index  $i$  signifies that this calculation is performed for each hour of the simulation.  $q_{CL,i}$  represents the rate of cooling that must be supplied to maintain constant indoor temperature. Thus, the hourly cooling load is estimated as  $q_{CL,i}$  times the hour time interval. Note that the cooling load includes loads when indoor temperature is below the indoor comfort temperature set point of 23.9°C. The portion of the cooling power that was covered by the sky radiation system, from storage and from the exposed condenser, is

$$\dot{q}_{RAD,i} = (k_{67}(T_7 - T_6) + k_{47*}(T_7 - T_{4*}))^+ \quad (63)$$

Auxiliary cooling is applied only when required to limit the indoor temperature  $T_7$  to no greater than 23.9°C, and is given by

$$\dot{q}_{AUX,i} = \dot{q}_{CL,i} - \dot{q}_{RAD,i} \quad (64)$$

with  $T_7 = 23.9^\circ\text{C}$ . The cooling load and auxiliary cooling were summed over the entire year. During times of non-cooling loads, the indoor temperature,  $T_7$ , was allowed to drift, but it was limited to a minimum of 18.3°C. No calculations were made for auxiliary heating of the space. The fraction of the total annual load served by the sky radiator is defined as the sky fraction,

$$f_{RAD} = 1 - \frac{\sum_{k=1}^{8760} \dot{q}_{AUX,i}}{\sum_{k=1}^{8760} \dot{q}_{CL,i}} \quad (65)$$

where 8760 is the number of hours in the year. Hourly theoretical radiative heat transfer assuming the sky to be a perfect black body is

$$\dot{q}_{BB,i} = \sigma(T_2^4 - T_8^4) \quad (66)$$

where  $\sigma$  is the Stefan-Boltzman constant, and the temperatures are from Tables 4 and 5.

The radiator efficiency is then defined as

$$\eta = \frac{\dot{q}_{rad,i}}{\dot{q}_{BB,i}} \quad (67)$$

### 3.3. RESULTS AND DISCUSSION

#### 3.3.1. Effects of Condensation on System Performance

Sky fractions in cities in each ASHRAE climate zone for a baseline sky radiation system (characteristics in Table 5) including condensation with zero, one and two covers are shown in Figure 16. Rock Springs, Seattle and San Diego achieved sky fractions of 1.0 with a system with no cover. For these cities, the annual cooling loads were calculated as 64.2, 34.6 and 74.0 kWh/m<sup>2</sup>, respectively (Figure 17). Among the cities simulated, these had the lowest annual cooling loads. For all cities with sky fraction less than 1.0, adding a cover increased the sky fraction. Adding a second cover produced smaller increases. Results are also shown in Figure 16 for a system with two covers without condensation. Neglecting condensation resulted in increases in performance of similar magnitude to adding a second cover.

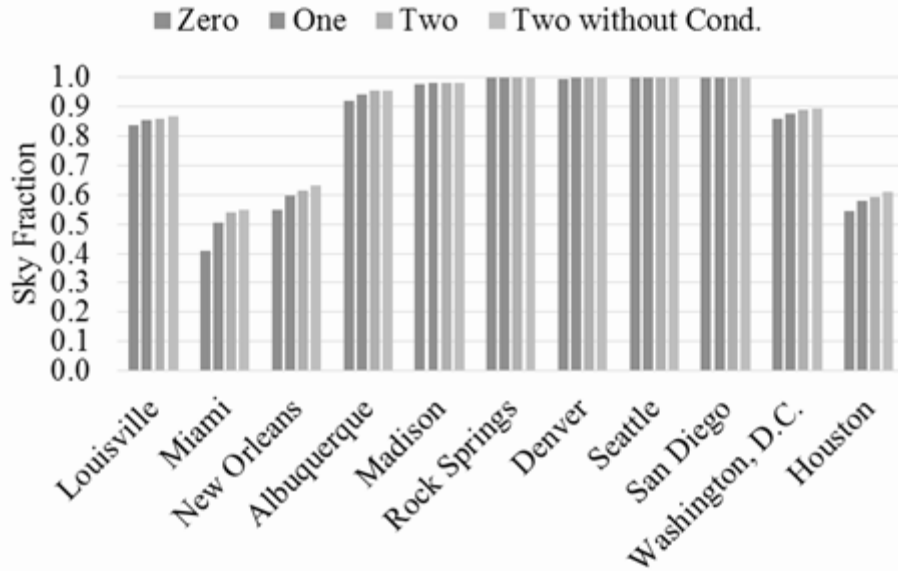


Figure 16. Annual sky fractions when condensation is included with zero, one and two cover(s).

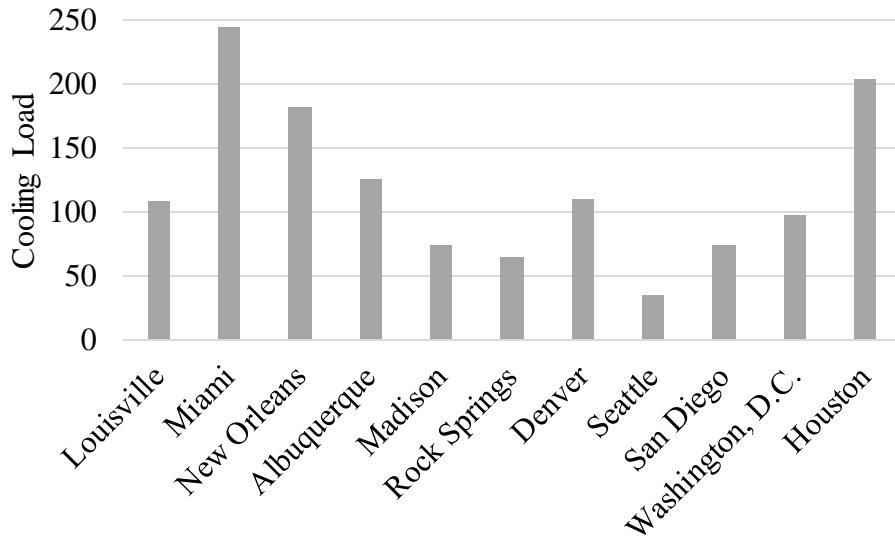


Figure 17. Calculated annual cooling loads for differing U.S. cities.

For each city, the hours during which condensation was present on the outermost surface of the sky radiation system with ambient air above 18°C were totaled. The greatest number of hours of condensation, 784 hours, occurred in New Orleans, and zero hours of condensation occurred in Rock Springs, Denver and Seattle (Figure 18). In all

climates, condensation was more likely during night time, due to the lack of solar heating, lower ambient temperature and higher humidity. Due to the increased heat rejection to the sky and the resulting lower temperature of the radiator, additional covers increased the amount of time that condensation occurred. Hydrophobic coatings and a small tilt could promote clearance of condensation. With less coverage of the windscreen, drop-wise condensation would have less performance.

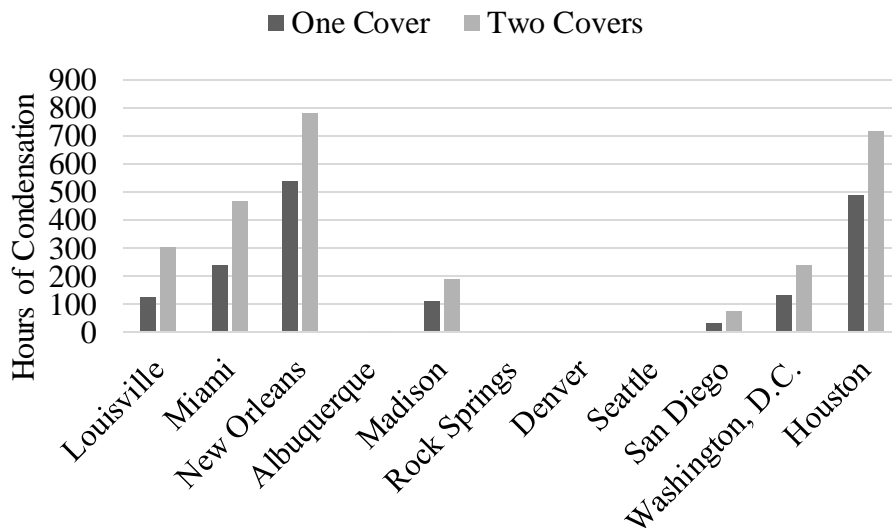


Figure 18. Time that condensation was found on the outer cover with one and two-cover systems.

Sky fraction decreased with increasing cooling load among the different cities (Figure 19). Since the radiator area and all other system parameters remain the same, this decrease is expected. However, the scatter reveals the influence of climate. The humid climates of Houston and New Orleans resulted in sky fractions below the linear trend line and the dry climates of Denver and Albuquerque produced performance above the trend line.

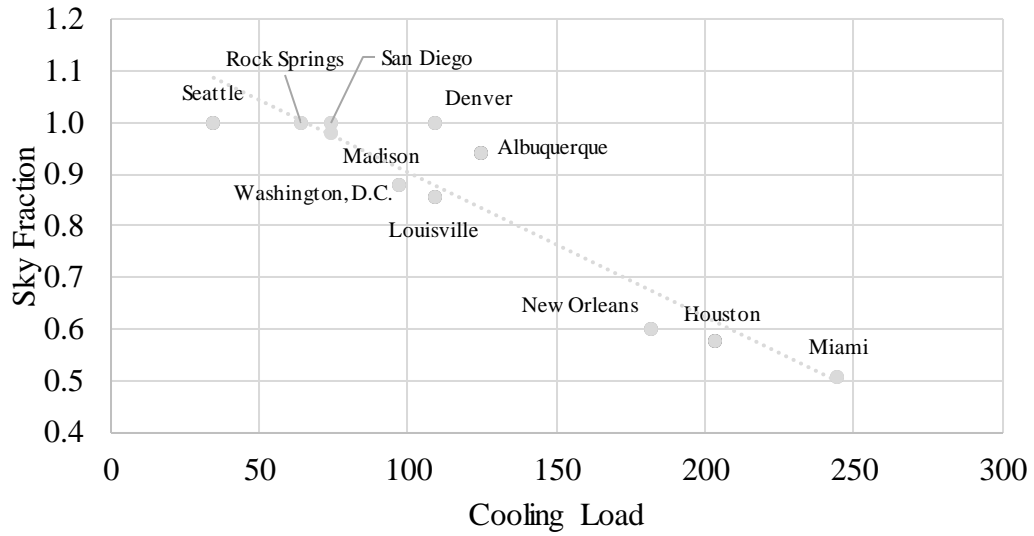


Figure 19. Comparison of sky fractions in all locations with cooling load of one cover system.

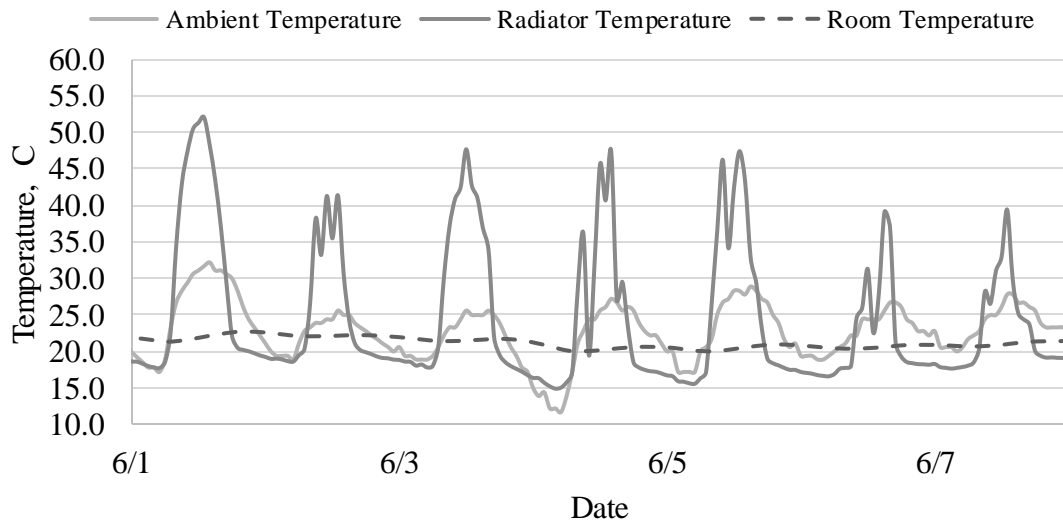


Figure 20. Comparison of room temperature, ambient temperature and radiator temperature during a week in June in Louisville, KY for the two cover system.

For the Louisville, KY climate, the thermal performance, during the daytime and night time, of the system with 2 covers including condensation is shown in Figure 20.

The first week in June is shown in the figure. Over this period, average nocturnal ambient, nocturnal room and nocturnal radiator temperature was 22 °C, 21 °C and 20°C,

respectively (Nocturnal is defined between 9:00 PM and 5:00AM.). As shown by the figure, a decrease in nocturnal radiator temperature of 2°C is slightly less than the results of Raman, *et al.* [2014] who achieved a 4°C to 5°C drop from ambient temperature during night-time and daytime.

### **3.3.2. Degradation of Polyethylene**

The effect of the date of annual replacement of the polyethylene cover is shown in Figure 21. The maximum sky fraction for the Louisville location occurs when the cover is changed in July, while the maximum sky fractions for Miami and New Orleans occur when the cover is changed in May and June, respectively. The mild climate of Louisville allows the cover to function sufficiently for the beginning of the cooling season, while in warmer regions, the cover needs to be replaced sooner. As modeled by equation 61, new polyethylene degrades from a maximum long-wave transmittance of 0.72 for a new cover to a minimum long-wave transmittance of 0.42 for the aged cover in 2486 hours or 103 days. Therefore, even if the cover is replaced in August, its transmittance has degraded to the minimum by May of the next year. Further, if the cover is replaced May 1, its transmittance has degraded to the minimum by the middle of August, before the end of the cooling season in these climates. Thus, all replacement dates result in the whole range of transmittance from maximum to minimum occurring during the cooling season. The benefits of different replacement dates are relatively small, and do not correlate with the peak of the cooling loads. Improvements in performance by early replacement in the two more challenging climates may be related to greater sky radiation potential earlier in the

summer. It is also shown in Figure 21 that neglecting degradation yields a significant increase in sky fraction.

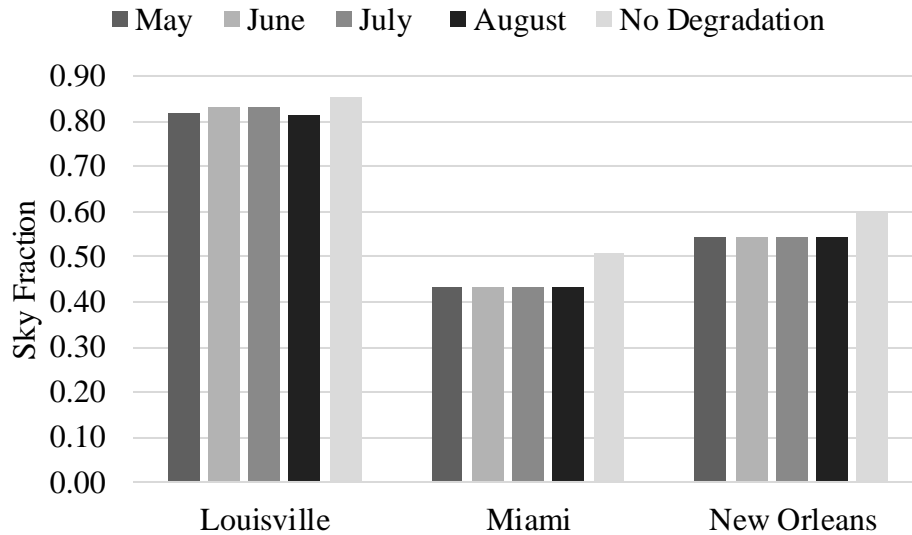


Figure 21. Annual sky fractions in Louisville, New Orleans and Miami, when the cover is replaced in the months shown.

In Figure 21, the degradation of the cover transmittance caused a significant decrease in sky fractions. Sky fraction in Louisville, Miami and New Orleans decreased by 3%, 14% and 9%, respectively, for aged versus new covers, suggesting that regular replacement is necessary, particularly in climates with large cooling loads. These results corroborate those of Pollet & Pieters [2000].

### 3.4. CONCLUSIONS

Because the performance of the sky radiator system was affected by dew on the cover in three climates (Louisville, Miami and New Orleans) in a previous study by Parsons & Sharp [2016], a wider range of climates and cover systems was investigated in this study. The addition of a cover enhanced sky fractions relative to no cover in all climates in which improvements were possible. A second cover caused smaller

improvements over one cover. Reductions in long-wave transmittance by additional covers had less influence than the reduction in convective gains.

As supported by previous studies, the inclusion of condensation decreased the overall performance of the system. For the Miami, New Orleans and Houston climates, including condensation caused a decrease in sky fraction by 2%, 3% and 3%, respectively, for the two-cover system. Including condensation in the calculations provided a more accurate depiction of how well a sky radiator will perform in these locations. It should be noted that other system configurations that cool to below ambient temperature, but not necessarily to a temperature low enough for direct cooling of room air [e.g., Goldstein, et al. 2017], may avoid condensation, but only partially offset cooling loads.

Regardless of the effects of condensation, using a sky radiator as a means of cooling is shown to be a viable option in climates across the US. Sky fractions of 100% were possible in cities with small cooling loads (Rock Springs, Seattle, San Diego) and also in Denver, which has a moderate cooling load, but low humidity and large diurnal temperature swings. Sky fractions of over 50% were achieved in New Orleans and Houston and over 40% in Miami, which have high cooling loads. Because the cooling loads in these three challenging climates are roughly three times those of the smallest, the raw energy savings are greater. Therefore, economic performance, which was not evaluated, may be better in warm climates.

Cover materials or treatments to reduce degradation would be helpful. Coatings to stabilize the film to ultraviolet radiation and mechanical erosion are commercially available, however documentation has focused largely on maintaining mechanical

properties [e.g., Dehbi, et al. 2016]. Some data is available for fresh coatings [e.g., Delgado, et al. 2011], but little information is available on long-term optical performance. Furthermore, even the transmittance of a new polyethylene cover (0.72 for long-wave radiation) is considerably less than that for a typical solar collector (> 0.9 for short-wave radiation for glass). New covers with higher transmittance represent an opportunity for materials development.

These results provide some initial insight into the significance of sky radiator design parameters and confirm the potential for passive cooling of buildings, and point towards avenues of future research to improve system performance.

CHAPTER IV  
CONTROL STRATEGIES AND DESIGN PARAMETERS FOR A COMBINED  
PASSIVE HEATING AND COOLING SYSTEM IN LOUISVILLE, KY

## 4.1. INTRODUCTION

### 4.1.1. Review of Passive Heating Systems

Many options exist for utilizing solar energy for heating buildings passively. Passive systems have the advantages of simplicity, long life and lower cost, while reducing heating loads in homes by an average of 70% [Balcomb 1992]. Passive heating systems are categorized as direct gain, indirect gain and isolated gain. Examples in the literature include optimal building design [Valladares-Rendon, *et al.* 2017], Trombe and water walls [Saadatian, *et al.* 2013, Hu, *et al.* 2017] (indirect gain), sunspaces [Mihalakakou 2002] (indirect gain), roof ponds [Hay and Yellot 1969, Sodha, *et al.* 1980, Kaushika and Rao 1983, Sharifi, *et al.* 2015] (indirect gain) and single-phase [Sadhishkumar & Balusamy 2014] and two-phase (heat pipe) [Susheela & Sharp 2001, Albanese, *et al.* 2012, Robinson, *et al.* 2013] thermosyphoning collectors (isolated gain).

One step toward minimizing space conditioning loads is to avoid overheating by passive solar systems. The effectiveness of four mechanisms for overheating reduction, as well as three strategies for employing the mechanisms, were evaluated for a solar heat pipe system, with positive results shown [Robinson & Sharp 2015a]. Additionally, features to provide cooling from systems designed primarily for heating have also been studied with success [Gan 1998, Mihalakakou 2002, Bataineh & Fayez 2011, Ghrab-Morcos, *et al.*

1993]. Incorporating components specifically for passive cooling could provide further benefits. For instance, roof ponds with moveable insulation can provide summertime cooling by evaporation during nighttime (see section 4.1.3).

#### **4.1.2. Review of Passive Cooling Systems**

Passive cooling is more challenging in varying climates due to the lower cooling capacities of ambient sources [Robinson, et al. 2015b] compared to passive solar heating. Passive cooling can be achieved through intelligent building design, such as shading, application of low solar absorptive materials, and building orientation. Additionally, passive cooling can be accomplished through application of a cooling system that utilizes an ambient energy source other than the sun. Givoni [2011] summarized these systems as naturally ventilated buildings, nocturnal ventilative cooling, radiant cooling, direct evaporative cooling, indirect evaporative cooling, and soil cooling. Common methods for passive cooling include solar chimneys [Yan, *et al.* 1991, dos S Bernardes, *et al.* 2003], solar roofs [Sodha et al. 1980, Srivastava & Tiwari 1984], and sky radiators [Santamouris 2007]. Lu et al. [2016] provided a comprehensive review of the current passive radiative cooling techniques used in buildings.

This study focuses on the use of passive radiant cooling, utilizing longwave radiant heat loss to the surroundings through a heat pipe. Since the effective black body radiant temperature of the clear night sky is substantially lower than ambient air in most climates [Berdahl & Fromberg 1982], radiant cooling is a viable means to condition a space [Frangoudakis, *et al.* 1989, Dobson 2005] and, in conjunction with thermal storage, can cool during the day and for longer periods. Therefore, the sky provides an attractive

thermal sink for cooling across a wide range of climates [Robinson, *et al.* 2015b]. Night sky temperature has been correlated to dry bulb and dew point temperatures and time [Berdahl & Martin 1984].

Recently, research on sky radiation for cooling has experienced a resurgence in attention. Performance depends on high surface emittance, as well as high thermal transmittance and low thermal absorbance and reflectance of the cover, if one is used. It is worth noting that ideal radiator properties are distinctly different than those for solar collectors, which are most efficient with surface properties optimized for capturing energy at solar temperatures and retaining energy at thermal temperatures. Radiator temperature as low as 11°C below ambient at night have been achieved with a white TiO<sub>2</sub> plate covered with polyethylene [Kimball 1985], and more recently temperatures as low as 5 °C were achieved using layers of HfO<sub>2</sub> and SiO<sub>2</sub> during the daytime [Raman, *et al.* 2014]. In addition, Zhai, *et al.* [2017] were able to achieve daytime cooling using more readily materials for their sky radiator.

#### **4.1.3. Review of Combined Passive Heating and Cooling**

Systems that combine passive heating and passive cooling without the use of active mechanical devices are less common. Some of the first were the cliff dwellings of the Pueblo Indians at Mesa Verde, Colorado. Entire buildings were located under overhangs to block the summer heat, yet were accessible to the warming rays of the winter sun. With the massive heat capacity of the surrounding rocks to provide cooling to ground temperature, they realized the principle of a passive heating and cooling system [Kreider, *et al.* 2009]. Chan, *et al.* [2010] offered a review of numerous individual

passive systems used for either solar heating or cooling, with a few integrated systems that would both heat and cool. The combined systems gain or trap heat through passive solar energy. The heat from the solar radiation is then absorbed, stored or used to preheat air. For passive cooling, the system generates and channels air flow, thereby removing heat and creating a cooling effect, most commonly by natural ventilation. Examples for combined systems listed in this study included Trombe wall or Trombe-Michel wall, solar chimney, and solar roofs. Moghasemi and Vadiie [2018] compiled a review of solar chimneys as a passive strategy for heating and cooling, and concluded that there is a need for additional research on combination systems that would provide thermal comfort in multiple climates. Coma, *et al.* [2015] compared two types of green roofs to a conventional roof in terms of energy consumption for heating and cooling periods, concluding that future work is needed to improve the design of green roof systems to reduce energy consumption during the winter periods.

The Atascadero, CA, Skytherm house utilized PVC water bags to form roof water ponds, which acted as solar heat collectors for heating and heat dissipaters for cooling [Haggard 1977]. This system provided 100% of the space heating and cooling requirements. Another Skytherm building system located in Phoenix, AZ utilized a water-covered roof with movable insulation panels and was able to keep the space in the comfort zone for 90% of the summer hours [Yellott 1973].

Reviews by Spanaki, *et al.* [2011] and Sharifi, *et al.* [2015] on numerous significant studies of roof ponds, suggest that using roof ponds as a means to passively heat and cool a space could provide an alternative to active heating and cooling. Roof ponds provide cooling benefits through indirect evaporative cooling and/or radiant

cooling, and use radiation and convection to cool the space. Heat is provided during the daytime when the water is exposed to solar radiation and solar energy is stored in the pond as sensible heat by the heat capacity of water. As in cooling, the stored energy is then transferred to the space by convection and radiation.

Joubert & Dobson [2017] tested a small model of a passive night-sky radiation cooling/solar heating system consisting of an unglazed radiator panel, a cold water storage tank, a hot water storage tank, a room and interconnecting pipework in Stellenbosch, South Africa. Sameti & Kasaeian [2015] used a lumped capacitance model of a passive heating and cooling system in the Louisville, KY, climate in which the storage tank was heated by solar radiation and cooled by night sky radiation. Hu et. al. performed numerical simulations and experimental validation of an air-based system [2018a] and a water-based system [2018b] of a combined diurnal solar heating and nocturnal radiative cooling system, although not entirely passive. Pumping power was needed to circulate the air and water. Hu, *et al.* [2019] proposed and manufactured a hybrid photo-thermal and radiative cooling collector coated with black acrylic paint. The system on a clear night, reached a net radiative cooling power of  $55.1 \text{ W/m}^2$ , while the nightly cooling energy gain of the photo-thermal and radiative cooling system was  $0.99 \text{ MJ}$  consecutively for  $11.5 \text{ h}$ , with a water temperature drop of  $3.9 \text{ K}$ . This manufactured system also used a pump to operate. The combined system in this study uses a similar method to heat and cool. Through the use of heat pipes, it is completely passive.

#### **4.1.4. Objective**

For the system discussed in this study, heat pipes are used as the heat transfer method to deliver solar heating in the winter as well as to radiate heat to the sky for cooling during the summer. In order to maximize the performance of the system, numerous simulations were conducted to determine relative performance of differing configurations. Two arrangements, a Combined System (CS) and Separate System (SS), of the passive heating and cooling subsystems were modeled and each were operated by four different control strategies to compare overall annual energy use for space conditioning. The Combined System operates with a single thermal mass connected to a dual-purpose solar absorber/sky radiator. The Separate System consists of a sky radiator and thermal mass separate from the solar absorber and its thermal mass. Of the four different control strategies, three are relatively simple control strategies and one is a more complicated weighted decision strategy.

## **4.2. METHODS**

The heating and cooling systems were simulated using the MATLAB computer software package with two different thermal networks, shown in Figure 22. For the passive heating system, the nodes included an absorber plate, condenser and evaporator ends of the heat pipe, thermal storage fluid (water), tank wall, room, and ambient air. Heat transfer between the nodes included solar flux through the cover to the plate, conduction from plate to heat pipe, two-phase heat transfer through heat pipe, natural convection from pipe to storage (water) and from water to tank wall, natural convection and radiation from tank wall to room, and overall heat loss from room to ambient. The passive cooling system thermal network differed from the heating system by including

nodes for the cover and for sky temperature. Condensation was simulated to occur on the cover when the cover temperature was equal to the dew point temperature of ambient air. Typical Meteorological Year (TMY3) weather data for Louisville, KY, was used in the simulations, and auxiliary heating and cooling was applied as needed to limit room temperature to a maximum of 23.9°C and a minimum of 18.3°C. Table 7 provides a description of the conductance and nodal temperatures used in the thermal networks shown in Figure 22, including modified values to account for condensation. In the computer program, nodal energy balance equations were simultaneously solved to obtain the nodal temperatures as functions of time. Five heat pipes were simulated with four heat pipes immersed in a thermal storage tank containing water, and one transferring heating/cooling directly into the space. Direct heating/cooling of room air is designed to provide immediate space conditioning that is more in phase with the typical peak daily thermal load. The heat pipe used R-124 refrigerant as the two-phase heat transfer fluid. This algorithm for heating was validated by experimental results from Robinson, *et al.* [2013]. The cooling model is the same as that developed by Parsons & Sharp [2018]. The heat transfer rate,  $q_{ij}$  per unit of collector area between nodes  $i$  and  $j$  is

$$q_{ij} = k_{ij}(T_j - T_i) \tag{68}$$

where  $k_{ij}$  is the heat transfer coefficient between nodal temperatures  $T_i$  and  $T_j$ , respectively. The energy balance for the  $i^{th}$  node is

$$m_i \frac{dT_i}{dt} = \sum_j (k_{ij}(T_j - T_i)) + E_i \tag{69}$$

where  $m_i$  is the capacitance per unit collector area,  $E_i$  is the solar energy received per unit collector area at the node and  $t$  is the time. Over a time step,  $\Delta t$ , equation 69 will become

$$\left[ \frac{2m_i}{\Delta t} + \sum_j k_{ij} \right] T_i - \sum_j k_{ij} T_j = \frac{2m_i T_{i-1}}{\Delta t} + \sum_j [k_{ij}(T_{j-1} - T_{i-1})] + [E_i + E_{i-1}] \quad (70)$$

where the  $-1$  in the subscripts denotes the previous time step. Thermal mass was included only for the water in the storage tank, thus  $m_i = 0$  for all other nodes. All the nodes were solved concurrently as functions of time from a set of initialized temperatures. For heat transfer coefficients dependent on the nodal temperatures, multiple iterations were used to solve for the value. Conductances, equation variables and nodal temperatures used in the thermal networks (Figure 22) are described in equations below, as well as in Table 7 and in Table 15 in the Appendix.

*Table 7. Description and baseline values of nodal temperatures and conductances.*

<b>Parameter Description</b>	<b>Variable</b>
Windscreen temperature <sup>T,R</sup>	$T_1$
(Radiator)/(Absorber) plate temperature <sup>T</sup>	$T_2$
Heat pipe (condenser)/(evaporator) end temperature <sup>T</sup>	$T_3$
Heat pipe (evaporator)/(condenser) end temperature <sup>T</sup>	$T_4$
Exposed heat pipe (evaporator)/(condenser) end temperature <sup>T</sup>	$T_{4*}$
Tank water temperature <sup>T</sup>	$T_5$
Tank wall temperature <sup>T</sup>	$T_6$
Room temperature <sup>T</sup>	$T_7$
Sky temperature <sup>T</sup>	$T_8$
Ambient temperature <sup>T</sup>	$T_9$
Solar flux (short and long wave radiation) to the radiator plate <sup>E,S</sup>	$E_{1H}$
Solar flux (short wave radiation) to the radiator plate <sup>E,R</sup>	$E_{1C}$
Solar flux (short wave radiation) to the windscreen <sup>E,R</sup>	$E_{2C}$
Natural convection and radiation from (plate to cover)/(cover to plate) <sup>H,R</sup>	$k_{12}$
Conduction from (plate to condenser)/(plate to evaporator) <sup>H</sup>	$k_{23}$
Conduction through insulation <sup>H</sup>	$k_{25}$

Two phase heat transfer from immersed (evaporator to condenser) /(condenser to evaporator) <sup>H</sup>	$k_{34}$
Two phase heat transfer from (exposed evaporator to condenser)/(condenser to evaporator) <sup>H</sup>	$k_{34*}$
Natural convection from (evaporator)/(condenser) to water <sup>H</sup>	$k_{45}$
Natural convection from (evaporator)/(condenser) to room <sup>H</sup>	$k_{4*7}$
Conduction through tank wall <sup>H</sup>	$k_{56}$
Natural convection and radiation <sup>H</sup>	$k_{67}$
Overall heat loss from room to ambient (LRR) <sup>H</sup>	$k_{79}$
Wind convection and long wave radiation from cover to ambient <sup>H,R,C</sup>	$k_{91}$
Long wave radiation from radiator plate to ambient <sup>H,R,C</sup>	$k_{92}$
Overall collector loss coefficient <sup>H,S</sup>	$k_{92}$
Long wave radiation from windscreen to sky <sup>H,R,C</sup>	$k_{81}$
Long wave radiation from radiator plate to sky <sup>H,R,C</sup>	$k_{82}$

T Indicates units of degrees Kelvin

E-Indicates units of W/m<sup>2</sup>

H- Indicates units of W/m<sup>2</sup>-K

C- Includes conduction through water layer when condensation is present

R-Indicates a sky radiator variable only

S-Indicates a solar heating variable only

For radiative cooling, sky temperature was modeled by [Berdahl, *et al.* 1984]

$$T_8 = T_o \left[ 0.711 + 0.0056T_{dp,o} + 0.00037T_{dp,o}^2 + 0.013 \cos(15t) \right]^{\frac{1}{4}} \quad (71)$$

where  $T_8$  and  $T_o$  are the sky and outdoor dry-bulb temperatures in degrees Kelvin,  $T_{dp,o}$  is the outdoor dew-point temperature in degrees Celsius, and  $t$  is the number of hours from midnight.

For the conductances shown in Figure 22, each conductance term was normalized by the radiator area and included view factors where needed.

Conductances described in equations 72, 75-77, 79-80 and 84 are used for calculating the nodal conductances in cooling only, while equations 78 and 81 describe heating-only conductances as described in Table 7. For cooling, the conductance from

ambient temperature to the outer windscreen including condensation (a cooling only parameter) is

$$k_{91} = \left( \left( \frac{1}{h_w} + \frac{L_{cond}}{k_{water}} \right)^{-1} + \tau_{Cond} e_{ws} \sigma (T_1^2 + T_9^2) (T_1 + T_9) \left( \frac{1 - \cos\beta}{2} \right) \right) \frac{A_{WS}}{A_{Rad}}. \quad (72)$$

The thickness of the condensation,  $L_{cond}$ , was modeled after Pieters & Deltour [1997] as the maximum condensate film thickness on polyethylene. Without condensation, the  $k_{91}$  conductance term is calculated the same as equation 72, but without the water conductance and the condensation transmissivity terms. The wind heat transfer coefficient [Burch & Luna 1980] is calculated by first finding the wind velocity [Sherman & Modera 1986]

$$V_j = WSV * \alpha_{building} \left( \frac{H_{building}}{H_{tower}} \right)^{Y_{building}} \quad (72)$$

Then the convection coefficient is

$$h_w = 2.8 + (4.8V_j) \quad (74)$$

The long wave radiation from radiator to ambient through one cover is

$$k_{92} = \tau_{Cond} \tau_{ws} e_{Rad} \sigma (T_2^2 + T_9^2) (T_2 + T_9) \left( \frac{1 - \cos\beta}{2} \right) \frac{A_{Rad}}{A_{Rad}}. \quad (75)$$

The far infrared radiation from the outer windscreen to the sky is

$$k_{81} = \tau_{Cond} e_{ws} \sigma (T_1^2 + T_8^2) (T_1 + T_8) \left( \frac{1 + \cos\beta}{2} \right) \frac{A_{WS}}{A_{Rad}}. \quad (76)$$

Similarly, the far infrared radiation from radiator to sky through one cover is

$$k_{82} = \tau_{Cond} \tau_{ws} e_{Rad} \sigma (T_2^2 + T_8^2) (T_2 + T_8) \left( \frac{1 + \cos \beta}{2} \right) \frac{A_{Rad}}{A_{Rad}}. \quad (77)$$

As in the cooling nodal diagram, a conductance for the overall collector loss coefficient was calculated for heating as described in Duffie & Beckman [2013]. It was calculated as

$$k_{92} = \left[ \frac{N}{520(1 - 0.000051\beta^2) \left( \frac{T_2 - T_9}{N + (1 + 0.089h_w - 0.1166h_w e_{Rad})(1 + 0.07866N)} \right)^{0.430 \left( 1 - \frac{100}{T_2} \right)}} + \frac{1}{h_w} \right]^{-1} + \frac{\sigma(T_2 + T_9)(T_2^2 + T_9^2)}{\frac{1}{e_{Rad} + 0.00591Nh_w} + \frac{2N + (1 + 0.089h_w - 0.1166h_w e_{Rad})(1 + 0.07866N) - 1 + 0.133e_{Rad} - N}{e_{WS}}} \quad (78)$$

The solar absorption of the outer windscreen and radiator was calculated from the model of Hay, Davies, Klucher and Reindl (HDKR) [Duffie & Beckman 2013]. The solar flux (short wave radiation) to the windscreen is

$$E_{2C} = (I_b + I_d A_i) R_b \alpha_{b_{ws}} + (I_d (1 - A_i) \alpha_{d_{ws}} \left( \frac{1 + \cos(\beta)}{2} \right) \left( 1 + f \sin^3 \left( \frac{\beta}{2} \right) \right) + I \rho_g \alpha_{g_{ws}} \left( \frac{1 - \cos(\beta)}{2} \right). \quad (79)$$

The solar flux (short wave radiation) through a single polyethylene windscreen to radiator plate for cooling is

$$E_{1C} = (I_b + I_d A_i) R_b (1.01 \tau_b \alpha_b)_{poly} + (I_d (1 - A_i) (1.01 \tau_d \alpha_d)_{poly} \left( \frac{1 + \cos(\beta)}{2} \right) \left( 1 + f \sin^3 \left( \frac{\beta}{2} \right) \right) + I \rho_g (\tau_g \alpha_g)_{poly} \left( \frac{1 - \cos(\beta)}{2} \right), \quad (80)$$

and the solar flux (short wave radiation) through a single glass windscreen to the radiator plate in heating is

$$E_{1H} = (I_b + I_d A_i) R_b (1.01 \tau_b \alpha_b)_{glass} + (I_d (1 - A_i) (1.01 \tau_d \alpha_d)_{glass} \left( \frac{1 + \cos(\beta)}{2} \right) \left( 1 + f \sin^3 \left( \frac{\beta}{2} \right) \right) + I \rho_g (\tau_g \alpha_g)_{glass} \left( \frac{1 - \cos(\beta)}{2} \right), \quad (81)$$

where  $A_i$ ,  $f$  and  $R_b$  are calculated based on equations in Duffie & Beckman [2013]. The factor 1.01 approximates the effect of multiple reflections. Isotropic beam radiation is

$$I_b = I - I_d . \quad (82)$$

The beam short-wave transmittance,  $\tau_b$ , was calculated using derived expressions from Fresnel [Duffie & Beckman 2013] for the reflection of un-polarized radiation passing from medium 1 with refractive index  $n_1$  to medium 2 with refractive index  $n_2$ . When condensation is not present, medium 1 is air, and medium 2 is the windscreen. When condensation occurs, medium 1 is water.

$$\tau_b = \exp \left( - \frac{KL}{\cos \theta_2} \right) 0.5 \left( \frac{1 - \frac{\tan^2(\theta_2 - \theta_1)}{\tan^2(\theta_2 + \theta_1)}}{1 + (2N - 1) \frac{\tan^2(\theta_2 - \theta_1)}{\tan^2(\theta_2 + \theta_1)}} + \frac{1 - \frac{\sin^2(\theta_2 - \theta_1)}{\sin^2(\theta_2 + \theta_1)}}{1 + (2N - 1) \frac{\sin^2(\theta_2 - \theta_1)}{\sin^2(\theta_2 + \theta_1)}} \right). \quad (83)$$

Beam absorptivity,  $\alpha_b$ , for the windscreen (polyethylene for cooling and glass for heating) and radiator, diffuse and ground-reflected transmittance or radiation ( $\tau_d$  and  $\tau_g$ ), diffuse and ground-reflected absorption of radiation ( $\alpha_d$  and  $\alpha_g$ ) and angle of refraction ( $\theta_1$  and  $\theta_2$ ) were calculated from Duffie & Beckman [2013]. The conductance between the windscreen and the radiator, a cooling only conductance, includes both radiation and convection

$$k_{12} = \frac{k_{Air} Nu_{Air}}{L_{W-R}} \left( \frac{A_{WS}}{A_{Rad}} \right) + \left( \frac{1}{\frac{1}{\epsilon_{Rad}} + \frac{1}{\epsilon_{WS}} - 1} \right) \sigma (T_1^2 + T_2^2) (T_1 + T_2) \left( \frac{A_{WS}}{A_{Rad}} \right), \quad (84)$$

where the Nusselt number is a function of Rayleigh number and tilt angle as found in experiments by Hollands, *et al.* [1976]

$$Nu_{Air} = 1 + 1.44 \left[ 1 - \frac{1708(\sin 1.8\beta)^{1.6}}{Ra_{Air} \cos \beta} \right] \left[ 1 - \frac{1708}{Ra_{Air} \cos \beta} \right]^+ + \left[ \left( \frac{Ra_{Air} \cos \beta}{5830} \right)^{\frac{1}{3}} - 1 \right]^+, \quad (85)$$

where the meaning of the + exponent is that only positive values of the terms in the square brackets are used. Zero is used if the term is negative. The Rayleigh number is

$$Ra = \frac{g\beta' \Delta T L_X^3}{\nu \alpha} \quad (86)$$

where  $L_X$  is the distance between windscreen and radiator.

The remaining conductance equations, 87-94, describe nodal conductances for both the heating and cooling systems. An equation developed by Susheela & Sharp [2001] is used for the conductance between the radiator plate and the condenser end of the heat pipe

$$k_{23} = \left( \frac{1}{\frac{1}{3k_{Rad}L_{Rad}} \left( \frac{W_{HP} - OD_{HP}}{2} \right)^2} \right) N_{fins} \left( \frac{A_{HP}}{A_{Rad}} \right). \quad (87)$$

The conductance of the heat pipe from condenser to evaporator end in the thermal storage fluid is [Susheela & Sharp 2001]

$$k_{34} = 0.04(N_{HP,room} \left( \frac{k_{HP}}{L_{HP}} \right) \left( \frac{A_{HP}}{A_{Rad}} \right) + N_{HP,tank} \left( \frac{1}{R_{evap} + R_{cond}} \right) \frac{1}{A_{rad}} + \frac{k_{Insul}}{L_{Insul}} \left( \frac{A_{Insul}}{A_{Rad}} \right)). \quad (88)$$

The conductance of the heat pipe from condenser to evaporator end exposed to room air is [Susheela & Sharp 2001]

$$k_{34*} = 0.25(N_{HP} \left( \frac{k_{HP}}{L_{HP}} \right) \left( \frac{A_{AHP}}{A_{Rad}} \right) + N_{HP} \left( \frac{1}{R_{evap} + R_{cond}} \right) \frac{1}{A_{rad}} + \frac{k_{Insul}}{L_{Insul}} \left( \frac{A_{Insul}}{A_{Rad}} \right)). \quad (89)$$

The convective conductance between the heat pipe evaporator end and thermal storage fluid is

$$k_{45} = \frac{N_{HP,W} k_{Water} Nu}{OD_{HP}} \left( \frac{A_{Evap}}{A_{Rad}} \right), \quad (90)$$

where the Nusselt number for the fluid in the tank is

$$Nu = \left( 0.60 + \frac{0.387R a^{\frac{1}{6}}}{\left( 1 + \left( \frac{0.559\nu}{a} \right)^{\frac{9}{16}} \right)^{\frac{8}{27}}} \right)^2, \quad (91)$$

where the Rayleigh number is calculated using equation 86. For the heat pipes exposed to the room, the convective conductance is

$$k_{47*} = \frac{N_{HP,R} k_{air} Nu}{OD_{HP}} \left( \frac{A_{Evap}}{A_{Rad}} \right), \quad (92)$$

where the Nusselt and Rayleigh numbers are calculated using equations 85 and 86, respectively. The conduction through the tank wall is

$$k_{56} = \frac{k_{Tank}}{L_{Tank}} \left( \frac{A_{Tank}}{A_{Rad}} \right). \quad (93)$$

The conductance due to convection and radiation from the tank wall to the room is

$$k_{67} = \frac{N_{Tank} k_{air} Nu}{L_{Tank}^*} \left( \frac{A_{Tank}}{A_{Rad}} \right) + e_{Tank} \sigma (T_6 + T_7) (T_6^2 + T_7^2) \left( \frac{A_{Tank}}{A_{Rad}} \right), \quad (94)$$

where the Nusselt number for the top and bottom of the tank [Susheela & Sharp 2001] and vertical sides [Bergman et al. 2011] are

$$Nu_{sides} = 0.68 + \frac{0.670 Ra^{\frac{1}{4}}}{\left( 1 + \frac{0.492}{P^{\frac{9}{16}}} \right)^{\frac{4}{9}}}, \quad Ra < 10^9$$

$$Nu_{sides} = \left( 0.825 + \frac{0.387 Ra^{\frac{1}{6}}}{\left( 1 + \frac{0.492}{P^{\frac{9}{16}}} \right)^{\frac{8}{27}}} \right)^2, \quad Ra > 10^9 \quad (95)$$

$$Nu_{Top} = 0.54 Ra^{0.25}, \quad 10^4 < Ra < 10^7,$$

$$Nu_{Top} = 0.15 Ra^{0.333}, \quad 10^7 < Ra < 10^{11},$$

(96)

$$Nu_{Bottom} = 0.27 Ra^{0.25},$$

The Rayleigh number is calculated using equation 86 for each surface of the tank. The final conductance,  $k_{79}$ , is the overall heat loss from room to ambient and a constant value of  $10 \frac{W}{m^2 K}$  is considered for the system.

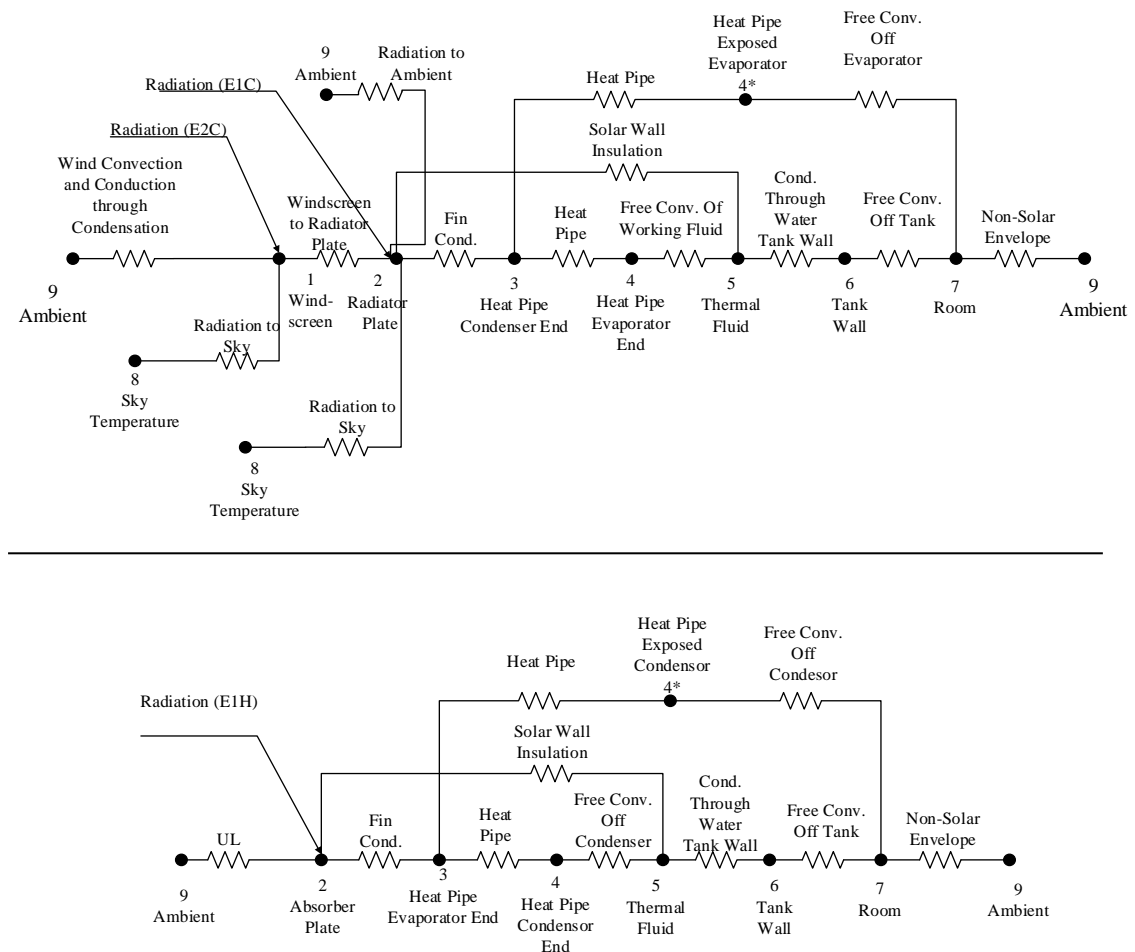


Figure 22. Nodal diagram depicting the thermal conductances for cooling (top) and heating (bottom) for a one cover system.

#### 4.2.1. Passive System Configurations

For this paper, two system configurations were studied. The first, the Separate System (SS), consists of a sky radiator and thermal mass separate from the solar absorber and its thermal mass (Figure 23). For the SS, differing attributes for the sky cooling and

the solar heater subsystems were assigned (Table 8). The storage tank in each subsystem of the SS is fully insulated from the indoor space until heating or cooling is required by the room. When heating or cooling is not needed, the tank continues to collect/reject heat from ambient sources.

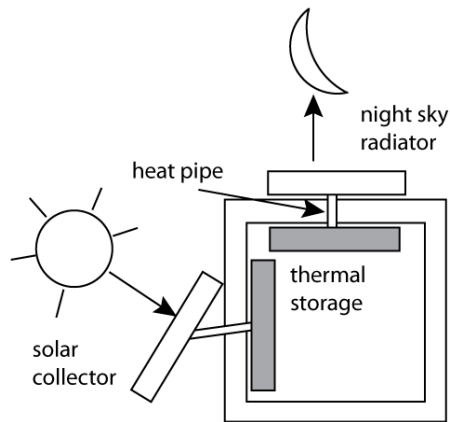


Figure 23. Separate System configuration.

Table 8. Separate System design parameters.

<b>Collector/Radiator Orientation</b>	
Sky cooling	0°
Solar heating	Latitude+15° (53°)
<b>Windscreen Material</b>	
Sky cooling	Polyethylene
Solar heating	Glass
<b>Collector/Radiator Surface</b>	
Sky cooling	White zinc oxide
Solar heating	Black chrome over nickel substrate

The second configuration, Combined System (CS), operates with a single thermal mass connected to a dual-purpose solar absorber/sky radiator (Figure 24).

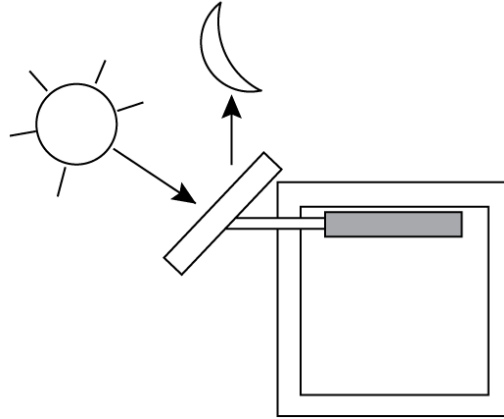


Figure 24. Combined System configuration with slope = latitude + 15°. (Slope = 0° was also simulated, but not depicted in this figure).

For the CS, four different designs were studied to identify the most beneficial parameter values for the Louisville, KY, climate. Two of the designs included attributes to maximize cooling or heating performance, respectively (Table 9). A mechanism to provide switching from heating to cooling functions was assumed, for instance, a mechanism that switches the tilt of the heat pipe as shown in Figure 25.

Table 9. Combined System design parameters for cooling versus heating schemes.

<b>CS with Sky Cooling Attributes</b>	
Orientation	0°
Windscreen Material	Polyethylene
Collector/Radiator Surface	White Zinc Oxide
<b>CS with Solar Heating Attributes</b>	
Orientation	Latitude+15° (53°)
Windscreen Material	Glass
Collector/Radiator Surface	Black Chrome over Nickel Substrate

For the third and fourth design, not listed in Table 9, cooling and heating attributes were switched to maximize performance based on the system's mode. The two variable systems were simulated at both 0° and 53° (Latitude+15°) slope. Mechanisms that would provide the attribute changes were assumed, for instance, by manual or

automatic switching of materials or by innovative photochromic, thermochromic or electrochromic materials. For both the SS and CS, Figure 22 depicts the nodal diagrams for the cooling and heating modes. Conductances are included to heat/cool the storage tank, as well as to heat/cool the room directly.

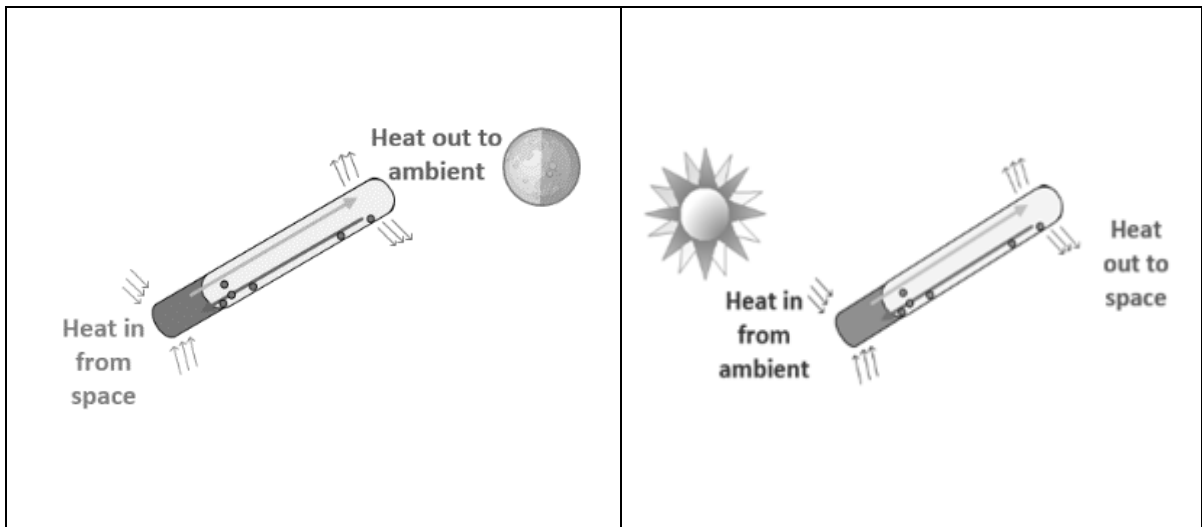


Figure 25. Combined System heat pipe configurations for cooling (left) and heating (right).

#### 4.2.2. System Control Strategies

Four strategies were evaluated to control the passive heating and cooling system based on typical control methods that a residential system might employ. These four control strategies were simulated for each of the systems. The first strategy, called Seasonal (S), was chosen to operate similar to a boiler/chiller system. This system switches to cooling-only on April 15<sup>th</sup> and back to heating-only on October 15<sup>th</sup>. These dates were chosen based on the Louisville, KY, climate, where heating degree days typically occur October through April and cooling degree days occur April through October.

The second strategy, Ambient (A), uses ambient temperature to determine the heating and cooling mode. The switching point was set to the traditional baseline of 18.3°C for heating and cooling mode.

[[http://www.cpc.ncep.noaa.gov/products/analysis\\_monitoring/cdus/degree\\_days/ddayexp.shtml](http://www.cpc.ncep.noaa.gov/products/analysis_monitoring/cdus/degree_days/ddayexp.shtml)]. For the Ambient control strategy, if ambient temperature is below 18.3°C the system is in heating mode, and if ambient temperature is above 18.3°C the system is in cooling mode, similar to an economizer.

For the third control strategy, user comfort was taken into consideration. For the Room temperature (R) control, two simulations (one with the system in heating mode and the other with the system in cooling mode) calculated room temperature after an hour. The heating or cooling mode that maintained the room temperature closest to 22.2°C was chosen (optimum operative temperature for a winter season, typical clothing and light sedentary activity [ASHRAE]). This temperature was chosen due to Louisville, KY, being a heating-dominated climate.

The final strategy, described as Matrix (M), uses forecasted weather data to make a process decision to heat or cool. Each variable was given a weight as shown in Figure 5. A total of +/-10 points was distributed based on the variables and process shown in Figure 26. The heating/cooling mode was determined by adding the points for each variable

$$\mathbf{Mode} = 2F_1(T_{high}) + 4F_2(T_9) + 2F_3(T_{avg}) + F_4(t) + F_5(m) \quad (98)$$

where the functions  $F_i$  take on values of 0 or 1 based on the thresholds shown in Figure 26, and  $T_{high}$  is the 24-hour high temperature,  $T_{avg}$  is the 24-hour average temperature,  $t$  is

the time of day and  $m$  is the month. A *Mode* value less than -2 calls for cooling mode and a value greater than or equal to -2 indicates heating mode. The settings for this strategy were created by simulating several iterations until good performance in the heating-dominated climate of Louisville, KY, was found. Appropriate weights would likely be different for other locations.

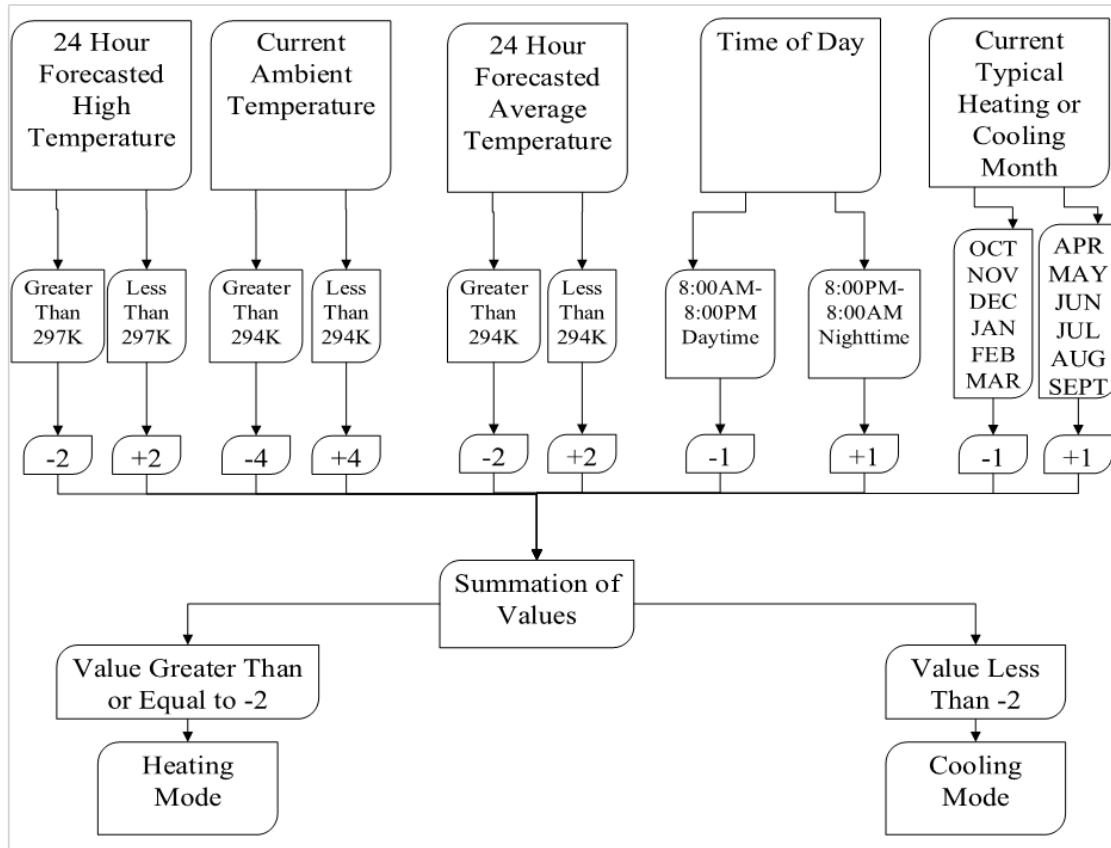


Figure 26. Process flowchart used to determine heating or cooling mode for the Matrix control strategy.

Table 10 displays all of the system control strategies and configurations evaluated in this study.

Table 10. Control strategies for varying system type and design parameters

<i>System Configuration</i>	<i>Control Strategy</i>	<i>Design Parameters</i>	<i>Abbreviation</i>
Separate System	Room Temperature	N/A	SS-R
Separate System	Matrix	N/A	SS-M

Separate System	Ambient	N/A	SS-A
Separate System	Seasonal	N/A	SS-S
Combined System	Room Temperature	Cooling Attributes	CS-R-C
Combined System	Matrix	Cooling Attributes	CS-M-C
Combined System	Ambient	Cooling Attributes	CS-A-C
Combined System	Seasonal	Cooling Attributes	CS-S-C
Combined System	Room Temperature	Heating Attributes	CS-R-H
Combined System	Matrix	Heating Attributes	CS-M-H
Combined System	Ambient	Heating Attributes	CS-A-H
Combined System	Seasonal	Heating Attributes	CS-S-H
Combined System	Room Temperature	Variable Attributes*	CS-R-V-0
Combined System	Matrix	Variable Attributes*	CS-M-V-0
Combined System	Ambient	Variable Attributes*	CS-A-V-0
Combined System	Seasonal	Variable Attributes*	CS-S-V-0
Combined System	Room Temperature	Variable Attributes*	CS-R-V-53
Combined System	Matrix	Variable Attributes*	CS-M-V-53
Combined System	Ambient	Variable Attributes*	CS-A-V-53
Combined System	Seasonal	Variable Attributes*	CS-S-V-53

\*Variable Attributes – this mode allowed the attributes in Table 9 to switch instantaneously depending on the mode selected by the strategy, with the slope of the absorber/radiator fixed as indicated by the number in the abbreviation.

#### 4.2.3. Energy Fractions

The baseline rate of heat gain during the cooling mode from outdoors to the room is

$$\dot{q}_{CL,i} = (k_{79}(T_9 - 18.3^\circ\text{C}))^+ \quad (99)$$

where  $k_{79}$  is the overall heat loss from room to ambient and  $T_9$  is ambient temperature.

The description of variables for equations 99-107 are given in Table 7. Similarly, the baseline rate of heat loss while in heating mode from the room to outdoors is

$$\dot{q}_{HL,i} = (k_{79}(18.3^\circ\text{C} - T_9))^+ \quad (100)$$

The index  $i$  signifies that this calculation is performed for each hour of the simulation.  $\dot{q}_{CL,i}$  represents the rate of cooling that must be supplied to maintain constant room temperature using a traditional baseline of 18.3°C. Thus, the baseline hourly cooling load is estimated as  $q_{CL,i}$  times the hour time interval. Similarly,  $\dot{q}_{HL,i}$  represents the rate of heating at the same traditional baseline temperature, which is the same as the lower limit of the room temperature range in these simulations. With this in mind, the baseline hourly heating load is estimated as  $q_{HL,i}$  times the hour time interval. The rates of cooling provided to the radiator and space, respectively, while in cooling mode, from storage and from the exposed evaporator, are

$$\dot{q}_{SYS,SR,i} = \left( \left[ \frac{1}{k_{91}+k_{12}} + \frac{1}{k_{92}} \right]^{-1} (T_2 - T_9) + k_{82}(T_2 - T_8) - E_{1c} \right)^+ \quad (\text{radiator}) \quad (101)$$

$$\dot{q}_{SYS,SR,i} = (k_{67}(T_7 - T_6) + k_{47*}(T_7 - T_{4*}))^+ \quad (\text{room}) \quad (102)$$

The rates of heating provided to the radiator and space, respectively, while in heating mode, from storage and from the exposed condenser, is

$$\dot{q}_{SYS,SHP,i} = (E_{1H} - k_{92}(T_2 - T_9))^+ \quad (\text{radiator}) \quad (103)$$

$$\dot{q}_{SYS,SHP,i} = (k_{67}(T_6 - T_7) + k_{47*}(T_{4*} - T_7))^+ \quad (\text{room}) \quad (104)$$

Auxiliary cooling is applied only when required to limit the indoor temperature  $T_7$  to a maximum of 23.9°C and is

$$\dot{q}_{AUX,C,i} = k_{79}(T_9 - 23.9^\circ\text{C}) - \dot{q}_{SYS,SR,i} \quad (105)$$

and auxiliary heating is applied only when required to limit the indoor temperature  $T_7$  to a minimum of 18.3°C and is

$$\dot{q}_{AUX,H,i} = k_{79}(18.3^\circ\text{C} - T_9) - \dot{q}_{SYS,SHP,i}. \quad (106)$$

The cooling, heating and auxiliary loads were summed over the entire year. The fraction of the total annual load served by the system is defined as the ambient energy fraction,

$$f = 1 - \frac{\sum_{i=1}^{8760} q_{AUX,C,i} + \sum_{i=1}^{8760} \dot{q}_{AUX,H,i}}{\sum_{i=1}^{8760} q_{CL,i} + \sum_{i=1}^{8760} \dot{q}_{HL,i}} \quad (107)$$

where 8760 is the number of hours in the year. This value was used to indicate the general performance of the system.

### 4.3. RESULTS AND DISCUSSION

Of the four control strategies, three spent most of the time in heating mode, since Louisville, KY, is a heating-dominated climate. The exception was the seasonal control strategy (Figure 27). The heating/cooling strategy that resulted the highest number of heating hours and lowest number of cooling hours was the Matrix strategy, which also produced the highest ambient energy fraction (0.707). The SSs that proved to be more effective with higher ambient energy fractions were those with slightly more hours for heating than the climate alone dictated (as indicated by the hours for the Ambient strategy). Those strategies, SS-M and SS-R, were in heating for 5,937 and 5,540 hours and in cooling for 2,823 and 3,220 hours, respectively.

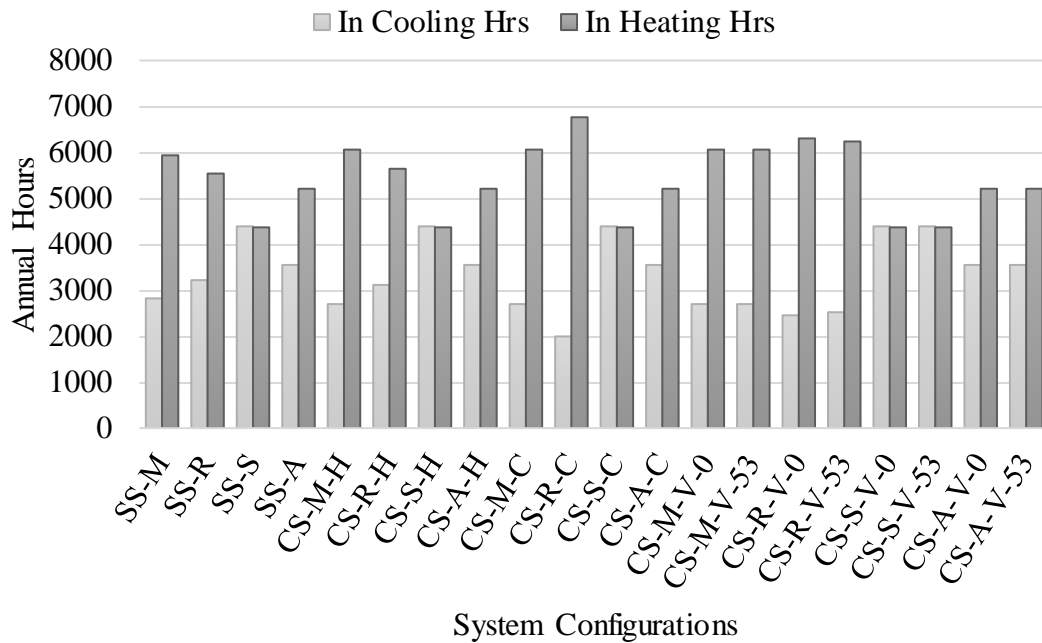


Figure 27. Heating and cooling mode hours for all control strategies (see Table 10).

For the SS-M, the annual ambient energy fraction (fraction of total heating and cooling load provided by the system, equation 107) was calculated as 0.707 (Figure 28). This system type and heating/cooling strategy produced the largest fraction of the systems/strategies. The CS-S-C had the lowest performance of the systems/strategies (0.296). Of the CS schemes modeled, those with variable attributes and slope of 53° (15°+Latitude) generally had the highest ambient energy fractions. With Louisville being a heating-dominated climate, the better heating tilt angle for heating provided greater incident radiation during the winter season, and the heating-oriented attributes retained more of the solar heat. For the CS, the fraction decreased by 58% when cooling (CS-M-C) rather than heating (CS-M-V-53) attributes were used for the system.

Most surprisingly of the control systems, the CS-M-V-53 control strategy proved to have the highest ambient energy fraction among the CS configurations with an annual

ambient energy fraction of 0.704 (Figure 28). Of all the strategies with V-53 design attributes, the Matrix control called for the second highest number of hours in heating (the Room strategy was highest), despite ambient temperature dictating fewer heating hours (see the heating hours for CS-A-V-53 in Figure 27, based on ambient temperature being below 18.3°C). It was beneficial to use multiple inputs to make the heating or cooling decision, as demonstrated by the higher fractions for the Matrix strategy across all equivalent system configurations. In higher-performing cases, the CS almost matched the fractions of the SS. For instance, the ambient energy fraction for CS-M-V-53 was only 1% lower than for SS-M. This is a surprising and convenient result, as it is potentially more economical to manufacture, transport and install only a single unit (the CS), rather than two separate units for heating and cooling (the SS). The monthly average and maximum system power delivered to the room (equations 102 and 104) and to the radiator (equations 101 and 103) for the heating and cooling seasons for the CS-M-V-53 are shown in Table 11. The results are displayed in two separate categories: power delivered at the radiator and power delivered at the room. The results for the maximum values of power delivered at the radiator during the cooling season show similar outcomes as Hu, *et al.* [2016] found in their study (Net cooling power for a clear night sky using a radiative cooling collector of 20-80 W/m<sup>2</sup> and their solar heating and radiative cooling collector having a net cooling power for a clear sky of 50.3 W/m<sup>2</sup>). The system in Hu, *et al.* [2016] study was an active combined system using sky radiation that utilized a composite surface on a flat plate solar collector. A later study of a similar system also performed by Hu, *et al.* [2019] on a clear night, reached a net radiative cooling power of 55.1 W/m<sup>2</sup>. The heat pipe system average heating/cooling powers

shown in Table 11. The average heating/cooling powers are significantly lower than the maximum heating/cooling powers because the system is either not able to provide power or the space is within the upper and lower comfort limits and additional power is not provided. The values for the table are over a 24 hour cycle. During the day, little cooling would be expected as the ambient temperature and solar radiation would dominate, and for heating, nocturnal heating would not be provided during winter months. Thus power provided would be zero, and included in the average values.

Table 11. The average and maximum system power for CS-R-V-53.

Month	System power at radiator $\left(\frac{W}{m^2}\right)$				System power at room $\left(\frac{W}{m^2}\right)$			
	Heating		Cooling		Heating		Cooling	
	Avg.	Max.	Avg.	Max.	Avg.	Max.	Avg.	Max.
<b>Jan</b>	89	783	--	--	89	526	--	--
<b>Feb</b>	116	843	--	--	115	593	--	--
<b>Mar</b>	114	852	11	51	94	571	--	5
<b>Apr</b>	111	815	18	54	97	576	3	18
<b>May</b>	--	--	17	58	--	--	4	17
<b>Jun</b>	--	--	17	51	--	--	5	16
<b>Jul</b>	--	--	16	44	--	--	7	14
<b>Aug</b>	--	--	17	44	--	--	7	15
<b>Sept</b>	--	--	15	44	--	--	6	14
<b>Oct</b>	133	877	17	35	94	644	7	12
<b>Nov</b>	113	855	--	--	101	594	--	--
<b>Dec</b>	87	777	--	--	84	517	--	--

Table 11 also shows a significantly lower power provided to the space compared to the power provided at the radiator. This is expected as the system would need ample energy to raise the temperature of the thermal fluid in the storage tank.

With multiple system configurations, the combined system provides more than half the total heating and cooling load (Figure 27). These results concur with previous simulation results of a combined system in the Louisville climate [Sameti & Kaseian 2015]. Among systems with the same M control strategy, the CS-M-V-0 and CS-M-V-53

exhibited 21% lower and less than 1% lower fractions, respectively, than the SS-M. A similar trend of slightly lower performance for the CS system with tilt of 53° and much lower performance for the CS system with tilt of 0° is evident for the R, S and A strategies also. These results suggest that it is more beneficial to have a slope appropriate for the dominate (heating) season than it is to have separate thermal masses for heating and cooling.

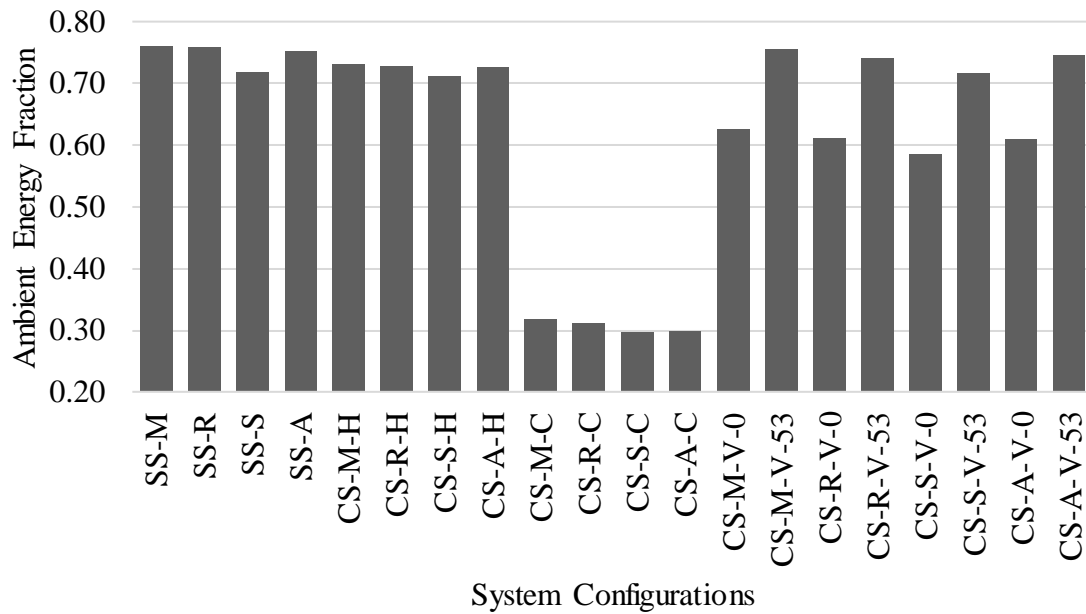


Figure 28. Ambient energy fractions for varying control strategies and attributes (see Table 10).

As discussed, the M control generally provided the highest annual ambient energy fractions among the differing strategies, only slightly higher than the SS-R. In Figures 29 and 30, room temperatures for a cooling and a heating period, respectively, are compared among the SS and the several CS systems with varying attributes. For the cooling period, Figure 29 depicts a warm period in July. After the first day, all systems and attributes begin in the evening with room temperature at the upper limit. When the systems are in

cooling mode and can provide cooling, the SS-M provides the greatest amount followed by the CS-M-C and CS-M-V-0. CS-M-V-53 also performs surprisingly well. The radiators for SS-M and CS-M-C have identical optical properties, but the cooling provided by SS-M is greater than that of CS-M-C due to switching from cooling to heating mode caused by cool nighttime temperatures. When the switching to heating mode occurs, CS-M-C discontinues cooling of its thermal storage, leaving less cooling available the next day, while SS-M always cools its cold thermal storage whenever possible. CS-M-C and CS-M-V-0 also have identical radiator properties when CS-M-V-0 is in cooling mode, but CS-M-V-0 switches to heating attributes and more effectively heats thermal storage, whether switching is appropriate or not. Remnants of this effect are evident during the first day of Figure 29, when storage for CS-M-V-0 starts warmer and provides less cooling. Throughout the period of Figure 29, both systems are continuously in cooling mode, thus their room temperatures converge after the first day. All systems provide some cooling, but the combined system with heating attributes (CS-M-H) provides the least, as expected. Due to poor optical properties of the cover and radiator

plate for cooling, the CS-M-H cannot cool as efficiently as the other configurations.

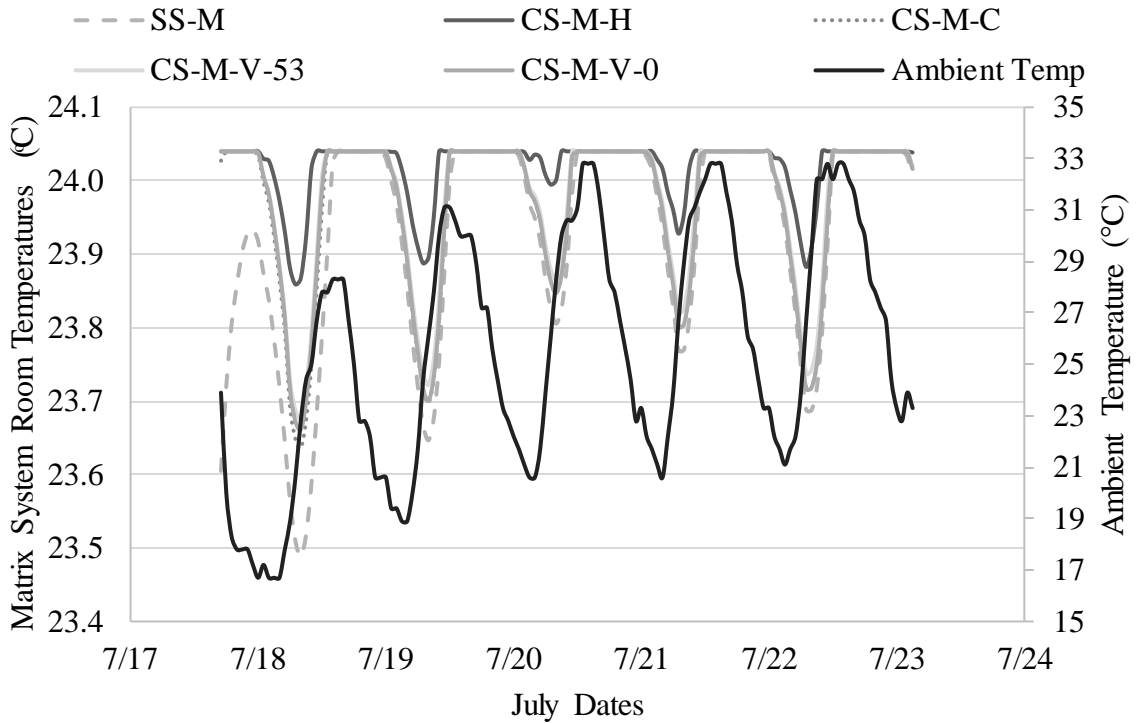


Figure 29. Room temperature during a cooling period for Matrix control strategy (see Table 10).

A heating period in March is shown in Figure 30. All systems and attributes begin this period with room temperature at the lower limit. When CS-M-V-53 is in heating mode, it has identical optical properties to SS-M and CS-M-H. Therefore, these three systems provide the greatest amount of heat to the room. The curves for these three systems are identical during this period. CS-M-V-0 has the same optical properties except for a slope that is detrimental for heating, thus its performance is lower. CS-M-C has optical properties designed for cooling, so it is ineffective in heating compared to the other systems.

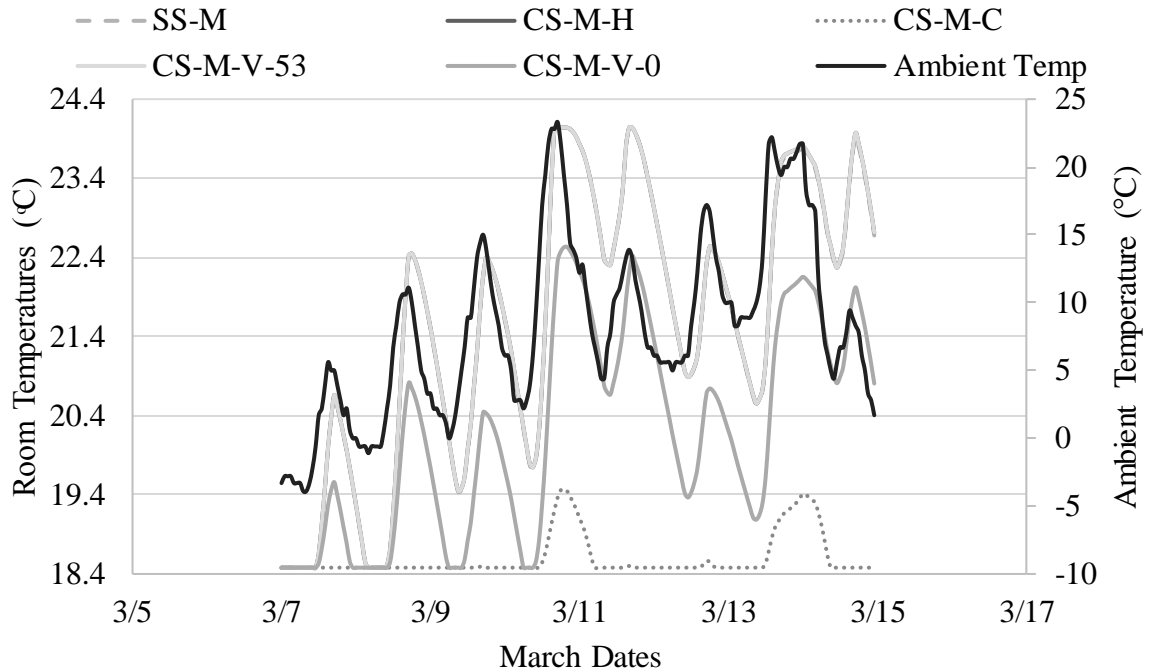


Figure 30. Room temperature during a heating period for Matrix control strategy (see Table 10).

Heating/cooling attributes had a significant effect on the ability to heat and cool. During the heating period (Figure 30), the CS-M-C system with cooling attributes shows little change in room temperature, meaning much auxiliary heating is required. During the cooling period (Figure 29), the CS-M-H system with heating attributes also provided the least amount of cooling, due to the inability to cool the radiator effectively. This is important to understand during the design phase for a building using this heat pipe system in a particular climate, because the heating/cooling attributes have important impacts on seasonal system performance. Separate subsystems for heating and cooling understandably maximize thermal performance, however for space and economic reasons, the combined system has potential benefits.

#### 4.4. CONCLUSIONS

Of the twenty system configurations simulated in this study, the SS-M provided the greatest annual ambient energy fraction of the overall building load. This control strategy allowed the system to change its cooling/heating mode in response to forecasted temperature anomalies that occur during the season, in contrast to the other strategies, which provide no such feedback and are based on climate, ambient temperature and room temperature.

As might be expected, the SS proved to be the slightly superior system configuration in terms of thermal performance. This is supported by simulation results that showed that the SS-M performed 21% better than the CS-M-V-0 and approximately 1% better than CS-M-V-53. For a combined system, variable attributes showed significantly higher performance compared to either constant heating or constant cooling attributes. This analysis supports that it is very beneficial to have switchable optical properties for the absorber/radiator and for the cover. Switching might be accomplished manually, i.e., by physically changing these components, or by the development of mechanisms for automatic switching, for instance, by innovative photochromic, thermochromic or electrochromic materials. The lowest performance occurred when cooling attributes were used exclusively in the Louisville, KY, climate. This caused a significant decrease of 58% in the fraction of total heating and cooling load provided by the system comparing CS-M-C to CS-M-V-53. These results show that having better heating attributes was extremely beneficial in the heating-dominated Louisville climate. Other climates could offer differing results.

For future studies, simulations are needed to investigate a wider range of climate

types to verify whether M control is always the preferred strategy for the SS and the CS, and whether climates and process controls exist for higher ambient energy fractions.

Also, additional studies should test the effect of switch-over dates for the seasonal control strategy and investigate the temperature set points that are most beneficial based on the climate.

## CHAPTER V ACTIVE CONTROL OF PASSIVE SYSTEMS FOR HEATING AND COOLING OF BUILDINGS

### **5.1. INTRODUCTION**

With the effects of climate change increasingly present, new ways are needed to alleviate the energy usage and environmental impacts of buildings, which comprise a large fraction of overall global energy demand and carbon production. Passive heating systems have a long history of development and applications, and passive cooling systems are receiving increasing attention in the research community, particularly those using sky radiative cooling. Combining passive heating and cooling presents challenges for appropriate operation of the two systems for thermal comfort, particularly during transitions between heating and cooling seasons and during unseasonable weather. This paper investigates the potential of integrating active control into these otherwise passive systems.

#### **5.1.1. Passive Heating and Cooling**

Passive building design has been implemented in a number of ways in previous studies. Critical features of traditional passive building design include greater insulation in the building envelope, controlled ventilation, thermal mass and solar gain through efficient windows, including shading devices and day lighting. This first level of passive design focuses primarily on managing losses and gains from the space to the surrounding

environment. Additionally, specific heating and cooling systems that harvest energy from the sun and other ambient sources may be added to the building. [Albayyaa et al., 2019]. Although not all are entirely passive systems, research on combined solar heating (SH) and sky cooling (SC) collectors is increasing. Through nocturnal radiant cooling, energy is radiated from the building (through the atmospheric window of transmittance of long-wave radiation) to the sky [Matsuta et al.,1987]. Wang et al. [2008] designed a tilted radiant panel as part of a solar heating and sky cooling system to absorb solar heat and dissipate heat to the sky. For a one-cover system in which polycarbonate and polyethylene film were used as covers, the maximum heat collecting efficiencies were 75% and 72%, the daily average heat collecting efficiencies were 61% and 58% and the cooling capacities were 50 W/m<sup>2</sup> and 36 W/m<sup>2</sup>, respectively. Yong et al. [2015] developed a small scale experimental solar heating and sky cooling panel system. For January in Tianjin, China, the daily average heat-collecting efficiency was 39% with the maximum of 65%, while during hot seasons the average cooling capacity reached 87 W/m<sup>2</sup>. When two different acrylic acid resin coatings were sprayed on the system, the daily average heat-collecting efficiencies were 39% and 27%, and had a cooling capacity of 30 W/m<sup>2</sup>. Hu et al. [2019] studied a hybrid photo-thermal and radiative cooling collector panel. The thermal efficiency at zero reduced temperature and cooling efficiency at zero dimensionless temperature difference were 63.0% and 58.3%, respectively under clear sky condition. The collector achieved a net radiative cooling flux of 55.1 W/m<sup>2</sup> on a clear night. Although the previously outlined research [Hu et al., 2019] used passive techniques to harvest energy, for the most part the subsystems used active

means to heat or cool the space. This study focuses on a completely passive heating and cooling system.

Hoy-Yen Chan et al. [2010] provided a review of individual passive systems used for either solar heating or sky cooling, with some integrated systems that both heat and cool. Spanaki et al. [2011] and Sharifi et al. [2015] provided reviews of roof ponds as a means of passive heating and cooling. Roof ponds provide cooling through evaporation and by long-wave radiation to the night sky. Heat is dissipated from the indoor space below the roof pond by conduction, convection and radiation. Roof ponds can also be used for passive heating during the winter. During the daytime, the pond is exposed to solar radiation and the thermal storage capacity of water is utilized to store solar energy in the pond as sensible heat. During nighttime, the pond is covered by insulating panels. Trombe or Trombe-Michel walls, solar chimneys, and solar roofs [Moghasemi and Vadiiee, 2018] can be used as multifunctional passive systems. A MATLAB-simulated passive system developed by Sameti & Kasaeian [2015] used a lumped-capacitance model of a passive heating and cooling thermal storage wall in the Louisville, KY, climate. The storage tank in the model was heated by solar radiation and cooled by night sky radiation. The authors concluded that 54% of annual heating demand and 53% of annual cooling demand could be supplied by the simulated passive system. In previous research, Parsons and Sharp [2019], simulated a passive solar heat pipe (for heating) and sky radiator (for cooling) system (SHP-SR) in the Louisville, KY, climate. Heat pipes transferred heat through the phase change of a working fluid. When a heat source is applied (for heating, the heat source is solar radiation and for cooling, the heat source is the indoor space) the fluid vaporizes and rises to the opposite end of the pipe. The fluid

then rejects the latent heat to an external heat sink (for heating, the heat sink is a storage tank and for cooling, the heat sink is the sky). With no external force required for pumping the fluid, heat pipes work as a completely passive system. In this study, the same SHP-SR system is simulated with differing control strategies and performance is evaluated.

### **5.1.2. Building Controls**

It is widely known that adding controls alone to a building can significantly decrease its energy usage. Previous studies have shown that intelligent controllers can reduce energy consumption from 7% to 50% [Afram et al. 2017]. Effective functioning of a building control system can lead to better occupant comfort and health, increased energy efficiency, increased equipment life cycle, reduced maintenance costs and reduced down time. Dynamic data-driven models are especially useful, as more advanced building controllers now use numerous input variables for smart decision making to ensure a building can operate efficiently. One objective of this project is to determine whether passive systems can similarly benefit from smart building controls to reduce the heating and cooling load and improve occupant comfort.

Three main types of advanced building control have been categorized: adaptive control, optimal control, and model predictive control. Adaptive control is characterized by adjustment of model parameters based on observed building response. Optimal control is based on the principle of maximizing or minimizing one or more system performance variables (for example, maximizing user comfort while minimizing costs), and model predictive control predicts future states of the system to deduce a beneficial sequence of

control states over a prediction horizon in the presence of disturbances and constraints [Killian & Kozek, 2016]. Numerous reviews have been presented on control methods for HVAC systems with emphasis on model predictive control (MPC) [Rossiter, 2003, Privara et al., 2011, Afram & Janabi-Sharifi, 2014, Afram et al., 2017]. The benefits of MPC control arise from exploiting predictions that accommodate stochastic disturbances, such as ambient temperature and solar radiation [Oldewurtel et al., 2012]. One of the essential contributors to successful MPC control is a well-identified model of the building. According to the knowledge of the MPC system utilized to formulate the models, the model-based supervisory control can be further divided into white box (physical model-based) control, black-box (phenomenologically based) control and gray-box (partially model-based) control [Wang & Ma, 2008]. Fouquier Aurélie, et al. [2013] gave an overview of these three approaches to system modeling for building load analysis. These methods are used in building load forecasting with an aim to quantify the improvements that could be made by using different control designs. For this study, the potential benefits of combining passive heating and cooling to reduce both heating and cooling loads for a building are readily evident. However, the effectiveness of different control strategies to maximize the performance of the combined system, particularly if components such as thermal storage are shared between the two subsystems, has not been investigated. This study uses a “white box” approach using a prediction horizon of 1-24 hour(s) for control.

### **5.1.3. Objective**

This study intends to compare control strategies for two configurations of the system, one with separate heating and cooling subsystems and another with combined subsystems, in the Louisville, KY, climate. The Combined System operates with a single thermal mass connected to a dual-purpose solar absorber/sky radiator. For the Combined System actively controlled attributes of the heat pipe tilt angle and optical properties of the cover were assumed for this simulation when switching mode (heating to cooling or cooling to heating). The Separate System consists of a sky radiator and thermal mass separate from the solar absorber and its thermal mass. Four different control strategies are simulated, Ambient temperature, Heating and cooling load, Room/Ambient temperature and Auxiliary load, with two strategies, Heating and cooling load and Auxiliary load, simulated over multiple prediction horizons.

## **5.2. METHODS**

### **5.2.1. MATLAB Computer Simulation**

The systems were simulated by two thermal networks [Parsons & Sharp, 2019] (Figure 31). The nodes for the passive heating system include an absorber plate, the condenser and evaporator ends of the heat pipe, a thermal storage fluid (water), the tank wall, room, and the ambient air. Heat transfer between the nodes included solar flux through the cover to the plate, conduction from plate to heat pipe, two-phase heat transfer through heat pipe, natural convection from pipe to storage (water) and from water to tank wall, natural convection and radiation from tank wall to room, and overall heat loss from room to ambient. The passive cooling system model was expanded from the heating

system to include nodes for the cover and for sky temperature. Condensation was simulated for the cooling system only and occurs on the cover when the cover temperature is equal to the dew point temperature of ambient air. Typical Meteorological Year (TMY3) weather data for Louisville, KY (cool humid climate), is used in the simulations, and auxiliary heating and cooling was applied as needed to limit room temperature to a maximum of 23.9°C and a minimum of 18.3°C. This algorithm for heating was modeled and validated by experimental results from Robinson, et al. [2013] in heating. The cooling model is a theoretical model the same as Parsons & Sharp [2018a].

Figure 31 displays the nodal diagrams for equations 107-109. The calculated heat transfer rate,  $q_{ij}$  per unit of collector area between nodes  $i$  and  $j$  is calculated using

$$q_{ij} = k_{ij}(T_j - T_i) \quad (107)$$

where  $k_{ij}$  is the heat transfer coefficient between nodal temperatures  $T_i$  and  $T_j$ ,

respectively. The energy balance for the  $i^{th}$  node is

$$m_i \frac{dT_i}{dt} = \sum_j (k_{ij}(T_j - T_i)) + E_i \quad (108)$$

where  $m_i$  is the capacitance per unit collector area,  $E_i$ , is the solar energy received per unit collector area at the node and  $t$  is the time. Over a time step,  $\Delta t$ , equation 108

becomes

$$\left[ \frac{2m_i}{\Delta t} + \sum_j k_{ij} \right] T_i - \sum_j k_{ij} T_j = \frac{2m_i T_{i-1}}{\Delta t} + \sum_j [k_{ij}(T_{j-1} - T_{i-1})] + [E_i + E_{i-1}]$$

where the  $-1$  subscript denotes the previous time step. All the nodes were solved concurrently as functions of time from a set of initialized temperatures. Some heat transfer coefficients were dependent on the nodal temperature. To calculate these coefficients, multiple iterations were performed to solve for the value. Conductances, equation variables and nodal temperatures used in the thermal networks (Figure 31) are described in equations 111-136 below [Parsons & Sharp, 2019]. All variables used in the equations are defined in Table 12 (below) and Table 16 (located in the Appendix).

*Table 12. Description and baseline values of nodal temperatures and conductances.*

<b>Parameter Description</b>	<b>Variable</b>
Windscreen temperature $T_{1,R}$	$T_1$
(Radiator)/(Absorber) plate temperature $T$	$T_2$
Heat pipe (condenser)/(evaporator) end temperature $T$	$T_3$
Heat pipe (evaporator)/(condenser) end temperature $T$	$T_4$
Exposed heat pipe (evaporator)/(condenser) end temperature $T$	$T_{4*}$
Tank water temperature $T$	$T_5$
Tank wall temperature $T$	$T_6$
Room temperature $T$	$T_7$
Sky temperature $T$	$T_8$
Ambient temperature $T$	$T_9$
Solar flux (short and long wave radiation) to the radiator plate $E_{1,S}$	$E_{1H}$
Solar flux (short wave radiation) to the radiator plate $E_{1,R}$	$E_{1C}$
Solar flux (short wave radiation) to the windscreen $E_{2,R}$	$E_{2C}$
Natural convection and radiation from (plate to cover)/(cover to plate) $H,R$	$k_{12}$
Conduction from (plate to condenser)/(plate to evaporator) $H$	$k_{23}$
Conduction through insulation $H$	$k_{25}$
Two phase heat transfer from immersed (evaporator to condenser)/(condenser to evaporator) $H$	$k_{34}$
Two phase heat transfer from (exposed evaporator to condenser)/(condenser to evaporator) $H$	$k_{34*}$
Natural convection from (evaporator)/(condenser) to water $H$	$k_{45}$
Natural convection from (evaporator)/(condenser) to room $H$	$k_{4*7}$
Conduction through tank wall $H$	$k_{56}$
Natural convection and radiation $H$	$k_{67}$
Overall heat loss from room to ambient (LRR) $H$	$k_{79}$
Wind convection and long wave radiation from cover to ambient $H,R,C$	$k_{91}$
Long wave radiation from radiator plate to ambient $H,R,C$	$k_{92}$

Overall collector loss coefficient <sup>H,S</sup>	$k_{92}$
Long wave radiation from windscreen to sky <sup>H,R,C</sup>	$k_{81}$
Long wave radiation from radiator plate to sky <sup>H,R,C</sup>	$k_{82}$

T Indicates units of degrees Kelvin

E-Indicates units of  $W/m^2$

H- Indicates units of  $W/m^2-K$

C- Includes conduction through water layer when condensation is present

R-Indicates a sky radiator variable only

S-Indicates a solar heating variable only

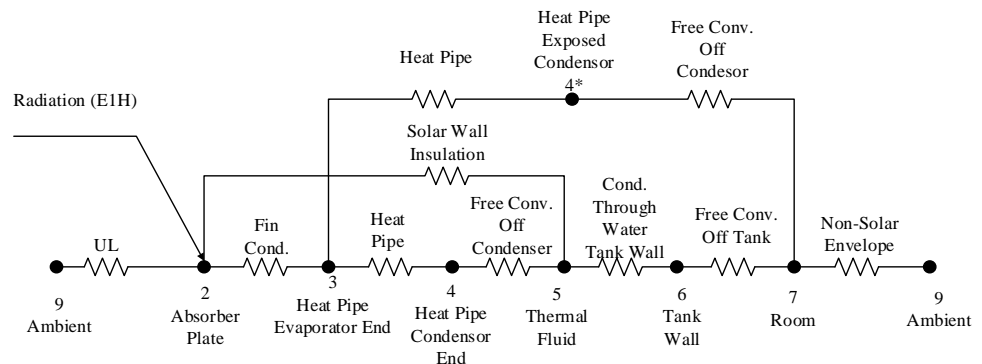
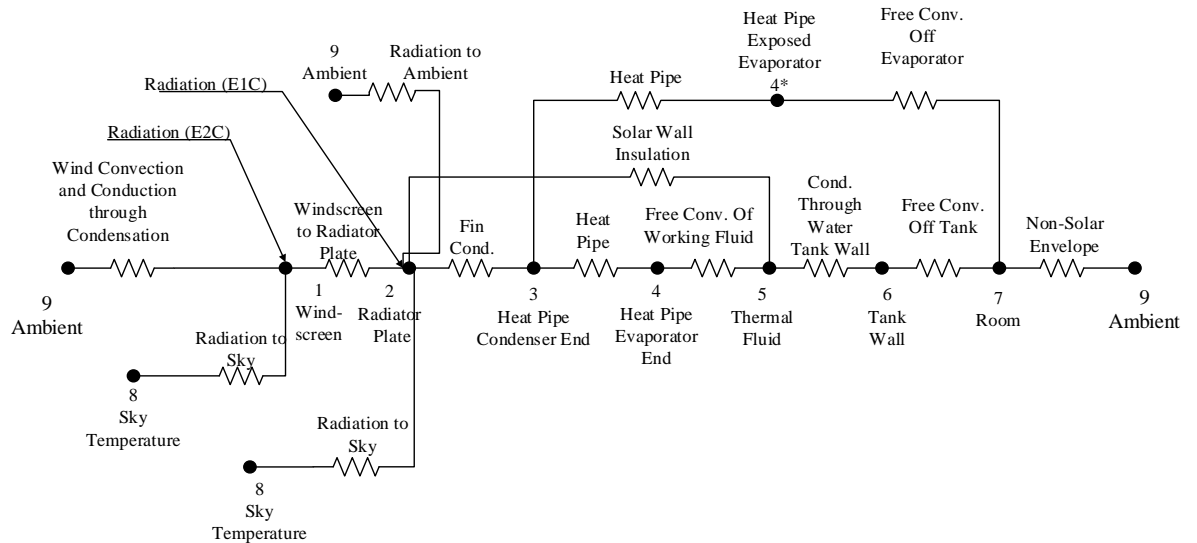


Figure 31. Nodal diagram depicting the calculations for thermal conductance for cooling (top) and heating (bottom) for a one cover system [Parsons & Sharp, 2019].

For radiative cooling, sky temperature was modeled by [Berdahl, *et al.* 1984]

$$T_8 = T_o [0.711 + 0.0056T_{dp,o} + 0.00037T_{dp,o}^2 + 0.013 \cos(15t)]^{\frac{1}{4}} \quad (110)$$

where  $T_8$  and  $T_o$  are the sky and outdoor dry-bulb temperatures in degrees Kelvin,  $T_{dp,o}$  is the outdoor dew-point temperature in degrees Celsius, and  $t$  is the number of hours from midnight.

For the conductances shown in Figure 31, each conductance term was normalized by the radiator area and included view factors where needed.

Conductances described in equations 111, 114-116, 118-119 and 123 are used for calculating the nodal conductances in cooling only, while equations 117 and 120 describe heating-only conductances as described in Table 12. For cooling, the conductance from ambient temperature to the outer windscreen including condensation (a cooling only parameter) is

$$k_{91} = \left( \left( \frac{1}{h_w} + \frac{L_{Cond}}{k_{Water}} \right)^{-1} + \tau_{Cond} e_{WS} \sigma (T_1^2 + T_9^2) (T_1 + T_9) \left( \frac{1 - \cos\beta}{2} \right) \right) \frac{A_{WS}}{A_{Rad}}. \quad (111)$$

The thickness of the condensation,  $L_{Cond}$ , was modeled after Pieters & Deltour [1997] as the maximum condensate film thickness on polyethylene. Without condensation, the  $k_{91}$  conductance term is calculated the same as equation 111, but without the water conductance and the condensation transmissivity terms. The wind heat transfer coefficient [Burch & Luna 1980] is calculated by first finding the wind velocity [Sherman & Modera, 1986]

$$V_j = WSV * \alpha_{Building} \left( \frac{H_{Building}}{H_{Tower}} \right)^{\gamma_{Building}} \quad (112)$$

Then the convection coefficient is

$$h_w = 2.8 + (4.8V_j) \quad (113)$$

The long-wave radiation from radiator to ambient through one cover is

$$k_{92} = \tau_{Cond} \tau_{ws} e_{Rad} \sigma (T_2^2 + T_9^2) (T_2 + T_9) \left( \frac{1 - \cos\beta}{2} \right) \frac{A_{Rad}}{A_{Rad}}. \quad (114)$$

The far infrared radiation from the windscreen to the sky is

$$k_{81} = \tau_{Cond} e_{WS} \sigma (T_1^2 + T_8^2) (T_1 + T_8) \left( \frac{1 + \cos\beta}{2} \right) \frac{A_{WS}}{A_{Rad}}. \quad (115)$$

Similarly, the far infrared radiation from radiator to sky through one cover is

$$k_{82} = \tau_{Cond} \tau_{ws} e_{Rad} \sigma (T_2^2 + T_8^2) (T_2 + T_8) \left( \frac{1 + \cos\beta}{2} \right) \frac{A_{Rad}}{A_{Rad}}. \quad (116)$$

As in the cooling nodal diagram, a conductance for the overall collector loss coefficient was calculated for heating as described in Duffie & Beckman [2013]. It was calculated as

$$k_{92} = \left[ \frac{N}{\frac{520(1 - 0.000051\beta^2)}{T_2} \left( \frac{T_2 - T_9}{N + (1 + 0.089h_w - 0.1166h_w e_{Rad})(1 + 0.07866N)} \right)^{0.430 \left( 1 - \frac{100}{T_2} \right)} + \frac{1}{h_w}} \right]^{-1} + \frac{\sigma (T_2 + T_9) (T_2^2 + T_9^2)}{\frac{1}{e_{Rad} + 0.00591N h_w} + \frac{2N + (1 + 0.089h_w - 0.1166h_w e_{Rad})(1 + 0.07866N) - 1 + 0.133e_{Rad} - N}{e_{WS}}}$$

(117)

The solar absorption of the windscreen and radiator was calculated from the model of Hay, Davies, Klucher and Reindl (HDKR) [Duffie & Beckman, 2013]. The solar flux (short-wave radiation) to the windscreen is

$$E_{2C} = (I_b + I_d A_i) R_b \alpha_{b_{WS}} + (I_d (1 - A_i) \alpha_{d_{WS}} \left( \frac{1 + \cos(\beta)}{2} \right) \left( 1 + f \sin^3 \left( \frac{\beta}{2} \right) \right) + I \rho_g \alpha_{g_{WS}} \left( \frac{1 - \cos(\beta)}{2} \right).$$
(118)

The solar flux (short-wave radiation) through a single polyethylene windscreen to radiator plate for cooling is

$$E_{1C} = (I_b + I_d A_i) R_b (1.01 \tau_b \alpha_b)_{WS} + (I_d (1 - A_i) (1.01 \tau_d \alpha_d)_{WS} \left( \frac{1 + \cos(\beta)}{2} \right) \left( 1 + f \sin^3 \left( \frac{\beta}{2} \right) \right) + I \rho_g (\tau_g \alpha_g)_{WS} \left( \frac{1 - \cos(\beta)}{2} \right),$$
(119)

and the solar flux (short wave radiation) through a single glass windscreen to the radiator plate in heating is

$$E_{1H} = (I_b + I_d A_i) R_b (1.01 \tau_b \alpha_b)_{WS} + (I_d (1 - A_i) (1.01 \tau_d \alpha_d)_{WS} \left( \frac{1 + \cos(\beta)}{2} \right) \left( 1 + f \sin^3 \left( \frac{\beta}{2} \right) \right) + I \rho_g (\tau_g \alpha_g)_{WS} \left( \frac{1 - \cos(\beta)}{2} \right),$$
(120)

where  $A_i$ ,  $f$  and  $R_b$  are calculated based on equations in Duffie & Beckman [2013]. The factor 1.01 approximates the effect of multiple reflections. Isotropic beam radiation is

$$I_b = I - I_d .$$
(121)

The beam short-wave transmittance,  $\tau_b$ , was calculated using derived expressions from Fresnel [Duffie & Beckman 2013] for the reflection of un-polarized radiation passing from medium 1 with refractive index  $n_1$  to medium 2 with refractive index  $n_2$ . When condensation is not present, medium 1 is air, and medium 2 is the windscreen. When condensation occurs, medium 1 is water.

$$\tau_b = \exp\left(-\frac{KL}{\cos\theta_2}\right) 0.5 \left( \frac{1 - \frac{\tan^2(\theta_2 - \theta_1)}{\tan^2(\theta_2 + \theta_1)}}{1 + (2N - 1) \frac{\tan^2(\theta_2 - \theta_1)}{\tan^2(\theta_2 + \theta_1)}} + \frac{1 - \frac{\sin^2(\theta_2 - \theta_1)}{\sin^2(\theta_2 + \theta_1)}}{1 + (2N - 1) \frac{\sin^2(\theta_2 - \theta_1)}{\sin^2(\theta_2 + \theta_1)}} \right). \quad (122)$$

Beam absorptivity,  $\alpha_b$ , for the windscreen (polyethylene for cooling and glass for heating) and radiator, diffuse and ground-reflected transmittance or radiation ( $\tau_d$  and  $\tau_g$ ), diffuse and ground-reflected absorption of radiation ( $\alpha_d$  and  $\alpha_g$ ) and angle of refraction ( $\theta_1$  and  $\theta_2$ ) were calculated from Duffie & Beckman [2013]. The conductance between the windscreen and the radiator, a cooling only conductance, includes both radiation and convection

$$k_{12} = \frac{k_{Air} Nu_{Air}}{L_{W-R}} \left( \frac{A_{WS}}{A_{Rad}} \right) + \left( \frac{1}{\frac{1}{e_{Rad}} + \frac{1}{e_{WS}} - 1} \right) \sigma (T_1^2 + T_2^2) (T_1 + T_2) \left( \frac{A_{WS}}{A_{Rad}} \right), \quad (123)$$

where the Nusselt number is a function of Rayleigh number and tilt angle as found in experiments by Hollands, *et al.* [1976]

$$Nu_{Air} = 1 + 1.44 \left[ 1 - \frac{1708(\sin 1.8\beta)^{1.6}}{Ra_{Air} \cos\beta} \right] \left[ 1 - \frac{1708}{Ra_{Air} \cos\beta} \right]^+ + \left[ \left( \frac{Ra_{Air} \cos\beta}{5830} \right)^{\frac{1}{3}} - 1 \right]^+, \quad (124)$$

where the meaning of the + exponent is that only positive values of the terms in the square brackets are used. Zero is used if the term is negative. The Rayleigh number is

$$Ra = \frac{g\beta' \Delta T L_X^3}{\nu \alpha}. \quad (125)$$

The remaining conductance equations, 126-133, describe nodal conductances for both the heating and cooling systems. An equation developed by Susheela & Sharp [2001] is used for the conductance between the radiator plate and the condenser end of the heat pipe

$$k_{23} = \left( \frac{1}{\frac{1}{3k_{Rad}L_{Rad}} \left( \frac{W_{HP} - OD_{HP}}{2} \right)^2} \right) N_{fins} \left( \frac{A_{HP}}{A_{Rad}} \right). \quad (126)$$

The conductance of the heat pipe from condenser to evaporator end in the thermal storage fluid is [Susheela & Sharp, 2001]

$$k_{34} = 0.04 \left( N_{HP,room} \left( \frac{k_{HP}}{L_{HP}} \right) \left( \frac{A_{HP}}{A_{Rad}} \right) + N_{HP,tank} \left( \frac{1}{R_{Evap} + R_{Cond}} \right) \frac{1}{A_{Rad}} + \frac{k_{Insul}}{L_{Insul}} \left( \frac{A_{Insul}}{A_{Rad}} \right) \right). \quad (127)$$

The conductance of the heat pipe from condenser to evaporator end exposed to room air is [Susheela & Sharp, 2001]

$$k_{34*} = 0.25 \left( N_{HP} \left( \frac{k_{HP}}{L_{HP}} \right) \left( \frac{A_{HP}}{A_{Rad}} \right) + N_{HP} \left( \frac{1}{R_{Evap} + R_{Cond}} \right) \frac{1}{A_{Rad}} + \frac{k_{Insul}}{L_{Insul}} \left( \frac{A_{Insul}}{A_{Rad}} \right) \right). \quad (128)$$

The convective conductance between the heat pipe evaporator end and thermal storage fluid is

$$k_{45} = \frac{N_{HP,Tank} k_{Water} Nu}{OD_{HP}} \left( \frac{A_{Evap}}{A_{Rad}} \right), \quad (129)$$

where the Nusselt number for the fluid in the tank is

$$Nu = \left( 0.60 + \frac{0.387Ra^{\frac{1}{4}}}{\left( 1 + \left( \frac{0.559v}{\alpha} \right)^{\frac{9}{16}} \right)^{\frac{8}{27}}} \right)^2, \quad (130)$$

where the Rayleigh number is calculated using equation 125. For the heat pipes exposed to the room, the convective conductance is

$$k_{47*} = \frac{N_{HP,Room} k_{Air} Nu}{OD_{HP}} \left( \frac{A_{Evap}}{A_{Rad}} \right), \quad (131)$$

where the Nusselt and Rayleigh numbers are calculated using equations 124 and 125, respectively. The conduction through the tank wall is

$$k_{56} = \frac{k_{Tank}}{L_{Tank}} \left( \frac{A_{Tank}}{A_{Rad}} \right). \quad (132)$$

The conductance due to convection and radiation from the tank wall to the room is

$$k_{67} = \frac{N_{Tank} k_{Air} Nu}{L_{Tank*}} \left( \frac{A_{Tank}}{A_{Rad}} \right) + e_{Tank} \sigma (T_6 + T_7) (T_6^2 + T_7^2) \left( \frac{A_{Tank}}{A_{Rad}} \right), \quad (133)$$

where the Nusselt number for the top and bottom of the tank [Susheela & Sharp, 2001]

and vertical sides [Bergman et al., 2011] are

$$Nu_{Sides} = 0.68 + \frac{0.670Ra^{\frac{1}{4}}}{\left( 1 + \frac{0.492}{P^{\frac{1}{16}}} \right)^{\frac{4}{9}}}, \quad Ra < 10^9$$

$$Nu_{Sides} = \left( 0.825 + \frac{0.387Ra^{\frac{1}{6}}}{\left(1 + \frac{0.492}{P^{\frac{9}{16}}}\right)^{\frac{8}{27}}}\right)^2, \quad Ra > 10^9$$
(134)

$$Nu_{Top} = 0.54Ra^{0.25}, \quad 10^4 < Ra < 10^7,$$

$$Nu_{Top} = 0.15Ra^{0.333}, \quad 10^7 < Ra < 10^{11},$$
(135)

$$Nu_{Bottom} = 0.27Ra^{0.25},$$
(136)

The Rayleigh number is calculated using equation 125 for each surface of the tank. The final conductance,  $k_{79}$ , is the overall heat loss from room to ambient, for which a constant value of  $10 \frac{W}{m^2 K}$  was used for all cases.

### 5.2.2. Ambient Energy Fraction

The load served by the passive system for heating and cooling was determined as a fraction of that based on a standard baseline indoor temperature of 18.3°C. Thus, the baseline rate of heat gain from outdoors to the room during the cooling mode is given by

$$\dot{q}_{CL,i} = (k_{79}(T_9 - 18.3^\circ C))^+$$
(137)

where  $k_{79}$  is the overall heat loss from room to ambient (LRR) and  $T_9$  is ambient temperature. Similarly, the baseline rate of heat loss from the room to outdoors while in heating mode is given by

$$\dot{q}_{HL,i} = (k_{79}(18.3^\circ\text{C} - T_9))^+ \quad (138)$$

The index  $i$  signifies that this calculation is performed for each hour of the simulation.

During the cooling mode, the contribution of the system to cooling the room from storage and from the exposed evaporator is

$$\dot{q}_{SR,Room,i} = (k_{67}(T_7 - T_6) + k_{47*}(T_7 - T_{4*}))^+ \quad (139)$$

In cooling mode the power supplied by radiator (neglecting ambient) is

$$\dot{q}_{SR,Rad,i} = (k_{82}(T_2 - T_8) - E_{1C})^+. \quad (140)$$

Thermal efficiency of the radiator in cooling was calculated by

$$\eta_{SR} = \frac{\dot{q}_{SR,Rad,i}}{\sigma A_{Rad}(T_2^4 - T_8^4)} \quad (141)$$

where  $A_{Rad}$  is the area of the radiator and cooling provided by ambient was neglected.

During the heating mode, the heat provided from storage and from the exposed condenser is

$$\dot{q}_{SHP,Room,i} = (k_{67}(T_6 - T_7) + k_{47*}(T_{4*} - T_7))^+. \quad (142)$$

In heating mode, the heat supplied by the absorber is

$$\dot{q}_{SHP,Abs,i} = (E_{1H} - k_{92}(T_2 - T_9))^+$$

(143)

Thermal efficiency of the absorber in heating was calculated by

$$\eta_{SHP} = \frac{\dot{q}_{SHP,Abs,i}}{E_{1H}A_{Abs}} \quad (144)$$

where  $A_{Abs}$  is the area of the absorber.

Auxiliary cooling is applied only when required to limit the indoor temperature  $T_7$  to a maximum of 23.9°C and is given by

$$\dot{q}_{Aux,C,i} = (k_{79}(T_9 - 23.9^\circ C) - \dot{q}_{SR,Room,i})^+, \quad (145)$$

and auxiliary heating is applied only when required to limit the indoor temperature to a minimum of 18.3°C

$$\dot{q}_{Aux,H,i} = (k_{79}(18.3^\circ C - T_9) - \dot{q}_{SHP,Room,i})^+. \quad (146)$$

The cooling, heating and auxiliary loads were summed over the entire year. The fraction of the total annual load served by the system is defined as the ambient energy fraction,

$$f = 1 - \frac{\sum_{i=1}^{8760} \dot{q}_{Aux,C,i} + \sum_{i=1}^{8760} \dot{q}_{Aux,H,i}}{\sum_{i=1}^{8760} \dot{q}_{CL,i} + \sum_{i=1}^{8760} \dot{q}_{HL,i}} \quad (147)$$

where 8760 is the number of hours in the year. The ambient energy fraction was used to signify the thermal performance of the passive system.

In addition to energy savings, passive systems can realize a significant cost savings. A review of the cost savings of the baseline system using the controls strategy with the results was included to quantify an estimated energy savings of the SHP-SR

system in Louisville, KY. Table 13 displays two types of rate structures used in the Louisville area by a service provider for residential and general service rate structures.

*Table 13. Louisville, KY Utility Electric Rate Structure*

<b>Residential Rate Structure</b>	
Energy Charge per kWh	\$0.09382
<b>General Service Rate Structure (&lt; 50kW)</b>	
Energy Charge per kWh	\$0.10297

### **5.2.3. System Configurations**

Two system configurations, Separate System (SS) and Combined System (CS) modeled after Parsons and Sharp [2019] (Figure 32), were compared in this study. The SS incorporates separate solar collector and sky radiator subsystems, each with its own thermal mass. Each thermal mass is fully insulated from the space until heating or cooling is needed. When heating or cooling is not needed, the tank continues to collect/reject heat from the ambient sources. For the CS, a single thermal mass is connected to another device that serves as both the solar collector and the sky radiator. For the CS, a passive mechanism was assumed that provides switching from heating to cooling functions as needed (including favorable design parameters for windscreen, radiator plate and heat pipe angles). For instance, a mechanism that changes the tilt of the heat pipe between the collector/radiator and thermal storage can serve this switching function. The slope of the CS radiator was fixed at Latitude +15°. Load to collector and load to radiator ratios are important and should be mentioned here. Additional design/optical parameters are listed in Table 16 of the Appendix.

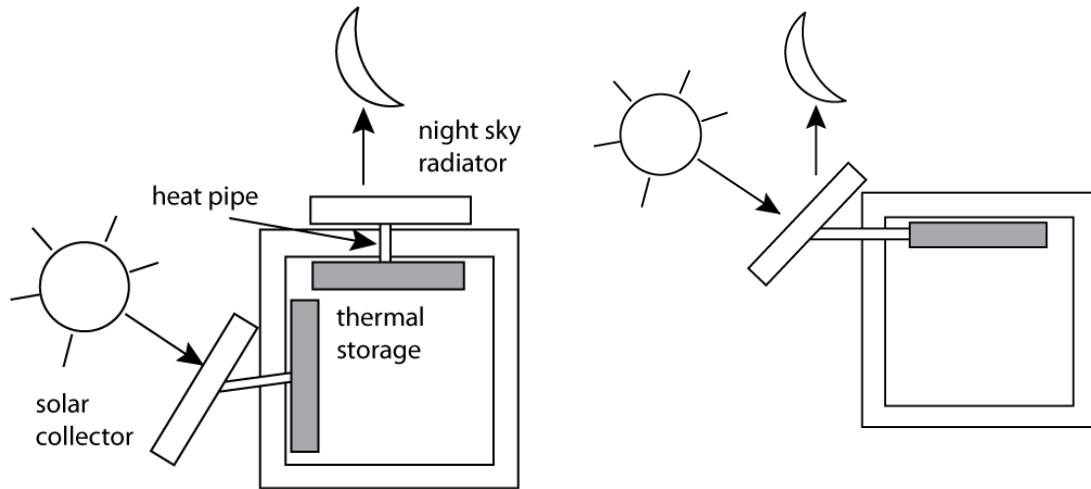


Figure 32. [Left] The SS configuration. [Right] The CS configuration with slope at latitude.

#### 5.2.4. Control Strategies

In previous work [Parsons and Sharp, 2019], three relatively simple control strategies (similar to a proportional derivative controller) and one, more complicated weighted decision strategy (adjustments of weighted model variables) were compared:

- An ambient temperature control strategy: Hourly heating/cooling decisions were based on whether ambient temperature was above or below 18.3°C
- A room temperature strategy: Hourly heating/cooling decisions were based on how close room temperature was to a set point (22.2°C)
- A seasonal control strategy: Hourly heating/cooling decisions were based on typical heating/cooling degree days for the month for the region simulated
- A weighted decision strategy: Hourly heating/cooling decisions were based on five weighted independent variables (24 hour forecasted high and average ambient temperature, current ambient temperature, time of day and typical heating and cooling month for the climate)

As expected, the weighted decision strategy provided higher ambient energy fractions than the other strategies. From that study, four enhanced decision strategies were developed for comparison:

- i. Ambient temperature (AT)
- ii. Heating and cooling load (BL)
- iii. Room/Ambient temperature (R/AT)
- iv. Auxiliary load (AUX)

The AT control strategy based the control on current and forecasted ambient temperature, as well as on the season (Figure 33). Specifically, the inputs were: current hourly ambient temperature, future 24-hour average ambient temperature, future 24-hour high ambient temperature, future 24-hour low ambient temperature and the seasonal month. Low-temperature thresholds of 12.8°C and 10°C were chosen instead of the baseline temperature (18.3°C) to prevent the system from going into heating at night during the summer (cooling season) months. These thresholds were based on multiple iterations to increase the ambient energy fraction. While the appropriate threshold values may be sensitive to the characteristics of the home and of the passive system, this control strategy is otherwise based only on external weather data.

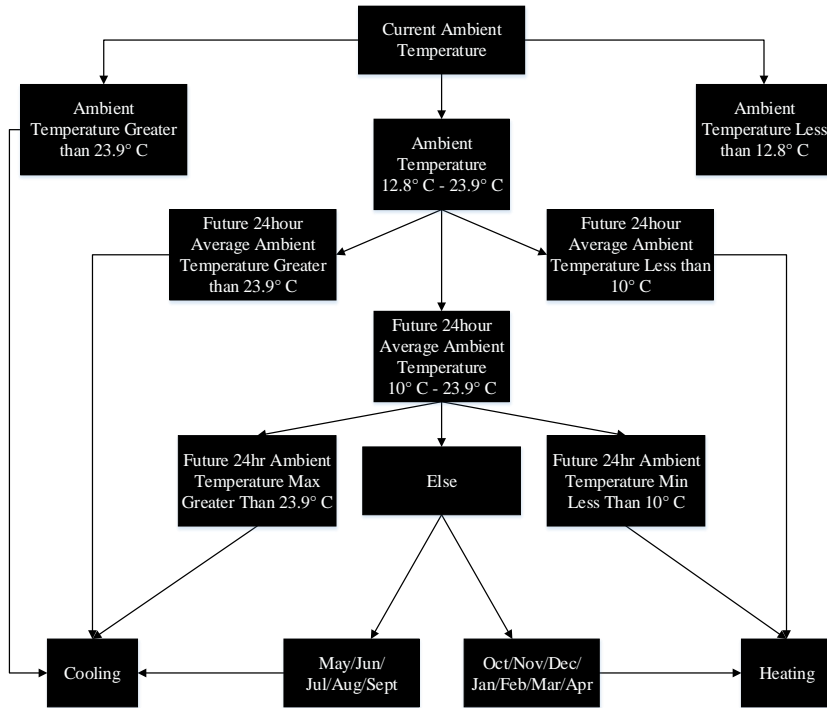


Figure 33. Ambient temperature (AT) implementation diagram

For the BL control, the cooling (equation 137) and heating (equation 138) loads were calculated using future time intervals of 1 hour, 6 hours, 12 hours, and 24 hours (Figure 34). For each time interval, the mode with the larger load is chosen. By using the baseline temperature, rather than the model-simulated room temperature, this strategy is based only on the weather data. It thus offers faster computations than model-based strategies.

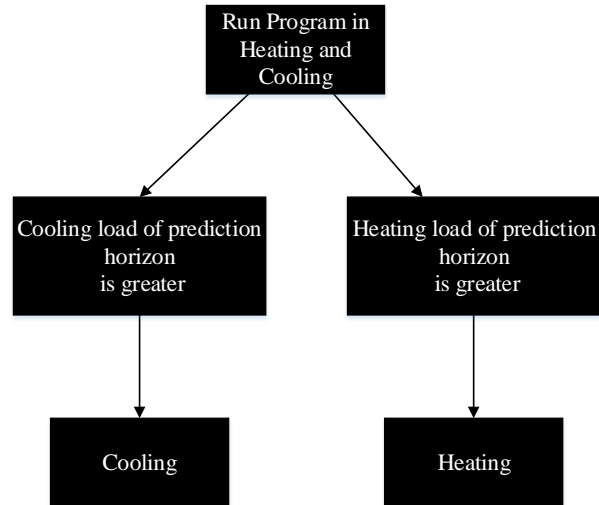


Figure 34. Building load (BL) implementation diagram.

The R/AT control modified the AT strategy by introducing model-simulated room temperature as a variable (Figure 35). The inputs for the partially model-based R/AT control included: future (1 hour) simulated room temperature, current hourly ambient temperature, future 24 hour average ambient temperature, and temperature difference of seasonal set point and future (1 hour) simulated room temperature. The control begins with two simulations, one in heating mode and the other in cooling mode. Only a prediction horizon of 1 hour was included. If the predicted room temperature is either above the upper comfort temperature or below the lower comfort temperature, heating or cooling is chosen, respectively. Otherwise, the mode may be chosen in intermediate steps based on ambient temperature similar to the AT strategy. Whereas the final step is purely seasonal for the AT strategy, the final step for the R/AT strategy compares the predicted room temperature to two seasonal set points. The set point for heating was 22°C (based on ASHRAE *Standard 55-1992* for optimum operative temperature during winter for a user with typical clothing and light sedentary activity) and for cooling was 23.9°C. (ASHRAE, *Standard 55-1992* suggests a set point of 24.5°C for the summer season,

assuming a user with light slacks and short sleeve shirt. However, since the room was limited to 23.9°C in this study, a set point of 23.9°C was used for a cooling hour.)

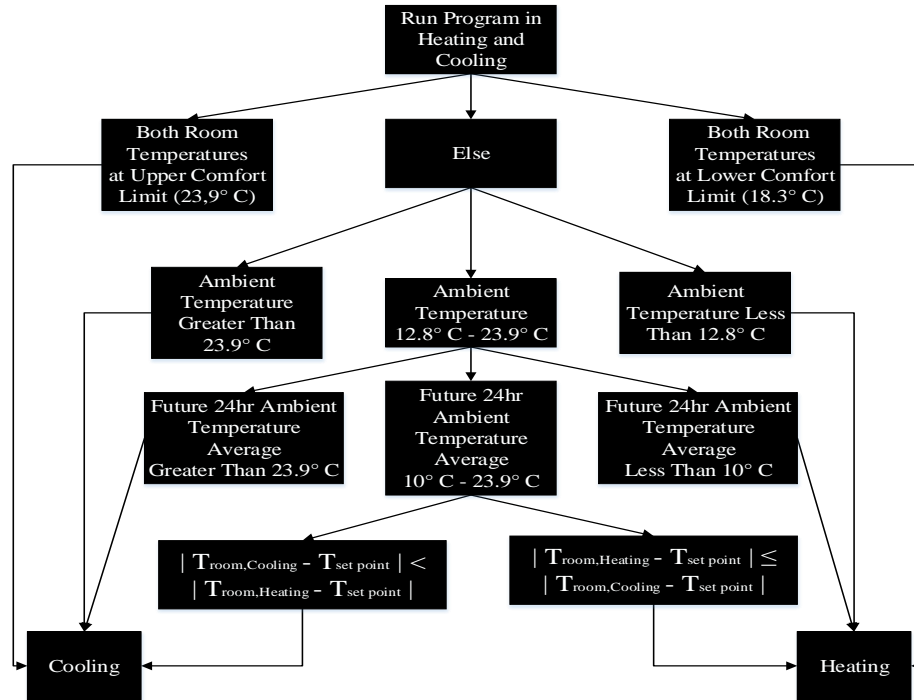


Figure 35. Room temperature (R/AT) implementation diagram.

The AUX strategy (Figure 36) was more fully model-based in that two simulations were run, one with the system in heating mode and the other in cooling mode, for prediction horizons of 1 hour, 6 hours, 12 hours, or 24 hours. The mode with the lowest auxiliary load was chosen. If the auxiliary was the same for each, a decision based on Louisville, KY, typical heating or cooling season was used. The most common condition for which the two auxiliary loads were the same was when both were zero (when the room temperature remained within the comfort limits for the for the entire time interval). For a short prediction horizon, the mode decision is thus often seasonal, but for longer times, auxiliary heating or cooling is more likely to be encountered, and the decision becomes more model-based.

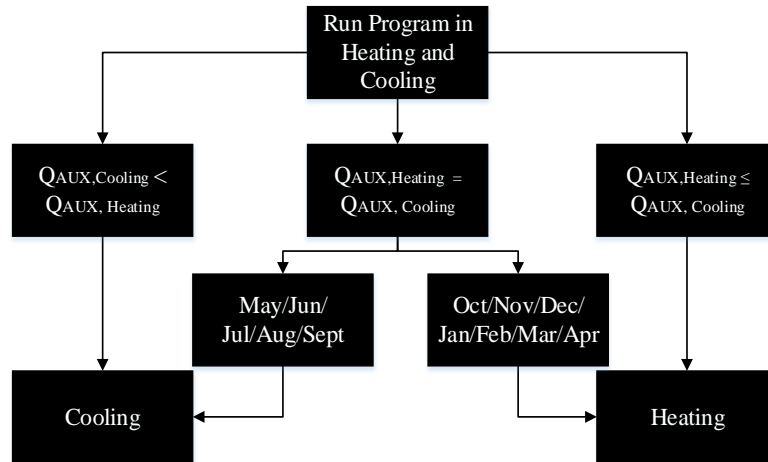


Figure 36. Auxiliary load (AUX) implementation diagram.

For all cases, auxiliary energy was added to maintain the room within comfort limits of 18.3°C to 23.9°C.

### 5.3. RESULTS AND DISCUSSION

#### 5.3.1. Annual performance of SS and CS

The SS performed only slightly better than the CS for control strategies other than AT (Figure 37). For the SS, the AUX-24HR strategy had the largest ambient energy fraction of 0.715. This strategy performed only 3% better than the BL-6HR strategy, which had the lowest ambient energy fraction for this strategy of 0.697. These small differences reflect the flexibility of the separate subsystems to independently heat and cool without substantial adverse impacts on the other subsystem. In particular, because the SS always harvests solar heat and sky cooling whenever possible to separate thermal storage units, the differences in performance among the strategies result from variation in

the decisions about when to deliver heat and cold to the room from each unit. When heating or cooling is delivered to the room, the temperature of the respective storage is affected, which has a secondary effect on its potential for collecting more energy. As is evident in Figure 37, this effect is small compared to the CS, which has only one storage unit. Decisions about whether to heat or cool storage have a much greater influence on performance. For instance, heating storage when cooling will be needed the following day may cause the storage temperature to be too high to provide the necessary cooling. The decisions that the different strategies make will be compared on an hour-by-hour basis in the next section.

Increasing the prediction horizon consistently increased the ambient energy fraction for the AUX control in both the CS and SS. For the AUX control, 6, 12 and 24-hour horizons yielded similar ambient energy fractions. Curiously, a 6-hour prediction horizon for the BL control produced a lower ambient energy fraction than 1-hour, and 12 and 24-hour horizons provided significant improvements. Considering that weather forecasts farther into the future have increased uncertainty, this suggests that AUX control may be more reliable. This result may also be climate dependent.

Similar to the SS, the AUX-24HR strategy had the largest ambient energy fraction (0.709) among all the CS cases. The AUX strategy again consistently increases ambient energy fraction with increasing prediction horizon. For the BL strategy, the ambient energy fraction for a 12 hour prediction horizon is slightly less than for 6 hours, again suggesting that the AUX strategy may be more reliable. Dissimilar from the SS, the CS strategy that performed the worst was the AT (0.589). This was due to the system being

in cooling mode significantly longer than the other models, despite Louisville, KY, being a heating dominated climate (Figure 38).

In previous work by Parsons and Sharp [2019], the maximum ambient energy fraction achieved for CS using a weighted decision strategy was 0.704. The AUX-24HR strategy improved the ambient energy fraction to 0.709. The revised strategy allowed the system to stay in cooling during cooler summer nights, and it extended the window of data used to make heating and cooling decisions.

In comparing the best performing control strategies of the SS and CS, the SS proved to perform only 1% better. With the CS and SS performing similarly, manufacturing a single system (CS) would require less initial costs than two separate systems, however a material would need to be developed that would allow the system's cover and radiator material to passively switch optical and radiative properties (similar to glass and polyethylene) and radiator tilt. Development of a mechanical system to accomplish the switch would also cause this to no longer be a passive system.

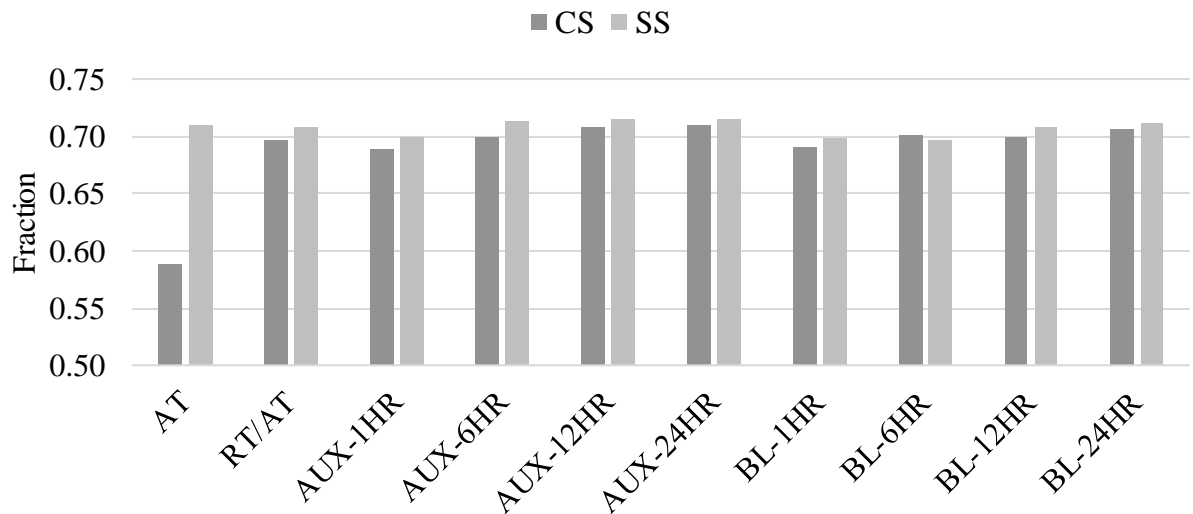


Figure 37. Ambient energy fractions for the differing SS control strategies in Louisville, KY.

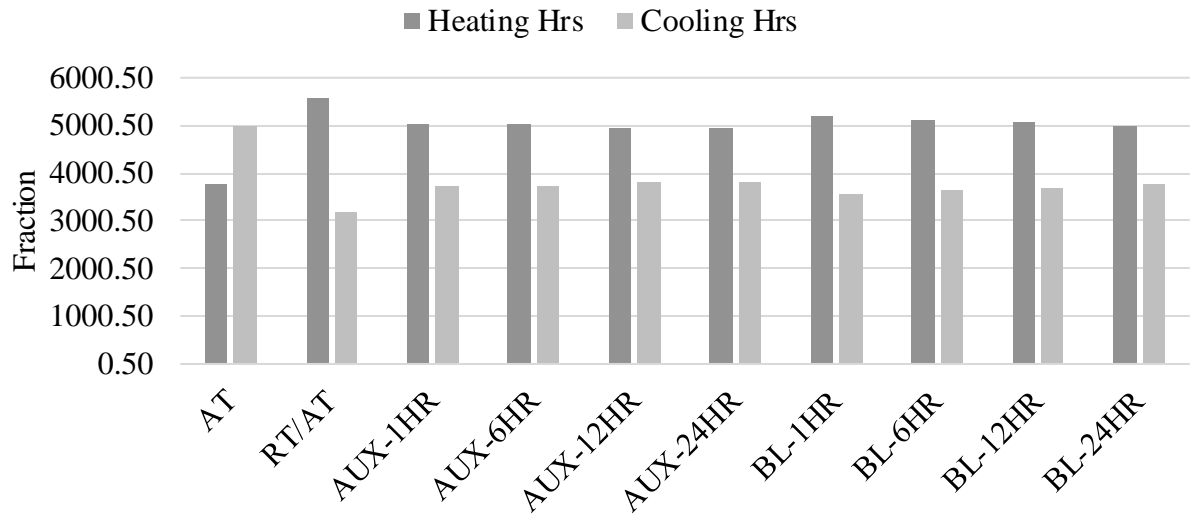


Figure 38. Heating and cooling hours for CS control strategies in Louisville, KY.

Along with performance, an additional consideration for this study was personal comfort. To assess this variable, the average annual temperature of each of the control strategies is shown in Figure 39, along with the standard deviation. As discussed in section 2.4, the optimal temperature for a winter season was taken as 22°C, and for the summer season a set point of 23.9°C was used. As expected, the control strategy that stayed closest to the limits was R/AT for both systems. Standard deviations for the simulations were similar for each control strategy, ranging from 0.91°C to 1.06°C. The largest deviation being CS-RT/AT and smallest SS-BL-1HR. With CS-RT/AT having the highest average temperature in a heating dominated climate it makes sense that the standard deviation for this control would be the largest. The upper and lower comfort limits for all strategies were 23.9°C and 18.3°C, respectively, which are evident in the figure.

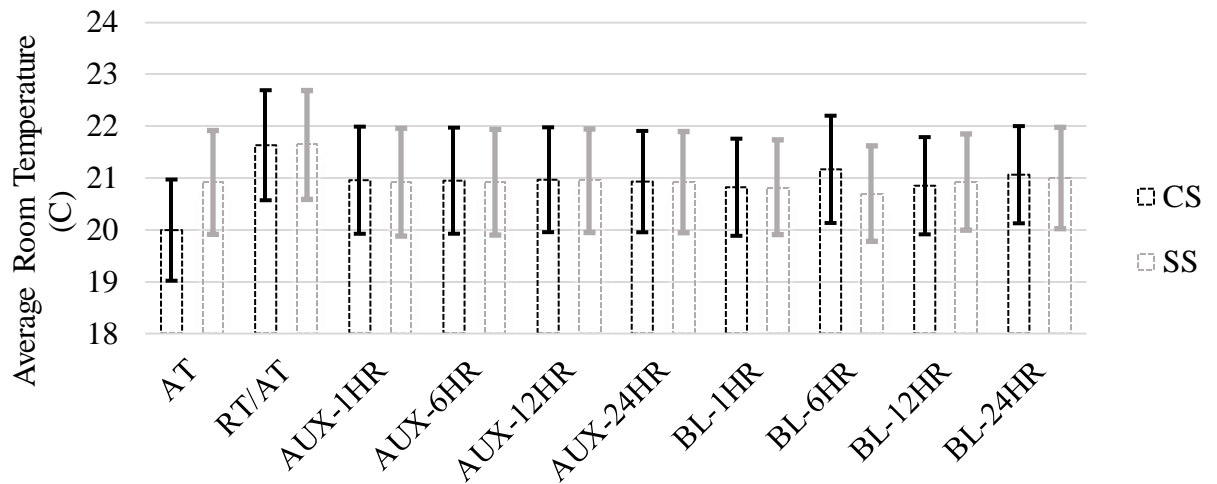


Figure 39. Average indoor temperatures and standard deviation ( $\sigma=0.5$ ) of the control strategies in Louisville, KY for SS and CS.

For most of the systems the average room temperature was approximately 21°C, which is cooler than both the seasonal set-point temperatures. Overall, most of the temperatures stayed within the low part the comfort limit range due to Louisville being a heating dominant climate, i.e., the space temperature drifted to the lower comfort limit (18.3°C) for much of the winter. The strategy (R/AT) that performed closest to the optimum seasonal temperatures had only a slightly lower energy fraction (1% less), so only a small tradeoff of decreased energy savings was necessary to achieve increased user comfort. This result exemplifies the need to match the objective function of the control strategy to the desired system performance variable.

Absorber and radiator efficiencies for the SS-AUX-24HR for January, a typical heating month for Louisville, KY, and July, a typical cooling month for Louisville, KY, are plotted in Figure 40 and 41, respectively. The peak absorber versus ambient

temperature difference in January reached 48°C, while the peak temperature difference between the radiator and sky reached 16°C, with a positive efficiency.

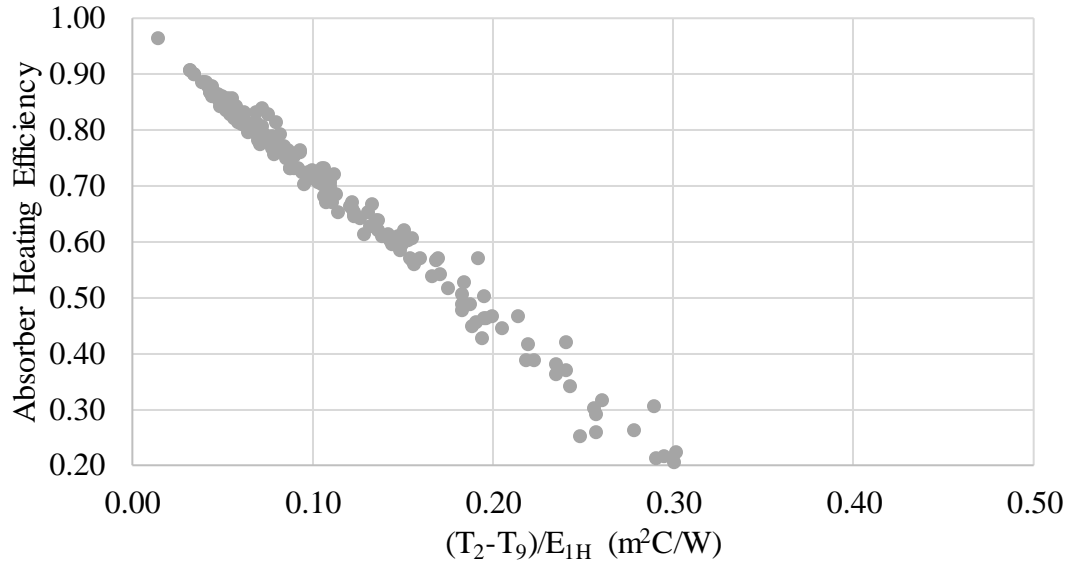


Figure 40. Absorber heating efficiency versus loss potential to insolation ratio in January of the SS-AUX-24HR.

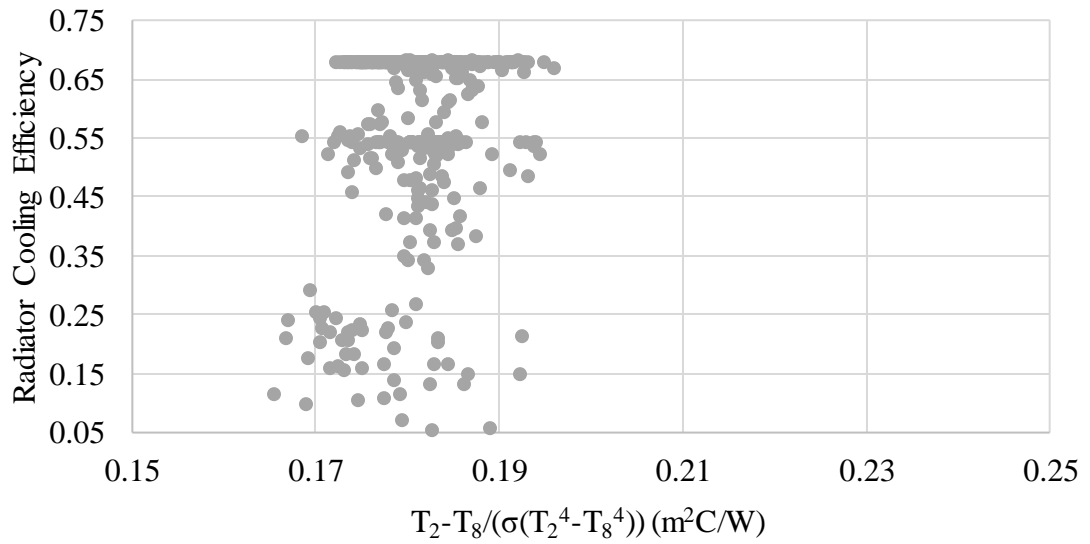


Figure 41. Radiator cooling efficiency in July of the SS-AUX-24HR at different sky-radiator temperature differences over black body radiation.

The results reported here can be compared to those of Hu et al. [2019], who studied a hybrid photo thermal and radiative cooling collector panel. The cooling efficiency for the collector at zero-dimensionless temperature (a concept proposed by Hu et al. [2019] to eliminate the effect of sky emissivity variation and temperature difference between the surroundings and water at the collector inlet for calculating cooling efficiency. The concept of dimensionless temperature is described as:

$$\tau = \frac{4(T_a - T_p)}{[1 - \varepsilon_s(T_a)]T_a}, \quad (148)$$

where  $T_a$  is ambient temperature,  $T_p$  is temperature of the panel, and  $\varepsilon_s$  is the emissivity of the sky) and cooling power was 58.3% and 55.1 W/m<sup>2</sup>, respectively. For the SHP-SR system in this study, the SS-AUX-24HR and CS-AUX-24HR control system obtained a maximum cooling efficiency and maximum power of 68%/68% and 54.9/45.6 W/m<sup>2</sup> at the radiator, for the month of July respectively, similar to Hu et al. [2019] hybrid heating and cooling system. For the both the SS-AUX-24HR and CS-AUX-24HR strategy in this study, a peak fluid tank temperature versus ambient temperature difference in January reached 38.8°C similar to a Hu et al. [2019] where a water tank temperature rise of 34.2K was cited.

Along with energy savings, an estimated cost savings was calculated. The cost savings provided in Table 14 only included the SS-AUX-24HR control and the energy rate structure for Louisville, KY (Table 13). As shown in Table 14 an annual cost savings between \$49-\$54/m<sup>2</sup> could be realized from the SHP-SR SS configuration. In other regions, additional demand charges, on peak and off peak energy rates, ratchet charges or power factor requirements may apply. For the Louisville, KY, region,

ambient energy fraction correlates directly with cost savings, thus optimization of the system control maximizes both simultaneously. However in regions with other rate structures, optimizing energy costs may require a distinctly different control strategy than for maximum ambient energy fraction. Most of the cost savings were during the heating season, which would be expected since Louisville, KY is a heating dominated climate.

*Table 14. Annual cost savings of SS-AUX-24HR passive system using Louisville, KY utility rate structures*

<i>Annual Residential Heating Cost Savings</i>	<b>\$44/m<sup>2</sup> USD</b>
<i>Annual Residential Cooling Cost Savings</i>	<b>\$5/m<sup>2</sup> USD</b>
<i>Annual General Service Heating Cost Savings</i>	<b>\$48/m<sup>2</sup> USD</b>
<i>Annual General Service Cooling Cost Savings</i>	<b>\$6/m<sup>2</sup> USD</b>

### **5.3.2. Hourly performance of CS**

Being able to forecast a change in heating or cooling was useful for the Louisville climate as shown by comparing the results of strategies that used model based inputs. The strategies BL (predicted building loads) and AUX (model-simulated auxiliary load) gave the highest ambient energy fractions of the control systems, 0.706 and 0.709 respectively. Despite AUX and BL having higher ambient energy fractions, it is important to note how well the R/AT model performed. The inputs for R/AT include: future (1 hour) simulated room temperature, current hourly ambient temperature, future 24 hour average ambient temperature, and temperature difference of seasonal set point and future (1 hour) simulated room temperature. Comparing this strategy to the AUX-1HR and BL-1HR it performed better than both while using only a 1 hour prediction window. It is important to note the R/AT used significantly less computing power than any of the AUX and BL models with future predictions longer than an hour.

An interesting finding from the simulations is the performance of the AUX strategy compared to BL. CS-AUX-24HR and CS-BL-24HR both use a prediction horizon of 24 hours and yielded ambient energy fractions were not significantly different for the CS (Figure 40). Therefore, the expectation might be that the two controls would perform similar on an hourly basis. However, the hourly decisions during the mild months were considerably different (Figure 42). The AUX control default is to heat during the month of March, however the warm ambient temperatures keep the system in cooling (hour 14 of first day to hour 17 of second day) until it recognizes a future decrease in ambient (hour 16 of March 25th to hour 7 of March 26th) and accounts for it. The BL control, despite a heating load (when ambient is below 18.3°C) between hour 22 of March 25th and hour 8 of the next day, calculates that the overall cooling load is greater for the 24 hour period and remains in cooling mode entirely. Although these two control strategies make different heating/cooling decisions for hour 18 of the first day to hour 10 of the second day, which reduces the downward drift of the room temperature for the AUX strategy compared to BL during this period, neither requires auxiliary energy during these two days. Though not shown in this plot, the AUX decisions made during the transition months (March, April, May, September, October and November) allows the system to stay within the upper and lower comfort temperature limits longer than the other strategies, which yields the highest ambient energy fraction.

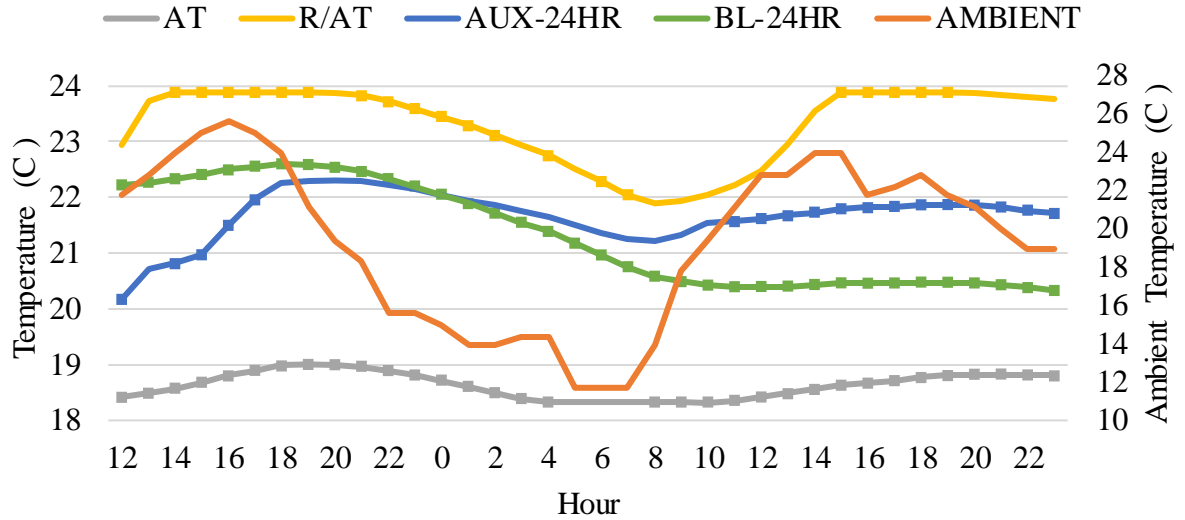


Figure 42. A 36 hour period in March (25-26th) of AT, R/AT, BL-24HR, and AUX-24HR room temperatures compared to ambient temperature of CS.  
 \*Markers indicate a cooling hour

Figure 42 also displays some of the drawbacks of the AT and R/AT control strategies. The AT control goes into cooling too soon in the spring, resulting in the room temperature being close to the lower comfort limit at the beginning of the plot. Throughout the afternoon of March 25, the AT strategy remains in cooling mode. Having not appropriately anticipated the sharp decrease in ambient temperature during the night of March 25, the AT strategy requires auxiliary heating during the early morning hours 5 to 7 of March 26. For the R/AT option, the opposite is true, the system tends to be in heating, and begins during this time interval near the upper comfort temperature limit. The system stays in heating too long, which leads to auxiliary cooling during hours 14 to 19 on March 25 and again during hours 15 to 19 on March 26.

For the CS, the importance of being able to anticipate large swings in temperatures during transitional months is clear. October is generally a mild heating month for Louisville, KY, with the large swings in temperature from day to nighttime (Figure 43).

In Figure 43, the AUX-24HR strategy stays in heating for the entire 36-hour period, because in October the default for AUX is to heat. This allows for an elevated room temperature before entering the nighttime and better user comfort on a cooler night. Similar to Figure 42, the AT control struggles due to being in cooling too often. This is the only strategy that needs auxiliary energy during the time period shown. Despite R/AT not providing an ambient energy fraction as high as AUX-24, in Figure 43 it shows good control overall, keeping the temperature close to the optimal comfort set point (22.2°C). The BL-24 strategy tries to adjust for the sharp increase in ambient temperature between hours 10-16, but little cooling could be provided during the day.

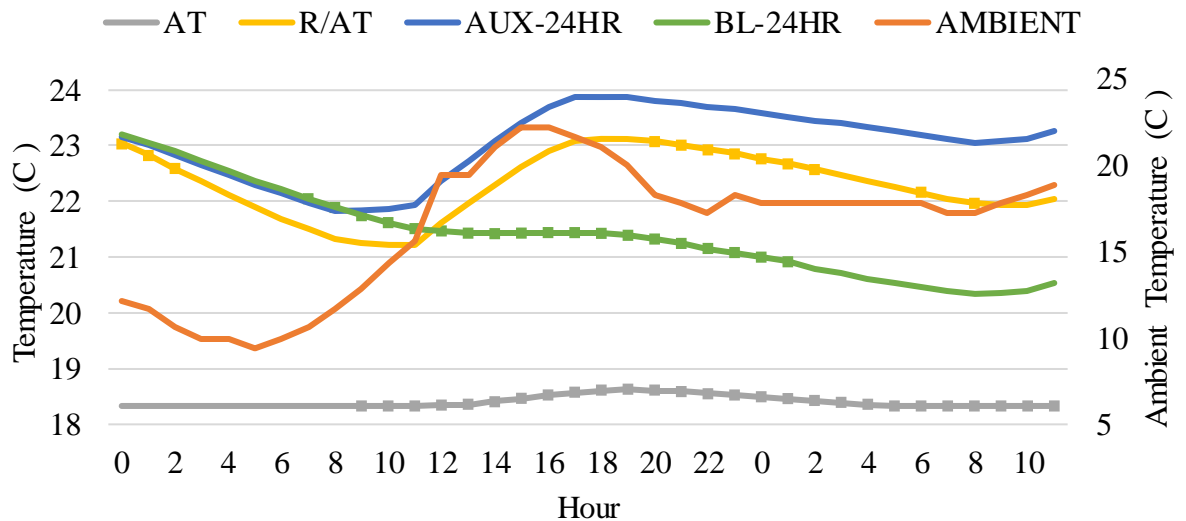


Figure 43. A 36 hour period in October (10-11<sup>th</sup>) of AT, R/AT, BL-24HR, and AUX-24HR room temperatures compared to ambient temperature of CS. \*Markers indicate a cooling hour

#### 5.4. CONCLUSIONS

For this study, with the Louisville, KY, climate simulated using a MATLAB model, the following conclusions were evident:

1. *For both SS and CS, the highest ambient energy fractions resulted with AUX-24HR control (0.715 and 0.709, respectively).*
2. *Differences in ambient energy fractions among the control strategies were small for SS, about 3% maximum. The type of control was more critical for CS, with about 20% maximum difference.*
3. *While the model-based AUX strategy provided the highest ambient energy fractions, the BL control gave nearly as good performance with less computational time for the same prediction horizon. However, the AUX strategy more reliably increased ambient energy fraction with increasing prediction horizon.*
4. *SS performed better than CS in all simulations, however, only about 1% better for strategies other than AT. Since the performances for the better strategies are similar, the lower cost of manufacturing a single system (CS) may provide more economical results.*
5. *For Louisville, KY, energy rates, cost savings of \$49-\$54 USD per square meter are possible with SS and AUX control.*

This study motivates a number of future investigations. Perhaps the most important is comparing the relative performance of control strategies across different climates, which have different ratios of heating to cooling loads, different solar and sky radiation potential, including more or less reliability of these ambient energy sources, and different ambient temperature fluctuations. These climate characteristics may influence how well strategies work relative to others, as well as the prediction horizon that is most effective. The model in this study neglected internal heat gains and thermal mass in the room. These factors can be expected to influence the performance of the building, and may impact the relative effectiveness of the control strategies. In addition, errors in weather prediction, which were not included in this study, would likely reduce the performance of all control strategies and perhaps change relative performance.

## CHAPTER VI CONCLUSIONS

### 6.1. SUMMARY OF RESULTS

This study evaluated several design parameters in a passive sky radiator system and multiple control strategies for a combined heating and cooling passive system. For the initial studies of the sky radiator system (cooling only), key findings included:

1. *In the Louisville climate, LRR and thermal storage capacity had strong effects on performance. These influences are as expected, in light of the well-documented importance of load to collector area ratio (LCR) and thermal storage capacity in passive and active solar heating systems.*
2. *Radiator slope had a surprisingly small impact in Louisville. This effect may be different in other climates.*
3. *Though relative humidity is modeled to increase sky temperature, ambient temperature and solar flux had stronger effects.*
4. *The addition of a cover enhanced sky fractions relative to no cover in all 11 ASRAE climates in which improvements were possible. A second cover caused smaller improvements over one cover.*
5. *Reductions in long-wave transmittance by additional covers had less influence than the reduction in convective gains.*
6. *Sky fractions of 100% were possible in cities with small cooling loads (Rock Springs, Seattle, San Diego) and also in Denver, which has a moderate cooling load, but low humidity and large diurnal temperature swings. Sky fractions of over 50% were achieved in New Orleans and Houston and over 40% in Miami, which have high cooling loads.*

These results provide some initial insight into the significance of sky radiator design parameters and confirm the potential for a heat pipe augmented system used for passive

cooling of buildings by radiation to the sky. These studies motivate the importance of modeling an all season heat pipe system used for both heating and cooling. The important findings of the final studies on modeling an all season heat pipe system with eight differing control strategies for a combined system and a separate system include:

1. *For both SS and CS, the highest ambient energy fractions resulted with AUX-24HR control (0.715 and 0.709, respectively).*
2. *Differences in ambient energy fractions among the control strategies were small for SS. The type of control was more critical for CS.*
3. *SS performed better than CS in all simulations (as one would expect).*

## **6.2. ADDITIONAL RECOMMENDATIONS**

This study motivates a number of future investigations for the all season (heating and cooling) heat pipe system. These results show that having better heating attributes was extremely beneficial in the heating-dominated Louisville climate. However, other climates could offer differing results. Perhaps the most important is comparing the relative performance of control strategies across different climates, which have different ratios of heating to cooling loads, different solar and sky radiation potential, including more or less reliability of these ambient energy sources, and different ambient temperature fluctuations. These climate characteristics may influence how well the control strategies work relative to others, as well as the prediction horizon that is most effective.

Additionally, the sky radiator (cooling only) and all season heat pipe model in this study neglected internal heat gains and thermal mass in the room. These factors can be expected to influence the performance of the building, and may impact the relative

effectiveness of the control strategies. In addition, errors in weather prediction, which were not included in this study, would likely reduce the performance of all models and perhaps change relative performance of the sky radiator and all season heat pipe system.

## REFERENCES

- Afram, A., & Janabi-Sharifi, F. "Review of modeling methods for HVAC systems." *Applied Thermal Engineering*, 67(1-2), 507-519, 2014.
- Afram, A., Janabi-Sharifi, F., Fung, A. S., & Raahemifar, K. "Artificial neural network (ANN) based model predictive control (MPC) and optimization of HVAC systems: A state of the art review and case study of a residential HVAC system." *Energy and Buildings*, 141, 96-113, 2017.
- Albanese MV, Brehob EG, Robinson BS & Sharp MK. Simulated and experimental performance of a heat pipe assisted solar wall. *Solar Energy* 86:5:1552-62, 2012.
- Albayyaa, Haider, et al. "Energy Conservation in Residential Buildings by Incorporating Passive Solar and Energy Efficiency Design Strategies and Higher Thermal Mass." *Energy & Buildings*, vol. 182, 2019.
- Andretta A, Bartoli B, Coluzzi B & Cuomo V. Selective Surfaces for Natural Cooling Devices. *J Physics* 42:1:423-30, 1981.
- Athienitis AK & Ramadan H. Numerical model of a building with transparent insulation. *Solar Energy* 67:1-3, 101-9, 1999.
- Agrawal PC. Review of passive systems and passive strategies for natural heating and cooling of buildings in Libya. *Intl J Energy Res* 6:2:101-17, 1992.
- ASHRAE, Standard 55-1992: Thermal Environmental Conditions for Human Occupancy. American Society of Heating, Refrigeration and Air-Conditioning Engineers, Atlanta, GA, 1992.
- Balcomb JD. *Passive Solar Buildings*. MIT Press, Cambridge, MA, 1992.
- Balemans L. Light interception by condensation droplets on plastics, a basic approach. *XXIII International Horticultural Congress*, Firenze, Italy, p. 2296, 1990.
- Bataineh KM & Fayez N. Analysis of thermal performance of building attached sunspace. *Energy and Buildings* 43:8:1863-68, 2011.

- Berdahl P & Fromberg R. The thermal radiance of clear skies. *Solar Energy* 29:4:299-314, 1982
- Berdahl P, Martin M & Sakkal F. Thermal performance of Radiative Cooling Panels. *International J Heat Mass Transfer* 26:6: 871-80, 1983.
- Berdahl P, Martin M & Sakkal F. Emissivity of clear skies. *Solar Energy* 32:5:663-664, 1984.
- Bergman T, Lavine A, Incropera F, & Dewitt D. *Fundamentals of Heat and Mass Transfer, Seventh Edition*. Chichester: John Wiley and Sons, Hoboken, NJ, 2011
- Bosi, S. G., Bathgate, S. N., & Mills, D. R. At Last! A Durable Convection Cover for Atmospheric Window Radiative Cooling Applications. *Energy Procedia*, 57, 1997-2004, 2
- Brandemuehl, M.J. and Beckman, Transmission of Diffuse Radiation through CPC and Flat-Plate Collector Glazings. *Solar Energy* 24: 511, 1980.
- Brunold, S., Investigations on the Potential of Radiation Cooling in Arid Climate Clusters. University of Freiburg, Freiburg, Diploma Thesis, 1989.
- Burch D.M & Luna D.E. A mathematical model for predicting attic ventilation rates required for preventing condensation on roof sheathing. *ASHRAE Transactions* 86:1:201-212, 1980.
- Catalanotti S, Cuomo V, Piro G, Ruggi D, Silvestrini V & Troise G. The Radiative Cooling of Selective Surfaces. *Solar Energy* 17:2: 83-89, 1975.
- Chan H-Y, Riffat S, Zhu J. Review of passive solar heating and cooling technologies. *Renewable and Sustainable Energy Reviews* 14:781-789, 2010.
- Chotivisarut, N., Nuntaphan, A., & Kiatsiriroat, T. Seasonal cooling load reduction of building by thermosyphon heat pipe radiator in different climate areas. *Renewable Energy*, 38(1), 188-194, 2012.
- Churchill, S. W., and H. H. S. Chu, Correlating Equations for Laminar and Turbulent Free Convection from a Horizontal Cylinder. *Int. J. Heat Mass Transfer* 18, 1049, 1975.
- Coma, Julià, et al. Thermal Assessment of Extensive Green Roofs as Passive Tool for Energy Savings in Buildings. *Renewable Energy*, vol. 85:1106–1115, 2016.
- Das AK & Iqbal M. A Simplified Technique to Compute Spectral Atmospheric Radiation. *Solar Energy* 39:2: 143-55, 1987.

- Dehbi A, Abdel-Hamid IM. Durability of mono-layer versus tri-layers LDPE films used as greenhouse cover: Comparative study. *Arabian J Chemistry* 9:S282–89, 2016.
- Delgado AE, Aperador W, & Bautista Ruiz JH. Optical properties of LDPE films with different additives. *Ingenieria y Ciencia* 7:14:49-70, 2011.
- Dobson, RT. Thermal modelling of a night sky radiation cooling system. *J Energy S Africa* 16:2:56-67, 2005.
- dos S Bernardes MA, Vo A & Weinrebe G. Thermal and technical analyses of solar chimneys. *Solar Energy* 75:6:511-24, 2003.
- Duffie JA & Beckman WA. *Solar Engineering of Thermal Processes*. Wiley, Hoboken, NJ, 2013.
- Fouquier, A, Robert, S., Suard, F., Stéphan, L., Arnaud, J. “State of the Art in Building Modelling and Energy Performances Prediction: A Review.” *Renewable and Sustainable Energy Reviews*, 23, 272–288, 2013.
- Frangoudakis A, Papadakis G, Kyritsis S. Influence of the geometrical configuration factors on the radiation heat exchange calculations in night sky radiators. *Intl J Solar Energy* 7:2:73-83, 1989.
- Gan G. Parametric study of Trombe walls for passive cooling of buildings. *Energy and Buildings* 27:1:37-43, 1998.
- Geoola F; Peiper U M; Geoola F. Outdoor testing of the condensation characteristics of plastic film covering materials using a model greenhouse. *J Agricultural Engineering Research* 57(3):167-172, 1994.
- Ghrab-Morcos N, Bouden C & Franchisseur R. Overheating caused by passive solar elements in Tunis. Effectiveness of some ways to prevent it. *Renewable Energy* 3:6-7:801-11, 1993.
- Givoni B. Indoor temperature reduction by passive cooling systems. *Solar Energy* 85:1692-1726, 2011.
- Goldstein, E., Raman, A. and Fan, S. Sub-ambient non-evaporative fluid cooling with the sky. *Nature Energy* 2(9), p.17143, 2017.
- Goldstein, E. Sub-ambient non-evaporative fluid cooling with the sky. *Emerging Water Technology Symposium*. Ontario, CA. May 15-16, 2018.
- Haggard, KL. Architecture of a passive system of diurnal radiation heating and cooling. *Solar Energy* 19:4:403-406, 1977.

- Hamza A, Saito H, Taha M, Kishinami K, & Ismail I. Effect of aging, thickness and color on both radiative properties of polyethylene films and performance of the nocturnal cooling unit. *Energy Conservation Mgmt* 39:1/2:87-93, 1998.
- Hollands KGT, Unny TE, Raithby GD, & Konicek L. Free Convective Heat Transfer Across Inclined Air Layers. *J Heat Transfer* 98:2:189-193, 1976.
- H.R. Hay and J. I. Yellott, Natural air-conditioning with roof pools and movable insulation. *ASHRAE Trans* 75, t65, 1969.
- Hu, M., Pei, G., Wang, Q., Li, J., Wang, Y., & Ji, J. Field test and preliminary analysis of a combined diurnal solar heating and nocturnal radiative cooling system. *Applied Energy*, 179, 899-908, 2016.
- Hu, M., Zhao, B., Ao, X., Su, Y. and Pei, G. Numerical study and experimental validation of a combined diurnal solar heating and nocturnal radiative cooling collector. *Applied Thermal Engineering* 145, pp.1-13, 2018.
- Hu, M., et al. "Parametric Analysis and Annual Performance Evaluation of an Air-Based Integrated Solar Heating and Radiative Cooling Collector." *Energy* 165:811–824, 2018.
- Hu, Mingke, et al. "Experimental Study on a Hybrid Photo-Thermal and Radiative Cooling Collector Using Black Acrylic Paint as the Panel Coating." *Renewable Energy* 139:1217–1226, 2019.
- Hu Z, Wei He, Jie Ji, Zhang S, A review on the application of Trombe wall system in buildings. *Renewable and Sustainable Energy Reviews* 70:976-987, 2017.
- IPCC Fifth Assessment Report, 2014,  
[http://ipcc.ch/pdf/assessment-report/ar5/syr/AR5\\_SYR\\_FINAL\\_SPM.pdf](http://ipcc.ch/pdf/assessment-report/ar5/syr/AR5_SYR_FINAL_SPM.pdf).
- Jakob M. Heat transfer in evaporation and condensation. *Mechanical Engineering* 58:729-739, 1936.
- Johnson TE. Radiation cooling of structures with infrared transparent wind screens. *Solar Energy* 17:173-178, 1975.
- Joubert, G., & Dobson, R. Modelling and testing a passive night-sky radiation system. *Journal of Energy in Southern Africa* 28(1), 76, 2017.
- Kaushika, N.d., and S.k. Rao. Non-Convective Roof Pond with Movable Insulation for Passive Solar Space Heating in Cold Climates. *Building and Environment* 18:1-2:9–17, 1983.

- Killian, M., & Kozek, M. "Ten questions concerning model predictive control for energy efficient buildings." *Building and Environment*, 105: 403-412, 2016.
- Kimball BA. Cooling Performance and Efficiency of Night Sky Radiators. *Solar Energy* 34:1: 19-33, 1985.
- Kreider JF, Curtiss P & Rabl A. Heating and Cooling of Buildings: Principles and Practice of Energy Efficient Design, 2nd ed. CRC, Taylor & Francis Group, Boca Raton, FL, 2009.
- Kummert M, Andre P & Nicolas J. Optimal heating control in a passive solar commercial building. *Solar Energy* 69:1-6:103-16, 2000.
- Lof GOG, ed. Active Solar Systems. MIT Press, Cambridge, MA, 1993.
- Lu, X., Xu, P., Wang, H., Yang, T., & Hou, J. Cooling potential and applications prospects of passive radiative cooling in buildings: The current state-of-the-art. *Renewable and Sustainable Energy Reviews*, 65, 1079-1097, 2016.
- Manz H, Egolf PW, Suter P & Goetzberger A. TIM-PCM external wall system for solar space heating and daylighting. *Solar Energy* 61:6:369-79, 1997.
- Matsuta M, Terada S, Ito H. "Solar heating and radiative cooling using a solar collector-sky radiator with a spectrally selective surface." *Solar Energy*, 39: 183e6, 1987.
- Mihalakakou G. On the use of sunspace for space heating/cooling in Europe. *Renewable Energy* 26:3:415-429, 2002.
- Monghasemi, Nima, and Amir Vadiee. A Review of Solar Chimney Integrated Systems for Space Heating and Cooling Application. *Renewable and Sustainable Energy Reviews*, 81:2714-2730, 2018.
- Oldewurtel, F., Parisio, A., Jones, C. N., Gyalistras, D., Gwerder, M., Stauch, V. Morari, M. "Use of model predictive control and weather forecasts for energy efficient building climate control." *Energy and Buildings*, 45: 15-27, 2012.
- Parsons A & Sharp MK. The potential of sky radiation with change in design parameters. *ASME 2016 Power and Energy Conversion Conference*, Charlotte, NC, Jun 26-Jun 30, 2016.
- Parsons, A. M., & Sharp, K. The effects of multiple covers with condensation and optical degradation of a polyethylene windscreens on the performance of a sky cooling system. *Intl J Sustainable Energy* 1-17. 2018.
- Parsons, A., & Sharp, M., "Control strategies and design parameters for a combined passive heating and cooling system in Louisville, KY." *Intl J Sustainable Energy*,

1-21, 2019.

- Pieters J & Deltour J. Performances of greenhouses with the presence of condensation on cladding materials. *Journal of Agricultural Engineering Research* 68: 125-137, 1997.
- Pollet I & Pieters J. Condensation and radiation transmittance of greenhouse cladding materials, Part3:Results for glass plates and plastic films. *J Agricultural Engineering Research* 77(4): 419-428, 2000.
- Poteat L & Sharp MK. Solar load parameters for a passive solar heat pipe system. ASME 9<sup>th</sup> Intl Conf Energy Sustainability, San Diego, CA, Jun 28-Jul 2, 2015.
- Prívarva, S., Šíroký, J., Ferkl, L., & Cigler, J. “Model predictive control of a building heating system: The first experience.” *Energy and Buildings*, 43(2-3): 564-572, 2011.
- Raman A, Anoma M, Zhu L, Rephaeli E, & Fan S. Passive radiative cooling below ambient air temperature under direct sunlight. *Nature* 515(7528): 540-544, 2014.
- Robinson BS, Chmielewski NE, Knox Kelecy A, Brehob EG & Sharp MK. Heating season performance of a full-scale heat pipe assisted solar wall. *Solar Energy* 87:76–83, 2013.
- Robinson BS & Sharp MK. Heating season performance improvements for a solar heat pipe system. *Solar Energy* 110: 39-49, 2014.
- Robinson BS & Sharp MK. Reducing unwanted gains during the cooling season for a solar heat pipe system. *Solar Energy* 115:16-32, 2015a.
- Robinson BS, Dorwart J, Sharp MK. US space cooling potentials for ambient sources with thermal energy storage. *Intl J Ambient Energy* 36:6:268-81, 2015b.
- Rossiter, J. “Model-based predictive control : A practical approach (Control series).” Boca Raton: CRC Press. 2003.
- Saadatian O, Sopian K, Lim C, Asim N, Sulaiman M. Trombe walls: A review of opportunities and challenges in research and development. *Renewable and Sustainable Energy Reviews* 16:6340-6351, 2012.
- Sadhishkumar S, Balusamy T. Performance analysis of a single-phase thermosiphon solar water heating system. *International Journal of Mechanical, Aerospace, Industrial, Mechatronic and Manufacturing Engineering* 8:10:1749-1752, 2014.
- Santamouris, Mat, 2007. Advances in Passive Cooling, Buildings. Radiative Cooling, Energy and Solar Technology Series, ISBN:1844072630 (Chapter 7).

- Sameti M, Kasaeian A. Numerical simulation of combined passive heating and radiative cooling for a building. *Building Simulation* 8:3, 2015.
- Schultz W & Bartnig KH. Evaluation of the non-drip properties of greenhouse cladding films. *Plasticulture* 111:23-35, 1996.
- Sharifi, Ayyoob, and Yoshiki Yamagata. “Roof Ponds as Passive Heating and Cooling Systems: A Systematic Review.” *Applied Energy* 160:336–357. 2015.
- Sherman M & Modera M. Comparison of measured and predicted infiltration using the LBL infiltration model. *Proceedings Measured Air Leakage Buildings, ASTM STP 904 ASTMS, Philadelphia, ASTM 325-347*, 1986.
- Sodha, M.S., Srivastava, A., Kumar, A., Tiwari, G.N., Heating and cooling buildings by flow of water over the roof. *Applied Energy* 7:229–242, 1980.
- Spanaki, Artemisia, et al. “On the Selection and Design of the Proper Roof Pond Variant for Passive Cooling Purposes.” *Renewable and Sustainable Energy Reviews* 15:8:3523–3533, 2011.
- Springer Z & Sharp MK. The potential of night sky radiation for humidity control. ASME 9<sup>th</sup> Intl Conf Energy Sustainability, San Diego, CA, Jun 28-Jul 2, 2015.
- Srivastava, A., Tiwari, G.N., Experimental validation of a thermal model of an evaporative cooling system. *Energy Convers Manag* 24:305–311, 1984.
- Susheela N & Sharp MK. A heat pipe augmented passive solar system for heating of buildings. *J Energy Eng* 127:1:18-36, 2001.
- The National Weather Service Climate Prediction Center.  
[http://www.cpc.ncep.noaa.gov/products/analysis\\_monitoring/cdus/degree\\_days/ddayexp.shtml](http://www.cpc.ncep.noaa.gov/products/analysis_monitoring/cdus/degree_days/ddayexp.shtml). Accessed 17 Nov. 2016.
- Vall S & Castell A. Radiative cooling as low-grade energy source: A literature review. *Renewable Sustainable Energy Rev* 77:803-20, 2017.
- Valladares-Rendon LG, Schmid G, & Shang-Lein Lo. Review on energy savings by solar control techniques and optimal orientation for the strategic placement of façade shading systems. *Energy and Buildings*, 140:458-479, 2017.
- Wang, Y., Cui, Y., Han, L. “Experiments on Novel Solar Heating and Cooling System.” *Energy Conversion and Management*, 49(8): 2083–2089, 2008.
- Wang, S., & Ma, Z. “Supervisory and Optimal Control of Building HVAC Systems: A Review.” *HVAC&R Research*, 14(1), 3-32, 2008.

- Yan MQ, Kridii GT, Sherif SA, Lee SS & Padki MM. Thermo-fluid analysis of solar chimneys. ASME Fluids Engineering Division (Publication) FED *Industrial Applications of Fluid Mechanics* 132:125-30, 1991.
- Yellott J. Utilization of sun and sky radiation for heating and cooling of buildings. *American Society of Heating Refrigerating and Air-Conditioning Engineers* 15:12:31-42, 1973.
- Yong, C., Yiping, W., & Li, Z. "Performance analysis on a building-integrated solar heating and cooling panel." *Renewable Energy*, 74, 627-632, 2015.
- Zaheer-Uddin M. Identifying the domain of overheating on the energy performance curves of a passive solar house. *Energy* 14:12:879-88, 1989.
- Zhai, Y., Ma, Y., David, S. N., Zhao, D., Lou, R., Tan, G., Yin, X. Scalable-manufactured randomized glass-polymer hybrid metamaterial for daytime radiative cooling. *Science*, 355(6329), 1062-1066, 2017.

APPENDIX

Table 15. Variables used in equations in Section 4.2.

<b>Variable</b>	<b>Description</b>	<b>Constant</b>
$A_{WS}$	Surface area of windscreen*	2.62 (m <sup>2</sup> )
$A_{Rad}$	Surface area of radiator*	2.62 (m <sup>2</sup> )
$A_{HP}$	Surface area of heat pipe*	5.18E-4 (m <sup>2</sup> )
$A_{Insul}$	Surface area of insulation*	2.62 (m <sup>2</sup> )
$A_{Tank}$	Surface area of tank*	4.17 (m <sup>2</sup> )
$A_{Evap}$	Surface area of evaporator*	0.104 (m <sup>2</sup> )
$A_i$	Anisotropy index	--
$\alpha_n$	Normal absorptivity (radiator)* (White ZnO/Black Chrome)	0.180/0.960
$\alpha_b$	Beam absorptivity (radiator)	--
$\alpha_{b_{WS}}$	Beam absorptivity (windscreen)	--
$\alpha_d$	Diffuse absorptivity (radiator)	--
$\alpha_{d_{WS}}$	Diffuse absorptivity (windscreen)	--
$\alpha_g$	Ground absorptivity (radiator)	--
$\alpha_{g_{WS}}$	Ground absorptivity (windscreen)	--
$\beta$	Radiator orientation*	0°, 53°
$e_{ws}$	Windscreen emissivity (long wave)* (Polyethylene/Glass)	0.150/0.880
$e_{Rad}$	Radiator emissivity (long wave)* (White ZnO/Black Chrome)	0.929/0.090
$e_{Tank}$	Tank emissivity*	0.930
$f$	Correction factor	--
$g$	Gravitational constant	9.81 (m/s <sup>2</sup> )
$H_{Building}$	Modeled building height*	3.00 (m)
$h_w$	Wind heat transfer coefficient [Sherman & Modera 1986]	--
$h$	Annual hour	--
$I$	Total radiation on horizontal surface (hourly)	TMY3 Data
$I_b$	Isotropic beam radiation (hourly)	--
$I_d$	Isotropic diffuse radiation (hourly)	TMY3 Data
$k_{Air}$	Conductivity of air	--
$k_{HP}$	Conductivity of heat pipe material*	401 (W/mK)
$k_{Insul}$	Conductivity of insulation material*	2.50E-2 (W/mK)
$k_{Rad}$	Conductivity of radiator material*	401 (W/mK)
$k_{Tank}$	Conductivity of tank*	0.500 (W/mK)

$k_{Water}$	Conductivity of thermal fluid (water)*	0.580
$K$	Extinction coefficient* (Polyethylene/Glass)	1.00E-5/4.0 (m <sup>-1</sup> )
$L$	Thickness of windscreen* (Polyethylene/Glass)	50E-6 /3.18E-3(m)
$L_{HP}$	Length of adiabatic section*	2.54E-2 (m)
$L_{Insul}$	Thickness of insulation*	0.700 (m)
$L_{Rad}$	Thickness of radiator*	3.18E-3 (m)
$L_{Tank}$	Thickness of tank wall*	3.18E-3(m)
$L_{Cond}$	Thickness of condensation*	1.20E-4 (m)
$L_{W-R}$	Distance between windscreen and radiator	2.54E-2 (m)
$n_1$	Refractive index (air)*	1.00
$n_2$	Refractive index* (Polyethylene/Glass)	1.54/1.53
$n_3$	Refractive index (water)*	1.33
$N$	Number of windscreens	1
$N_{Fins}$	Number of fins*	5
$N_{HP}$	Number of heat pipes*	5
$N_{HP,room}$	Number of heat pipes exposed to room*	1
$N_{HP,tank}$	Number of heat pipes in thermal fluid*	4
$N_{Tank}$	Number of tanks*	1
$Nu$	Calculated Nusselt number	--
$OD_{HP}$	Outside diameter of heat pipe*	2.86E-2 (m)
$\rho_g$	Ground reflectance*	0.3
$R_b$	Beam radiation Ratio	--
$R_{Cond}$	Resistance of condenser end*	8.58E-5 (K/W)
$R_{Evap}$	Resistance of evaporator end*	9.13E-5 (K/W)
$\sigma$	Stefan Boltzmann constant*	5.67 E-8 (W/m <sup>2</sup> K <sup>4</sup> )
$\tau_b$	Beam transmissivity	--
$\tau_d$	Diffuse transmissivity	--
$\tau_g$	Ground transmissivity	--
$\tau_{WS}$	Windscreen long wave transmissivity* (Polyethylene/Glass)	0.73/0.10
$\tau_{Cond}$	Condensation long wave transmissivity*	0.80
$W_{HP}$	Distance between heat pipe centers*	0.359 (m)
$LRR$	Load to radiator ratio*	10 (W/mK)
	Radiator plate material*	Copper
	Radiator plate selective surface*	White Zinc Oxide/Black Chrome
	Radiator plate height*	2.10 (m)
	Radiator plate width*	1.25 (m)
	Radiator plate height*	2.10 (m)
	Radiator plate width*	1.25 (m)
	Heat pipe two phase heat transfer fluid*	R-124

	Heat pipe material*	Copper
	Water tank height*	1.42 (m)
	Water tank length*	1.11 (m)
	Water tank width*	0.203 (m)

\*Constant values in program

-- Indicates a calculated value

Table 16. Variables and parameters used in MATLAB simulation and design.

Variable	Description	Constant
$\alpha$	Thermal diffusivity	--
$\alpha_n$	Normal absorptivity (radiator)* (White ZnO/Black Chrome)	0.180/0.960
$\alpha_b$	Beam absorptivity (radiator)	--
$\alpha_{b_{WS}}$	Beam absorptivity (windscreen)	--
$\alpha_d$	Diffuse absorptivity (radiator)	--
$\alpha_{d_{WS}}$	Diffuse absorptivity (windscreen)	--
$\alpha_g$	Ground absorptivity (radiator)	--
$\alpha_{g_{WS}}$	Ground absorptivity (windscreen)	--
$\alpha_{Building}$	Terrain Parameter, Class III	0.850
$A_{WS}$	Surface area of windscreen*	2.62 (m <sup>2</sup> )
$A_{Rad}$	Surface area of radiator*	2.62 (m <sup>2</sup> )
$A_{HP}$	Surface area of heat pipe*	5.18E-4 (m <sup>2</sup> )
$A_{Insul}$	Surface area of insulation*	2.62 (m <sup>2</sup> )
$A_{Tank}$	Surface area of tank*	4.17 (m <sup>2</sup> )
$A_{Evap}$	Surface area of evaporator*	0.104 (m <sup>2</sup> )
$A_i$	Anisotropy index	--
$\beta$	Radiator orientation*	0°, Latitude+15°
$\beta'$	Thermal expansion coefficient	--
$e_{ws}$	Windscreen emissivity (long wave)* (Polyethylene/Glass)	0.150/0.880
$e_{Rad}$	Radiator emissivity (long wave)* (White ZnO/Black Chrome)	0.929/0.090
$e_{Tank}$	Tank emissivity*	0.930
$f$	Correction factor	--
$g$	Gravitational constant	9.81 (m/s <sup>2</sup> )
$\gamma_{Building}$	Terrain Parameter, Class III	0.200
$H_{Building}$	Modeled building height*	3.00 (m)
$H_{Tower}$	Estimated height of weather tower*	10.0 (m)
$h_w$	Wind heat transfer coefficient [Sherman & Modera, 1986]	--

$h$	Hour	--
$I$	Total radiation on horizontal surface (hourly)	TMY3 Data
$I_b$	Isotropic beam radiation (hourly)	--
$I_d$	Isotropic diffuse radiation (hourly)	TMY3 Data
$k_{Air}$	Conductivity of air	--
$k_{HP}$	Conductivity of heat pipe material*	401 (W/mK)
$k_{Insul}$	Conductivity of insulation material*	2.50E-2 (W/mK)
$k_{Rad}$	Conductivity of radiator material*	401 (W/mK)
$k_{Tank}$	Conductivity of tank*	0.500 (W/mK)
$k_{Water}$	Conductivity of thermal fluid (water)*	0.580
$K$	Extinction coefficient* (Polyethylene/Glass)	1.00E-5/4.0 (m <sup>-1</sup> )
$L$	Thickness of windscreen* (Polyethylene/Glass)	50E-6 /3.18E-3(m)
$L_{HP}$	Length of adiabatic section*	2.54E-2 (m)
$L_{Insul}$	Thickness of insulation*	0.700 (m)
$L_{Rad}$	Thickness of radiator*	3.18E-3 (m)
$L_{Tank}$	Thickness of tank wall*	3.18E-3(m)
$L_{Cond}$	Thickness of condensation*	1.20E-4 (m)
$L_{W-R}$	Distance between windscreen and radiator	2.54E-2 (m)
$L_X$	Characteristic Length	--
$LRR/LCR$	Load to radiator ratio*	10.0 (W/mK)
$n_1$	Refractive index (air)*	1.00
$n_2$	Refractive index* (Polyethylene/Glass)	1.54/1.53
$n_3$	Refractive index (water)*	1.33
$N$	Number of windscreens	1
$N_{Fins}$	Number of fins*	5
$N_{HP}$	Number of heat pipes*	5
$N_{HP,room}$	Number of heat pipes exposed to room*	1
$N_{HP,tank}$	Number of heat pipes in thermal fluid*	4
$N_{Tank}$	Number of tanks*	1
$Nu$	Calculated Nusselt number	--
$OD_{HP}$	Outside diameter of heat pipe*	2.86E-2 (m)
$P$	Prandtl number	
$\rho_g$	Ground reflectance*	0.3
$Ra$	Rayleigh number	--
$R_b$	Beam radiation Ratio	--
$R_{Cond}$	Resistance of condenser end*	8.58E-5 (K/W)
$R_{Evap}$	Resistance of evaporator end*	9.13E-5 (K/W)
$\sigma$	Stefan Boltzmann constant*	5.67 E-8 (W/m <sup>2</sup> K <sup>4</sup> )
$\Delta T$	Temperature difference	--
$T_O$	Outdoor dry-bulb Temperature	--

$T_{dp,o}$	Outdoor dew-point Temperature	--
$t$	Number of hours from midnight	--
$\theta_1/\theta_2$	Angles of refraction	--
$\tau_b$	Beam transmissivity	--
$\tau_d$	Diffuse transmissivity	--
$\tau_g$	Ground transmissivity	--
$\tau_{ws}$	Windscreen long wave transmissivity* (Polyethylene/Glass)	0.73/0.10
$\tau_{Cond}$	Condensation long wave transmissivity*	0.80
$V_j$	Wind velocity	--
$\nu$	Kinematic viscosity	--
$W_{HP}$	Distance between heat pipe centers*	0.359 (m)
$WSV$		
<b>Description of Design Parameters</b>		
Radiator plate material*		Copper
Radiator plate selective surface*		White Zinc Oxide/Black Chrome
Radiator plate height*		2.10 (m)
Radiator plate width*		1.25 (m)
Radiator plate height*		2.10 (m)
Radiator plate width*		1.25 (m)
Heat pipe two phase heat transfer fluid*		R-124
Heat pipe material*		Copper
Water tank height*		1.42 (m)
Water tank length*		1.11 (m)
Water tank width*		0.203 (m)

\*Constant values in program

## CURRICULUM VITA

**NAME:** Adrienne Marie Parsons

**ADDRESS:** 2609 Landor Ave.

**DOB:** Cincinnati, OH – June 23, 1986

**EDUCATION:** B.S., Mechanical Engineering  
University of Louisville  
2004-2008

M.S., Mechanical Engineering  
University of Louisville  
2008-2009

Ph.D., Mechanical Engineering  
University of Louisville  
Expected August 2019

**PROFESSIONAL SOCIETIES  
AND TRAINING:** Professional Engineer of Commonwealth of  
Kentucky, NCEES, 2013 – Present

Certified Energy Manager, The Association of  
Energy Engineers, 2011 – 2017

Infrared Thermographer, Level I, 2011 – Present

Delphi University, Delphi U Online, June 2016-  
August 2016

Delphi Center for Teaching & Learning, Course  
Redesign Institute for Active Learning, May 2017

Delphi Center for Teaching & Learning, Faculty  
Learning Community: Classroom Response  
System, 2018-2019

## **PUBLICATIONS & PRESENTATIONS:**

Parsons, A., Sharp, M. K. (June 2016). The potential of sky radiation with change in design parameters. *ASME 2016 Power and Energy Conversion Conference*.

Parsons, A., Sharp, M. K. The cooling potential of sky radiation with variation in system parameters. *Journal of Solar Energy Engineering*. Published January 2019.

Parsons, A., Sharp, M. K. The Effects of Multiple covers with Condensation and Optical Degradation of a Polyethylene Windscreen on the Performance of a Sky Cooling System. *International Journal of Sustainable Energy*. Published October 2018.

Parsons, A., Sharp, M. K. (June 2018) Presentation: Control strategies and design parameters for a combined passive heating and cooling system in Louisville, KY. *ASME 2018 Power and Energy Conference & Exhibition*.

Parsons, A., Sharp, M. K. Control strategies and design parameters for a combined passive heating and cooling system in Louisville, KY. *International Journal of Sustainable Energy*. Published May 2019.

Parsons, A., Sharp, M. K. (June 2016) Poster Presentation: Solar heat pipe sky radiator. *The U.S. Clean Energy Education & Empowerment Women in Clean Energy Symposium*.

Bego, C. R., Thompson, A. K., Ralston, P. A., Crush, G. J., Parsons, A. (in press). Flipping the Differential Equations Classroom: Changes Over Time. *2018 ASEE Annual Conference and Exposition*.